
**Branching Fraction Measurement of $B^\pm \rightarrow \chi_{c1}\pi^+\pi^-K^\pm$ and
Search for a Narrow Resonance with the Belle Experiment**

Dissertation

zur Erlangung des mathematisch-naturwissenschaftlichen Doktorgrades
„Doctor rerum naturalium“
der Georg-August-Universität Göttingen

im Promotionsprogramm ProPhys
der Georg-August University School of Science (GAUSS)

vorgelegt von

Elisabeth Patricia Panzenböck

aus Mainz

Göttingen, 2014

Betreuungsausschuss

Prof. Dr. Ariane Frey

II. Physikalisches Institut, Georg-August-Universität Göttingen

Prof. Dr. Arnulf Quadt

II. Physikalisches Institut, Georg-August-Universität Göttingen

Mitglieder der Prüfungskommission:

Referent: Prof. Dr. Ariane Frey

II. Physikalisches Institut, Georg-August-Universität Göttingen

Koreferent: Associate Prof. Kenkichi Miyabayashi (Doctor of Science)

Faculty Division of Natural Sciences, Research Group of Physics, Nara Women's University, Nara, Japan

Weitere Mitglieder der Prüfungskommission:

Prof. Laura Covi, PhD

Institut für Theoretische Physik, Georg-August-Universität Göttingen

PD Dr. Jörn Große-Knetter

II. Physikalisches Institut, Georg-August-Universität Göttingen

Prof. Hisaki Hayashii (Doctor of Science)

Faculty Division of Natural Sciences, Research Group of Physics, Nara Women's University, Nara, Japan

Prof Satoru Hirenzaki (Doctor of Science)

Faculty Division of Natural Sciences, Research Group of Physics, Nara Women's University, Nara, Japan

Tag der mündlichen Prüfung: 2. Dezember 2014

Referenz: II.Physik-UniGö-Diss-2014/06

Branching Fraction Measurement of $B^\pm \rightarrow \chi_{c1}\pi^+\pi^-K^\pm$ and Search for a Narrow Resonance with the Belle Experiment

Dissertation

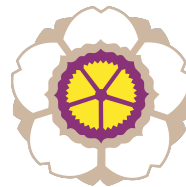
in
Research Cooperation
and
Joint Doctoral Supervision
between

the Faculty of Physics,
Georg-August University School of Science (GAUSS),
Georg-August-University, Göttingen, Germany

and

the School of Interdisciplinary Research of
Scientific Phenomena and Information,
Graduate School of Humanities and Sciences,
Nara Women's University, Nara, Japan

submitted by
Elisabeth Patricia Panzenböck



Göttingen, 2014

Abstract

The effective QCD colour potential can be derived by studying quarkonia through spectroscopy to determine their masses. In the charmonium spectrum, which is well understood and precisely measured below the $D\bar{D}$ production threshold, not all predicted states above that threshold have been observed yet and others cannot be assigned to conventional charmonium states. To fathom the nature of the latter so-called exotic or charmonium-like states motivates this thesis. A first observation and measurement of the branching fraction of the four-body B meson decay $B^\pm \rightarrow \chi_{c1}\pi^+\pi^-K^\pm$ is presented. In addition, the $\chi_{c1}\pi^+\pi^-$ invariant mass spectrum is studied in order to search for contributions of any intermediate charmonium(-like) resonance. This study is based on a 772×10^6 $B\bar{B}$ pairs data sample produced at a center-of-mass energy of $\sqrt{s} = 10.58$ GeV/ c^2 corresponding to the $\Upsilon(4S)$ resonance and collected by the Belle detector at the KEKB asymmetric-energy e^+e^- collider located at KEK, Japan. The signal yield is extracted by an unbinned maximum likelihood fit to the difference-to-beam energy ΔE distribution and the B decay branching fraction is obtained to be

$$\mathcal{B}(B^+ \rightarrow \chi_{c1}\pi^+\pi^-K^+) = (3.89 \pm 0.19 \text{ (stat)} \pm 0.20 \text{ (syst)}) \times 10^{-4}.$$

Using the $\chi_{c1}\pi^+\pi^-$ mass spectrum, an upper limit including both statistical and systematic uncertainties is given for a new decay mode of the exotic $X(3872)$ charmonium-like state,

$$\mathcal{B}(B^\pm \rightarrow X(3872)K^\pm) \times \mathcal{B}(X(3872) \rightarrow \chi_{c1}(1P)\pi^+\pi^-) < 1.4 \times 10^{-6} \text{ @ 90\% C.L.},$$

as well as a preliminary upper limit for the still undiscovered conventional charmonium $\chi_{c1}(2P)$ following a mass assumption of 3920 MeV/ c^2 ,

$$\mathcal{B}(B^\pm \rightarrow \chi_{c1}(2P)K^\pm) \times \mathcal{B}(\chi_{c1}(2P) \rightarrow \chi_{c1}(1P)\pi^+\pi^-) < 1.1 \times 10^{-5} \text{ @ 90\% C.L.}.$$

These results favour the hypothesis of $X(3872)$ being an admixture of a $D^0\bar{D}^{*0}$ molecule state and a conventional charmonium.

Kurz-Zusammenfassung

Das effektive QCD-Farbpotential kann aus der Untersuchung von Quarkonia durch Spektroskopie zur Bestimmung ihrer Massen abgeleitet werden. Im unterhalb der $D\bar{D}$ -Produktions-Schwelle gut verstandenen und präzise vermessenen Charmoniumspektrum wurden noch nicht alle vorhergesagten Zustände oberhalb der Schwelle beobachtet, und andere können keinen konventionellen Charmoniumzuständen zugeordnet werden. Das Ergründen der Natur der letzteren sogenannten exotischen oder Charmonium-ähnlichen Zuständen stellt die Motivation dieser Arbeit dar. Es wird die erste Beobachtung und Messung des Verzweigungsverhältnisses des Vierkörper- B -Meson-Zerfalls $B^\pm \rightarrow \chi_{c1}\pi^+\pi^-K^\pm$ präsentiert. Zusätzlich wird das invariante Massenspektrum von $\chi_{c1}\pi^+\pi^-$ untersucht, um nach Beiträgen von Charmonium-(-ähnlichen) Zwischenresonanzen zu suchen. Diese Arbeit basiert auf einem Datensatz von 772×10^6 $B\bar{B}$ -Paaren, die bei einer Schwerpunktsenergie von $\sqrt{s} = 10,58$ GeV/c², der $\Upsilon(4S)$ -Resonanz entsprechend, vom Belle-Detektor am energetisch-asymmetrischen e^+e^- -Beschleuniger KEKB am KEK, Japan, gesammelt wurden. Die Signalausbeute wird aus einem ungebinnten Maximum-Likelihood-Fit der Differenz-zu-Strahl-Energie ΔE -Verteilung gewonnen und daraus das B -Zerfalls-Verzweigungsverhältnis zu

$$\mathcal{B}(B^+ \rightarrow \chi_{c1}\pi^+\pi^-K^+) = (3,89 \pm 0,19 \text{ (stat)} \pm 0,20 \text{ (syst)}) \times 10^{-4}$$

bestimmt. Im invarianten Massenspektrum von $\chi_{c1}\pi^+\pi^-$ wird eine obere Grenze einschließlich statistischer und systematischer Unsicherheiten für eine neue Zerfallsmode des exotischen, Charmonium-ähnlichen Zustands $X(3872)$ mit

$$\mathcal{B}(B^\pm \rightarrow X(3872)K^\pm) \times \mathcal{B}(X(3872) \rightarrow \chi_{c1}(1P)\pi^+\pi^-) < 1,4 \times 10^{-6} @ 90\% \text{ C.L.},$$

als auch eine vorläufige obere Grenze des weiterhin unbeobachteten, konventionellen Charmoniums $\chi_{c1}(2P)$, bei einer vorhergesagten Masse von 3920 MeV/c², mit

$$\mathcal{B}(B^\pm \rightarrow \chi_{c1}(2P)K^\pm) \times \mathcal{B}(\chi_{c1}(2P) \rightarrow \chi_{c1}(1P)\pi^+\pi^-) < 1,1 \times 10^{-5} @ 90\% \text{ C.L.}$$

gegeben. Diese Ergebnisse begünstigen die Hypothese, dass $X(3872)$ einen Mischzustand aus einem $D^0\bar{D}^{*0}$ -Molekül und einem konventionellen Charmonium darstellt.

本論文の概要

QCD 有効カラーポテンシャルは、クォークoniumに関する分光学により種々の状態の質量を決定することにより導出できる。チャーモニウムのスペクトルは $D\bar{D}$ 閾値よりも小さい質量の領域では精密に測定され、よくわかっているが、その閾値よりも大きな質量のものについては、予言されたすべての状態が確認されてはおらず、かつ、いくつかのものは通常のチャーモニウムで未発見のものと解釈するのが難しい。後者のエキゾチックなチャーモニウム似の状態についてその本質を測りたいということが本論文の動機である。世界で最初に $B^\pm \rightarrow \chi_{c1}\pi^+\pi^-K^\pm$ なる四体崩壊の存在を確認し、さらにこの四体崩壊過程における $\chi_{c1}\pi^+\pi^-$ 系の不変質量スペクトラムにより、中間状態におけるチャーモニウム (似) 共鳴の寄与の有無を調べた。本研究は高エネルギー加速器研究機構 (KEK) において KEKB 非対称エネルギー電子・陽電子衝突型加速器と Belle 測定器を用いて $\Upsilon(4S)$ すなわち重心系エネルギー 10.58 GeV で収集した 7億7千200万 $B\bar{B}$ 事象のデータをもとにしている。 B 中間子崩壊の信号は B 中間子候補と重心系でのビームエネルギーとの差である ΔE なる量の分布に対して最尤度法フィットを適用することにより抽出した。得られた崩壊分岐比は

$$B(B^+ \rightarrow \chi_{c1}\pi^+\pi^-K^+) = (3.89 \pm 0.19 \text{ (stat)} \pm 0.20 \text{ (syst)}) \times 10^{-4}$$

であった。

$\chi_{c1}\pi^+\pi^-$ 系の不変質量スペクトラムからは、統計誤差および系統誤差の両方を考慮してエキゾチックなチャーモニウム似の状態である $X(3872)$ について

$$B(B^\pm \rightarrow X(3872)K^\pm) \times B(X(3872) \rightarrow \chi_{c1}(1P)\pi^+\pi^-) < 1.4 \times 10^{-6} @ 90\% \text{ C.L.}$$

を得た。同様に、これまで未発見のチャーモニウムである $\chi_{c1}(2P)$ に質量 3920 MeV/ c^2 を仮定して

$$B(B^\pm \rightarrow \chi_{c1}(2P)K^\pm) \times B(\chi_{c1}(2P) \rightarrow \chi_{c1}(1P)\pi^+\pi^-) < 1.1 \times 10^{-5} @ 90\% \text{ C.L.}$$

を得た。これらの結果は、 $X(3872)$ が $D^0\bar{D}^{*0}$ のメソン分子状態と通常のチャーモニウムが混合したものであるとの仮説を支持する。

Table of Contents

1. Preface	1
2. Introduction to Particle Physics	5
2.1. Elementary Particles of the Standard Model	5
2.2. Interactions of the Standard Model	6
2.2.1. Electroweak Unification and The Flavour Changing Weak Interaction	7
The Higgs Mechanism	7
<i>CP</i> Violation and the CKM Matrix	9
2.2.2. The Strong Interaction and Hadronisation	10
3. Motivation	13
3.1. The Charmonium Spectrum	13
3.1.1. The As Yet Unseen $\chi_{c1}(2P)$ - A Conventional Charmonium	15
3.2. Exotic Charmonium(-like) States	15
3.2.1. The Puzzling $X(3872)$ - An Exotic Charmonium	18
3.3. <i>B</i> Meson Decays as a Source for Charmonium	22
4. The Belle Experiment	25
4.1. The KEKB Accelerator	26
4.2. The Belle Detector	27
The Silicon Vertex Detector SVD	28
The Central Drift Chamber CDC	28
The Time-of-Flight Counter TOF	29
The Aerogel Cherenkov Counter ACC	29
The Electromagnetic Calorimeter ECL	29
The K_L^0 and Muon Detector KLM	30
Trigger and Data Acquisition	30
4.3. Particle Identification	32
4.4. Data Sample	33
5. Event Selection	35
5.1. Monte Carlo Simulation Dataset	35
5.2. Reconstruction of χ_{c1} Candidates	36
5.3. Selection of Light Meson Candidates	38
5.3.1. Low Transverse Momentum Pion Selection	38
5.4. Reconstruction of <i>B</i> Candidates	40

5.5. Properties of the reconstructed B Candidate	40
6. Monte Carlo Studies	45
6.1. Background Estimation	45
6.1.1. Expected Background in ΔE	45
6.1.2. Figure of Merit	46
6.1.3. Expected Background in $M_{\chi_{c1}\pi\pi}$	47
6.2. Fitting Strategy and Observable Extraction	49
6.2.1. ΔE Fit and Efficiency Estimation	49
ΔE Signal Fit	49
Efficiency Estimation for different Masses of an Intermediate State	51
Background Fit for ΔE	53
Total PDF for ΔE in PHSP	54
6.2.2. Fitting of the Invariant Mass Spectrum $M_{\chi_{c1}\pi\pi}$	54
$M_{\chi_{c1}\pi\pi}$ Signal Fit	54
Expected Signal Yield in $M_{\chi_{c1}\pi\pi}$ in $X(3872)$ Case	56
Background Fit for $M_{\chi_{c1}\pi\pi}$	57
Total PDF for $M_{\chi_{c1}\pi\pi}$ in $X(3872)$ Case	57
7. Results and Discussion	59
7.1. ΔE Distribution	59
7.2. Weighted Detection Efficiency Estimation	60
7.3. Efficiency Correction and Systematic Uncertainty	62
7.4. Branching Fraction of $B^\pm \rightarrow \chi_{c1}\pi^+\pi^-K^\pm$	64
7.5. $\chi_{c1}\pi^+\pi^-$ Invariant Mass Spectrum	65
7.6. Upper Limit for $X(3872)$ decaying to $\chi_{c1}\pi^+\pi^-$	66
7.7. Upper Limit for $\chi_{c1}(2P)$ decaying to $\chi_{c1}(1P)\pi^+\pi^-$	67
8. Conclusion	69
A. Cut Selection for π^0 Veto	73
B. Estimated ΔE Distribution in the Larger Window	74
C. Expected Signal Yield in the ΔE Distribution in the Phase Space	75
D. Upper Limit Calculation	76
E. Other Invariant Mass Combinations	77
Bibliography	i
Acknowledgements	vi
Curriculum Vitæ	viii

1. Preface

The grand questions of mankind, what are the innermost structures of matter, space and time, and which laws are the basis for the fundamental forces in the universe, have not yet been answered completely. But it seems like we are getting closer: The well established theory of particle physics, the Standard Model, has been proven right over and over again, not least with the prediction and discovery of the Higgs boson in 2012. However, because of its nature as a renormalisable quantum field theory, many parameters of the Standard Model need experimental results as input to be determined and cannot be deduced from first principle calculations: When a quantity is found to become finite by the procedure of renormalisation, an experimental result is required to settle that quantity's absolute value.

Many weak decay transition rates and CP violation phenomena have been measured to determine the four weak effective couplings in the quark sector as formulated in the Cabibbo-Kobayashi-Maskawa (CKM) matrix. This matrix includes one irreducible complex phase that leads to violation of CP invariance. A comprehensive method to test if the measured effective couplings match with the CKM framework is provided by the so-called *unitarity triangle*.

On the other hand, there is only one gauge coupling in the strong interaction, the running coupling constant $\alpha_s(q^2)$. Its absolute value has been determined to a precision of a few percent through various measurements at τ lepton hadronic decays, deep inelastic scattering and hadron production at e^+e^- colliders. The strong interaction's characteristics such as asymptotic freedom and the non-Abelian nature of quantum chromodynamics (QCD), the gauge group describing the strong interaction, are proven and the standard explanation of confinement of quarks in hadrons is widely established. However, even in 2014, 40 years after the ground-breaking discovery of the J/ψ meson in November 1974 led to the golden age of charmonium spectroscopy, some aspects of QCD are still posing a riddle. In the non-perturbative regime of α_s , two basic questions are not yet solved satisfactorily about the issue of exotic hadrons: While there is no explicit prohibition rule to form hadrons having unusual constituent configurations like tetraquarks, meson-meson molecules etc, there have been very few implications or evidence. On the other hand, some of the states in the charmonium spectrum are predicted, but have not been identified yet; others remain unconfirmed. The suppression mechanism is unknown. Also, the constituent quarks are not always a good approximation to be regarded as building blocks to form hadrons. Thus, a more appropriate picture is required to be deduced, especially for excited states.

With these exotic hadrons the question arises if there is an exceptional yet unknown mechanism related to excited states, and if so to what consequences such a concept might lead us in our understanding of the universe. Thus, the rigorous survey of the charmonium and bottomonium spectra is still pursued with much enthusiasm.

It should be noted that a particular excited state may largely affect the evolution of our universe: Carbon forms at the interior of burning stars in what is called the triple-alpha process. Here, the ^{12}C as we know it is not produced directly, but rather in an excited state 7 MeV above the ground state, called the Hoyle state.

The existence of such a state as an argument for stable carbon was predicted by Hoyle in 1954 [34, 43]. This excited state is playing an essential role in the currently observed abundance of ^{12}C in the universe. And even though there is no obvious link between exotic hadrons and the time evolution of the universe after the big bang, it offers a great motivation to further explore excited hadron states and look for something unexpected that might broaden our understanding of the world around us.

As vast a field particle physics may be,

One of the greatest intellectual challenges of modern physics is
to understand confinement not just as a phenomenon but
to comprehend it quantitatively from the theory of the strong force.

So it was written in the *Physics Performance Report* of the PANDA experiment where I did my graduate studies. And it is a great way to summarise the goal that motivates the enormous efforts that have been made in my current field of research - quarkonium spectroscopy. In this thesis, I will describe and explain the Ph.D. research work which led to the worldwide first observation of the $B^\pm \rightarrow \chi_{c1} \pi^+ \pi^- K^\pm$ final state along with the search for any intermediate charmonium(-like) state in this particular decay mode. There are two hypotheses pursued for a resonance decaying to $\chi_{c1} \pi^+ \pi^-$.

Now, the general structure of this work is as follows: The purpose of Chapter 2 is to provide a brief introduction to the Standard Model of particle physics. In particular, an overview of the fundamental particles and the interactions between these particles is given. Emphasis is put on the flavour changing weak interaction as it is the source to create charmonium in B meson decays. Another important point is the investigation of hadronisation and thus the quark-quark potential. The latter is picked up in Chapter 3 which provides a motivation to further explore the charmonium spectrum and look for so-called exotic charmonium(-like) states.

Here, the main goal of this work is defined, namely the study of a new aspect of the established but still not well understood $X(3872)$ and the search for the yet to be discovered $\chi_{c1}(2P)$. In Chapter 4 the Belle experiment is introduced as the experimental apparatus to do so. The KEKB accelerator as well as the Belle detector with its sub-detectors are briefly characterized. Event selection criteria to reconstruct B meson candidates and a look at their properties are described in Chapter 5. Using a best candidate selection and narrowing down the sample of reconstructed B candidates to the signal region of interest, Monte Carlo simulation studies are pursued to estimate potential background and reconstruction efficiencies as well as constructing

fitting routines for observable extraction. These methods and the calculation of systematic uncertainties are presented in Chapter 6. Results from this thesis research work and their discussion can be found in Chapter 7. Chapter 8 concludes this work with a summary and outlook.

Much of particle physics is concerned with the high-energy interactions of relativistic particles. S.I. based units are used to present e.g. luminosity, its unit is inverse barn where $1 \text{ barn} = 10^{-28} \text{ m}^2$. A system of units commonly used in particle physics is the so-called *natural units*. To simplify the expression of quantities we conveniently choose: $c = \hbar = 1$, where c is the speed of light in vacuum and \hbar the unit of action in quantum mechanics. Therefore, masses are presented in GeV rather than GeV/c^2 and momenta in GeV as well instead of GeV/c . The Einstein energy-momentum relation $E^2 = p^2c^2 + m^2c^4$ becomes $E^2 = p^2 + m^2$.

2. Introduction to Particle Physics

Particle physics is about exploring, understanding and giving a description of the visible matter in our Universe. It is at the heart of our understanding of the laws of nature. Bringing together a variety of theories and experimental observations throughout the latter half of the 20th century concluded in the so-called *Standard Model of Particle Physics* which provides a unified picture of the fundamental building blocks and the interactions between them.

2.1. Elementary Particles of the Standard Model

While it seems that almost all commonly encountered phenomena can be described in terms of the electron, electron neutrino, proton and neutron, it was observed that at higher energy scales, further structure becomes apparent. Eventually, in the Standard Model we find 12 spin-half particles (fermions) which can be divided into leptons and quarks as shown in Tab(2.1). The first generation consists of the lightest particles, the electron e^- , the electron neutrino ν_e , the up u and down quark d . As far as we know, those are elementary point-like particles and not composite structures with a sub-structure. These light fermions represent the basic components of the low-energy Universe. Each of these particles has two identical siblings that only differ in their higher masses. The second generation includes the muon μ , muon neutrino ν_μ , strange s and charm quark c . The third generation consists of the tau-lepton τ , tau neutrino ν_τ , top t and bottom quark b . [40] The fact that one fermion doublet forms one generation originates in the $SU(2)$ gauge symmetry of the electroweak interaction.

	Leptons			Quarks		
	Particle	Q (e)	Mass (GeV)	Particle	Q (e)	Mass (GeV)
1st generation	electron e^-	-1	0.0005	down d	$-1/3$	0.003
	neutrino ν_e	0	$< 10^{-9}$	up u	$+2/3$	0.005
2nd generation	muon μ^-	-1	0.106	strange s	$-1/3$	0.1
	neutrino ν_μ	0	$< 10^{-9}$	charm c	$+2/3$	1.3
3rd generation	tau τ^-	-1	1.78	bottom b	$-1/3$	4.5
	neutrino ν_τ	0	$< 10^{-9}$	top t	$+2/3$	174

Table 2.1.: Particles of the Standard Model [81].

2.2. Interactions of the Standard Model

The fermions interact with each other through four fundamental forces: gravity, electromagnetism, the strong and the weak force. The first is not yet included in the Standard Model description due to its negligible strength compared to the other three forces at the currently achievable energy scale. This leads to the many free parameters that can only be determined through experiments and the large difference between electroweak and grand unification scales. The SM could be considered an effective theory only valid at energies far below the Planck scale. An overview of the forces can be found in Tab(2.2).

Force	Boson	Spin	Mass (GeV)
Strong	8 Gluons g	1	0
Electromagnetic	Photon γ	1	0
Weak	W Bosons W^\pm	1	80.4
	Z Boson Z^0	1	91.2

Table 2.2.: Interactions of the Standard Model.

Each force is described by a Quantum Field Theory (QFT) corresponding to the exchange of gauge bosons, spin-1 force-carrying particles. In these QFTs, particles are described as fields that are solutions of the Euler-Lagrange equations. The Euler-Lagrange equation contains terms for the free particle fields as well as the interactions (vertex factors): $\mathcal{L} = \mathcal{L}_{\text{free}} + \mathcal{L}_{\text{interaction}}$. The forces' nature therefore is determined by the properties of the gauge bosons and the way in which they couple to the spin-half fermions. The dynamics of each of the 12 fundamental fermions are described by spinors ψ . Their interaction with the field is given by the Dirac equation of relativistic quantum mechanics, which is equivalent to the Lagrangian

$$\mathcal{L}_{\text{Dirac}} = \bar{\psi}(x)(i\gamma^\mu \partial_\mu - m)\psi(x).$$

The so-called gamma matrices γ^μ are given by the following, where σ^i denotes the Pauli matrices:

$$\gamma^0 = \begin{pmatrix} \mathbf{1} & 0 \\ 0 & -\mathbf{1} \end{pmatrix}, \gamma^i = \begin{pmatrix} 0 & \sigma^i \\ -\sigma^i & 0 \end{pmatrix}.$$

The Lagrange density has to be renormalisable and invariant under local gauge transformations. Its solutions satisfy the proper relativistic dispersion relation.

A particle couples to a force-carrying boson only if it carries the charge of the interaction. The coupling strength of the gauge bosons to the fermions is described by an associated coupling constant g for each type of interaction. Often α is used, representing a more convenient associated dimensionless constant with $\alpha \propto g^2$. A factor of the coupling constant for each interaction vertex is included in the quantum-mechanical transition matrix element \mathcal{M} for an interaction process. The Feynman rules can be deduced from the Lagrange equations and allow to calculate the transition probabilities between two quantum mechanical states using Fermis Golden Rule. They are proportional to the matrix element squared $|\mathcal{M}|^2$.

2.2.1. Electroweak Unification and The Flavour Changing Weak Interaction

The unification of the electromagnetic and the weak force was formulated by Glashow, Weinberg and Salam (GWS) [85]. The electroweak theory is represented by the gauge group $SU(2)_L \times U(1)_Y$, where L refers to left-handedness as the charged weak interaction only couples to fermions of left-handed chirality, and Y is the hypercharge. Y is related to the isospin I and the electric charge Q by the Gell-Mann-Nishijima equation: $Q = I_3 + Y/2$.

The group has four generators that lead to four massless fields that do not directly correspond to observable particles: $W_1^\mu, W_2^\mu, W_3^\mu$ generated by the weak isospin and B_μ^0 generated by the hypercharge. These massless bosons mix to form the physical particles resulting in the following relation for the neutral currents:

$$\begin{pmatrix} Z^0 \\ \gamma \end{pmatrix} = \begin{pmatrix} \cos \theta_W & \sin \theta_W \\ -\sin \theta_W & \cos \theta_W \end{pmatrix} \begin{pmatrix} B^0 \\ W_3^\mu \end{pmatrix}$$

with θ_W being the weak mixing angle (Weinberg angle). This angle can be expressed using g and g' , the coupling constants of the $SU(2)$ and $U(1)$ gauge groups, respectively,

$$\cos \theta_W = \frac{g}{\sqrt{g^2 + g'^2}} = \frac{M_W}{M_Z}.$$

The W^\pm bosons of the charged-current interactions are similarly treated by mixing the $W_{1,2}$ fields:

$$W^\pm = \frac{1}{\sqrt{2}}(W_1^\mu \mp iW_2^\mu).$$

All 12 fermions of the Standard Model are participating in the weak interaction. The charged W^\pm bosons consequently couple together fermions differing by one unit of electric charge. This charged-current weak interaction is the only known force to introduce a change of quark and lepton flavour, and is therefore particularly important when considering particle decays. The weak neutral-current interaction is mediated by the electrically neutral Z^0 boson. It has been shown that here flavour changing neutral-currents are forbidden in the lowest order.

In the above sketched electroweak theory, the original fields are massless; massive gauge bosons would lead to violation of local gauge invariance. This is in contradiction to measurements of the actually observed gauge bosons with exception of the photon and gluon. The W^\pm and Z^0 bosons are in fact very massive objects: $M_W \approx 80$ GeV and $M_Z \approx 91$ GeV.

The Higgs Mechanism

In the Standard Model, the explicit addition of vector boson and fermion masses to the Lagrangian leads to a breakdown of the local $SU(2)_L \times U(1)_Y$ gauge invariance. The Higgs mechanism solves this issue assuming that the symmetry is broken spontaneously.

A scalar field that couples to the fermions and gauge bosons is added. Interaction with the symmetry breaking vacuum allows the W and Z bosons as well as all the matter fields to acquire masses. The theory was formulated by Brout & Englert and Guralnik, Hagen & Kibble and Higgs [33, 39, 42, 41] and introduces the Higgs field as a doublet of complex scalar fields with four real components:

$$\phi = \frac{1}{\sqrt{2}} \begin{pmatrix} \phi_+ \\ \phi_0 \end{pmatrix} = \frac{1}{\sqrt{2}} \begin{pmatrix} \phi_1 + i\phi_2 \\ \phi_3 + i\phi_4 \end{pmatrix}.$$

The Higgs field Lagrangian's corresponding potential is represented as

$$V(\phi) = \mu^2(\phi^\dagger\phi) + \lambda(\phi^\dagger\phi)^2$$

where λ needs to be > 0 in order for a stable minimum to exist. Choosing $\mu^2 < 0$, the potential shows a non-zero vacuum expectation value v with $v = -\mu^2/\lambda$ and resembles the famous "mexican hat" shape, with many possible ground states. This leads to the so-called *spontaneous symmetry breaking* of the electroweak theory.

Expanding the field ϕ in the new minimum leads to an excitation of the Higgs field in form of a new massive scalar, the Higgs boson, with a mass of $m_H = \sqrt{2\mu}$. It is the interaction of the initially massless particles with this non-zero Higgs field that gives them their masses: The new Lagrangian contains terms that assign mass to the W^\pm and Z^0 bosons, while the Yukawa coupling λ_f to the Higgs field generates the fermion masses

$$M_W = \frac{1}{2}v\sqrt{g^2 + g'^2} \quad \text{and} \quad M_Z = \frac{1}{2}v \quad \text{and} \quad M_f = \frac{1}{\sqrt{2}}\lambda_f v.$$

The fermion flavour difference as well as the heavy quark masses are thought to be due to Yukawa coupling with the Higgs boson. The light quarks' effective masses are mainly coming from dynamical effects caused by being surrounded by sea quarks, i.e. due to chiral symmetry breaking.

After non-significant "observations" of a Higgs boson with a mass around 115 GeV at LEP, and measurements from Tevatron neither confirming nor discarding these hints [3, 68], a new particle consistent with the Standard Model Higgs boson was finally reported with a significance of 7σ in July 2012 by the ATLAS and CMS experiments at CERN's LHC [71, 78, 69]. The Higgs boson decays predominantly into a $b\bar{b}$ or a $WW^* \rightarrow \ell\nu\ell\nu$ pair, searches have also been performed in the $\tau^+\tau^-$ channel.

A very clean signal, offering the best mass resolution, is provided by the decays $H \rightarrow ZZ^* \rightarrow 4\ell$ and $H \rightarrow \gamma\gamma$, even though they have relatively small branching ratios. The Higgs mass is measured in these channels by both ATLAS and CMS resulting in a combined mass: $m_H = 125.36$ GeV based on data collected at 7 and 8 TeV with an integrated luminosity of 25 fb^{-1} [72].

Further studies show the Higgs boson not being a spin-1 particle due to its decay to two photons [50, 86] but rather, having positive parity, favouring spin-0 [70].

CP Violation and the CKM Matrix

To explain the observed matter-antimatter asymmetry in the Universe, Sakharov [61] originally formulated three conditions of which one was the possibility of CP violation in the weak interactions of quarks and leptons. And indeed, contrary to its conservation in QED and QCD, parity and charge-conjugation are maximally violated in the weak interaction. It was found that the weak interaction acts only on left-handed particles and right-handed antiparticles in the weak charged current which is formulated as a $V - A$ interaction, where V and A are vector and axial vector couplings, respectively. CP violation, the combination of charge conjugation and parity is not kept under some exceptional conditions, which was confirmed experimentally in the decay of neutral K mesons in 1964 [29]. It has to date been observed in the quark sector only.

The coupling strength of the weak interaction for quarks can be determined from the study of nuclear β -decays and was found to differ at certain quark weak interaction vertices. The effective coupling for a particular quark-quark transition can be expressed as the product of the universal weak coupling and a factor for mixing between the mass and the weak eigenstates. The weak interactions of quarks are described in terms of the unitary Cabibbo-Kobayashi-Maskawa (CKM) matrix [25, 48]. The weak eigenstates are related to the mass eigenstates by

$$\begin{pmatrix} d' \\ s' \\ b' \end{pmatrix} = \begin{pmatrix} V_{ud} & V_{us} & V_{ub} \\ V_{cd} & V_{cs} & V_{cb} \\ V_{td} & V_{ts} & V_{tb} \end{pmatrix} \begin{pmatrix} d \\ s \\ b \end{pmatrix}.$$

The absolute value of the matrix elements of this unitary matrix were determined experimentally:

$$\begin{pmatrix} |V_{ud}| & |V_{us}| & |V_{ub}| \\ |V_{cd}| & |V_{cs}| & |V_{cb}| \\ |V_{td}| & |V_{ts}| & |V_{tb}| \end{pmatrix} \approx \begin{pmatrix} 0.974 & 0.225 & 0.004 \\ 0.225 & 0.973 & 0.041 \\ 0.009 & 0.040 & 0.999 \end{pmatrix}.$$

The diagonal entries have been found to be close to one while the off-diagonal elements are rather small which implies that the rotation angles between the quark mass and weak eigenstates are relatively small. Consequently, the weak interactions between quarks of different generations are suppressed the most for the couplings between first and third generation quarks, ub and td .

Among several possible conventions of the CKM matrix, we often use the Wolfenstein parametrisation, where the matrix is conveniently expressed as an expansion in the small parameter $\lambda = \sin \theta_c = 0.225$ written in terms of four real parameters:

$$\begin{pmatrix} V_{ud} & V_{us} & V_{ub} \\ V_{cd} & V_{cs} & V_{cb} \\ V_{td} & V_{ts} & V_{tb} \end{pmatrix} = \begin{pmatrix} 1 - \lambda^2/2 & \lambda & A\lambda^3(\rho - i\eta) \\ -\lambda & 1 - \lambda^2/2 & A\lambda^2 \\ A\lambda^3(1 - \rho - i\eta) & -A\lambda^2 & 1 \end{pmatrix} + \mathcal{O}(\lambda^4).$$

In order to let CP violation occur in the quark sector, the matrix needs to contain an irreducible complex phase corresponding to $\eta \neq 0$. Such a complex phase can be accommodated in the quark mixing matrix if there are six quark flavours, equivalent to three generations. Now, the large numbers of B and \bar{B} mesons produced at the Belle and BaBar experiments allowed precise measurements of the branching ratios for semi-leptonic decays as well as various CP asymmetries and from that determination of the elements of the CKM matrix and the angles of the unitarity triangle.

2.2.2. The Strong Interaction and Hadronisation

The gauge group of the strong interaction is the non-abelian $SU(3)_C$ group with the eight generators being the force mediating massless gluons. The dynamics of quarks and gluons are described by the gauge invariant Quantum Chromodynamic (QCD) Lagrangian. QCD's equivalent of electric charge is known as colour, an additional quantum number of the quarks, that takes three conserved values *red*, *green* and *blue*. It has been introduced to avoid a violation of the Pauli principle which was encountered with the observation of the Δ^{++} resonance consisting of three up-quarks with parallel spin. If the quarks can be distinguished by colour, the Pauli-principle remains valid. Only particles that have non-zero colour charge, namely quarks and gluons, couple to gluons, which is the reason for leptons not to feel the strong force. As gluons connect quark states of different colour they must carry colour charge themselves in order for colour conservation. Quarks have never been observed directly as free, fractionally charged particles despite an abundance of experimental evidence of their existence. The non-observation is explained by the hypothesis of colour confinement: quarks are always observed to be confined to bound, colourless states. This behaviour is thought to originate from gluon-gluon self-interaction, since the generators of the $SU(3)_C$ group do not commute.

A qualitative understanding of colour confinement, for which there is currently no analytic proof, can be given by looking at two quarks becoming separated. The interaction between the quarks can be described in terms of an exchange of attractively self-interacting virtual gluons. The effect of these interactions is to form a flux tube of interacting gluons of approximately constant energy density and squeeze the colour field between the quarks into this tube. At some point it becomes energetically favourable to create a new quark-antiquark pair, instead of allowing the tube to extend further. Colour confinement therefore places strong restrictions on the structure of possible hadronic states; the allowed combinations of quarks and antiquarks are those where a colourless state can be formed: mesons as a pair of quark and antiquark ($q\bar{q}$), baryons made of three quarks (qqq) and antibaryons formed from three antiquarks ($\bar{q}\bar{q}\bar{q}$). Hadronic states thus correspond to and can be labelled by different combinations of quark flavours and different angular momenta states J^P , where J is the total angular momentum, P the parity eigenvalue. In processes such as $e^+e^- \rightarrow q\bar{q}$, as a consequence of colour confinement, quarks do not propagate freely. This process is known as fragmentation and hadronisation: high-energetic quarks and gluons produce jets of colourless particles, the hadrons, with all quark flavours that are energetically accessible, see Fig(2.1).

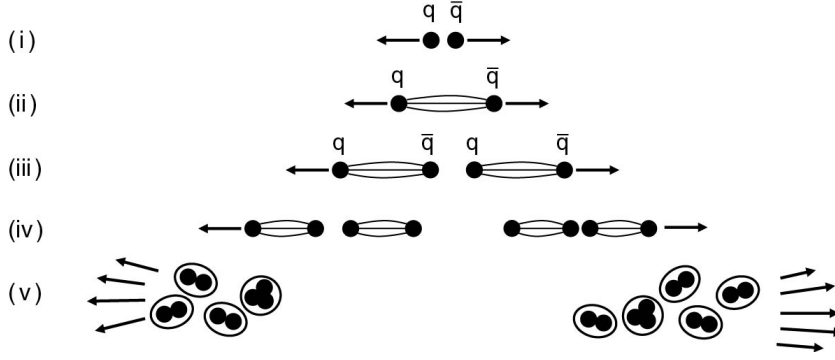


Figure 2.1.: Illustration of hadronisation: A flux tube forms and breaks up into colourless final state particles [81].

At low-energy scales, QCD processes such as the hadronisation process are currently not calculable from first-principles using traditional perturbation theory as the coupling constant of QCD becomes large, $\alpha_S \sim \mathcal{O}(1)$, and therefore the perturbation expansion does not converge rapidly. Here, lattice QCD studies are being carried out as a promising alternative.

On the other hand, the value of α_S depends on the energy scale of the interaction. Consequently at the typical scale for modern high-energy collider experiments, α_S becomes sufficiently small to make the usage of perturbation theory feasible due to the property of QCD being known as asymptotic freedom. Admittedly, unlike QED, higher-order corrections still cannot be neglected. But in this regime the quarks can be treated as quasi-free particles, rather than being strongly bound within hadrons.

It should accordingly be mentioned that hadronic states are often treated as bound states of simplified light valence quarks with constituent masses but are, as discussed above, far more complex, most of the mass of hadrons originating from the energy of the strongly interacting sea of virtual quarks and gluons within the bound state. While current masses of light quarks are just a few MeV, the constituent masses can be thought of as the effective masses of the quarks as they move within and interact with the QCD potential. Whilst this is valid for light quarks, in case of heavy quarks the masses given by the Higgs mechanism and Yukawa coupling would be dominant.

The non-relativistic QCD potential as a function of the distance r between a heavy quark and a heavy antiquark given as

$$V_{q\bar{q}}(r) = -\frac{4}{3} \frac{\alpha_S}{r} + \kappa r$$

can be used to predict a spectrum of $q\bar{q}$ bound states. The linear term becomes dominant at larger radii. It is believed to be responsible and setting the length scale for confinement for heavy quark states.

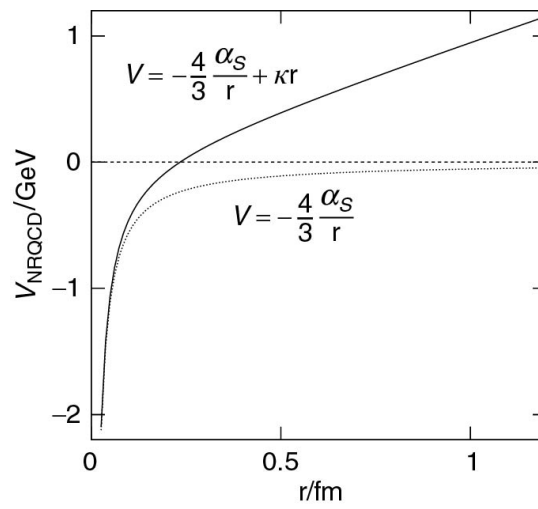


Figure 2.2.: Illustration of the form of the non-relativistic QCD potential for a bound heavy $q\bar{q}$ state, assuming $\alpha_S = 0.2$ and $\kappa = 1$ GeV/fm. [81]

3. Motivation

On the trail of the QCD colour potential, flavorless meson systems of a heavy quark and its own antiquark, so-called *quarkonia* provide a fruitful environment for spectroscopy of their bound states. Quarkonia, as strongly interacting systems, have been studied in an analogous manner to hydrogen atoms or positronium; from the measured spectrum and transition probabilities between the states one can derive the effective potential.

When describing charmonium formation from $c\bar{c}$ pairs that are produced in B decays or in e^+e^- annihilation, effective field theories are used. They are found to work quite well because of the large masses of the heavier charmonium ($c\bar{c}$) and bottomonium ($b\bar{b}$) systems. Those systems can be treated by approximation as non-relativistic because of their velocities being relatively low with $\beta \equiv v/c \sim 0.3$ and $\beta \sim 0.1$, respectively. Large masses are functioning as a natural cut off permitting the use of perturbation theory, most often non-relativistic QCD.

3.1. The Charmonium Spectrum

Charmonium bound states possessing quantum numbers $J^{PC} = 1^{--}$ are observed as resonances in e^+e^- annihilation at centre-of-mass energies between 3 and 4.5 GeV. This series of resonances can be found in a scan by varying the beam energy. They show as enhancements in the total hadronic cross section and charmonia having other quantum numbers are identified in consecutive decay modes. The resultant assignments to the various charmonium states are shown in Fig(3.1). The lowest state with these quantum numbers is the $1S$ ψ , for historical reasons called J/ψ , with a mass of 3097 MeV [13, 12]. Using methods of spectroscopy, particles can be named with their spectroscopic notation or their mass, sometimes excitation series are used: e.g. ψ' being the $\psi(2S)$ state. At centre-of-mass energies of ~ 10 GeV, another group of resonances can be seen, the bound states of the bottomonium system. The $b\bar{b}$ spectrum is very similar to that of $c\bar{c}$ which leads to the important conclusion that the QCD potential is universally applicable for different heavy quark flavours.

In general, heavy quarkonia show the following four kinds of decays:

1. Radiative decays, e.g. $\chi_{c1} \rightarrow J/\psi\gamma$:

The charmonium states have a limited life time and decay mainly through the strong interaction. Excited states can convert via de-excitation by emitting photons. Through electromagnetic transitions, a change in orbital angular momentum or spin, energetically lower states can be reached. An example would be the decay of the first radially excited charmonium state $\psi(2S)$ to the $1P$ triplet system of χ_{cJ} states.

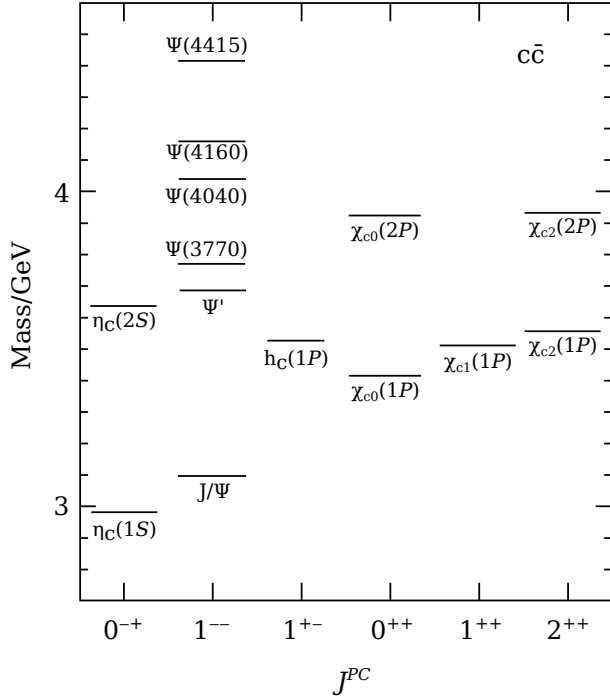


Figure 3.1: Spectrum with masses and J^{PC} of the observed and assigned charmonium bound states; based on [81]

2. Annihilation of the $q\bar{q}$ pair, e.g. $J/\psi \rightarrow \ell^+\ell^-$.
3. Feed down by pion pair emission, e.g. $\psi' \rightarrow J/\psi\pi^+\pi^-$.
4. Addition of light $q\bar{q}$ pairs, e.g. $\psi(3770) \rightarrow D^0\bar{D}^0$:

The light $q\bar{q}$ pairs are taken from vacuum production via formation of light mesons. This decay mechanism can only take place above a certain energy threshold as the light $q\bar{q}$ pair has to be made from the excitation energy of the quarkonium.

Okubo, Zweig and Iizuka formulated the so-called *OZI rule* to describe the suppression mechanism in the case if the Q-value is not sufficient to create a $q\bar{q}$ pair from an open-charm meson pair. Then, the OZI suppressed amplitude of decaying to a lower charmonium state by emitting a pion pair is the allowed strong decay. In the case where an open-charm meson pair cannot be produced, no quark current exists continuing from initial to final state. Such an amplitude cannot be large, and therefore the second decay mechanism is suppressed compared to the third. Thus the charmonia which are below the so-called *open-charm* or $D\bar{D}$ threshold at 3740 MeV that decay only via weak, electromagnetic and strong but OZI-suppressed processes have narrow decay widths, e.g. $\Gamma = 0.088$ MeV in case of J/ψ .

On the other hand, above that threshold, strong decays to a D meson pair predominantly take place as it is in general the simplest strong decay. Due to these available new decay possibilities, states decay faster which results in wide decay widths. $\psi(3770)$ is the first state above threshold and has a 93% probability to decay to $D\bar{D}$, as expected [58]. Looking at the more strongly bound bottomonium the decay to b quarks and mesons does not take place till the third excitation, $\Upsilon(4S)$ at 10.58 GeV, which is the first one to decay to $B\bar{B}$ among the $J^{PC} = 1^{--}$ bottomonium states.

3.1.1. The As Yet Unseen $\chi_{c1}(2P)$ - A Conventional Charmonium

The $\chi_{c1}(1P)$ is the lightest axial vector meson containing a $c\bar{c}$ pair with a mass of 3510 MeV. Its radial excitation with spectroscopic notation 2^3P_1 , the $\chi_{c1}(2P)$ (or χ'_{c1}), is predicted but still undiscovered. Its quantum numbers are $J^{PC} = 1^{++}$ and it is part of a spin triplet.

The mass prediction for the $\chi_{c1}(2P)$ lies above the open-charm threshold and is expected around 3920 MeV [84]. In this energy region Belle has reported the observation of two resonant structures denoted by $Y(3940)$ and $Z(3930)$ [28, 27]. The temporarily dubbed $Z(3930)$ was observed as an enhancement in the $D\bar{D}$ mass spectrum from $e^+e^- \rightarrow e^+e^-D\bar{D}$ events where $\gamma\gamma \rightarrow D\bar{D}$ takes place and is now interpreted as the $\chi_{c2}(2P)$ [83]. Since 2014, the $Y(3940)$ has been identified as the same state as $X(3915)$ and is recognized as the $\chi_{c0}(2P)$ [58]. Looking at the total decay widths of these two states, $\Gamma_{\text{tot}}(\chi_{c0}(2P)) = (20 \pm 5)$ MeV and $\Gamma_{\text{tot}}(\chi_{c2}(2P)) = (24 \pm 6)$ MeV, it comes at a natural choice to assume a width of approximately 20 MeV for $\chi_{c1}(2P)$. In the beginning of this study the comparison with the well known $\psi' \rightarrow J/\psi\pi^+\pi^-$ as one of the major decay modes led to the speculation that $\chi_{c1}(2P)$ has a significant branching fraction to a $\chi_{c1}(1P)\pi^+\pi^-$ final state. Based on the assumption that $\mathcal{B}(\chi_{c1}(2P) \rightarrow \chi_{c1}\pi^+\pi^-) \approx \mathcal{B}(\psi(2S) \rightarrow J\psi\pi^+\pi^-)$, ignoring quantum number differences, $\chi_{c1}(2P)$ was thought to be a narrow resonance.

It is noteworthy that decays predicted as major decay modes, $\chi_{c1}(2P) \rightarrow J/\psi\gamma$ and $\chi_{c1}(2P) \rightarrow \psi(2S)\gamma$, have not been observed nor has a peak been seen in the $D^0\bar{D}^{*0}$ spectrum at 3920 MeV. This leaves the $\chi_{c1}(2P) \rightarrow \chi_{c1}\pi^+\pi^-$ as the almost only remaining decay mode to search for $\chi_{c1}(2P)$. The decay $\chi_{c1}(2P) \rightarrow D\bar{D}$ is forbidden by parity conservation, while the $\chi_{c1}(2P)$ could decay into $D\bar{D}^*$, if energetically allowed. The absence of radiative decays and no decay to a charmed meson pair give a hint that the $\chi_{c1}(2P)$ might be another special case and deviate from the conventional charmonium spectrum. This will become important when looking at possible interpretations of the $X(3872)$ state later in this chapter.

This thesis, studying the $B^\pm \rightarrow \chi_{c1}\pi^+\pi^-K^\pm$ final state, is motivated by a search for the yet unseen intermediate state of $\chi_{c1}(2P)$ in the invariant mass distribution of $\chi_{c1}(1P)\pi^+\pi^-$.

3.2. Exotic Charmonium(-like) States

So far, all of the predicted $c\bar{c}$ states below the $D\bar{D}$ threshold at 3740 MeV have been observed and measured with high precision. They were found to have properties that are well described by the charmonium model. In addition, all the $J^{PC} = 1^{--}$ states with a mass $> 2m_D$ were identified. But there are still predicted but unconfirmed states above the open-charm threshold.

Charmonium is the best understood hadronic system and is much cleaner with regard to the dense spectrum of light states where mixing of neutral mesons plays an important role because of the $SU(3)$ flavour symmetry. So-called *exotic states* containing $c\bar{c}$ are expected to be identified easier than the ones predicted in the light spectrum of hadrons comprised of light quarks (u, d, s)

Strong evidence for meson-like states that do not fit into the simple $q\bar{q}$ scheme has been steadily accumulating during the past decade. Especially above the open-charm threshold, several charmonium-like states with unusual characteristics have been reported [59].

These so-called XYZ states are charmonium-like and bottomonium-like hadrons that do not fit into any of the remaining predicted but still undiscovered states in the $c\bar{c}$ and $b\bar{b}$ spectra as shown in Fig(3.2). X , Y and Z are temporary names usually followed by their mass, indicating that there are still open questions about these particles' properties and their place in the spectra.

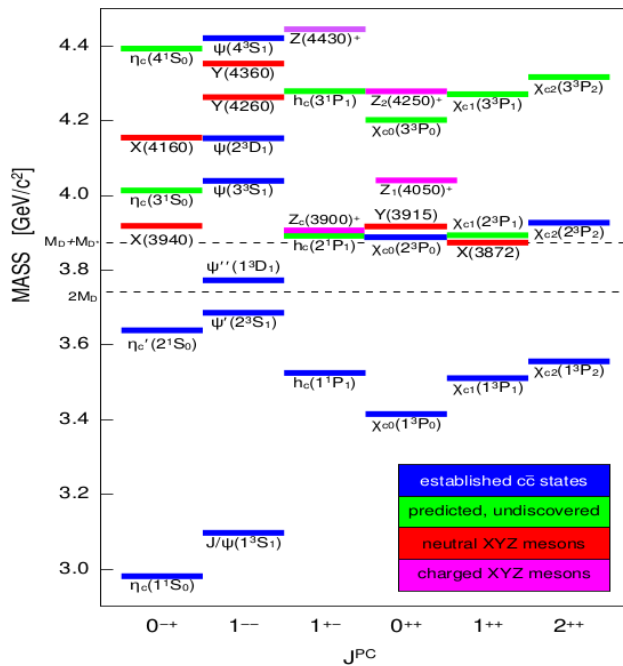


Figure 3.2: Spectrum with masses and J^{PC} of established, predicted but undiscovered, and XYZ states; based on [59].

To identify exotic states, further studies of the quarkonium model that specifies the allowed states of a $q\bar{q}$ system are necessary; if a quarkonium-like hadron decays into a final state with properties that do not match the expected ones of any of the unfilled levels in the associated quarkonium spectrum, it is consequently called exotic. Some indications for an exotic hadron candidate are a large branching fraction to anything but $D\bar{D}$, an unusually narrow decay width or a decay mode that cannot be explained as a charmonium state. Since the c and b quarks are heavy, their production from the vacuum in the fragmentation process is heavily suppressed. Thus, heavy quarks that are seen among the decay products of a hadron must have existed among its original constituents.

QCD-motivated models predict the existence of hadrons of more complex structure than conventional mesons or baryons. Even though, up-to-date experimental searches have passed without conclusive evidence for specifically QCD-motivated exotic hadrons, all confirmed hadrons seem to be either mesons or baryons. Information on the many discovered exotic charmonium-like states is rather limited. There are four main interpretations to explain the observed exotic states such as hybrids and multi-quark states or molecular configurations.

Multiquarks: Tetra- and Pentaquarks

There are two types of multiquark states for which there is no explicit suppression rule in QCD. Originally, the idea of a tetraquark was introduced to explain the properties of light scalar mesons like some of the f_0 and a_0 states as they seemed to lie outside the existing quark model classifications [46]. A *tetraquark* is an exotic meson, a tightly bound four-quark state, that is suggested as a diquark-diantiquark structure in which the quarks interact dominantly by a gluon exchange. Strong decay modes are expected to proceed via rearrangement processes, followed by disassociation. The $c\bar{c}$ states that might be classified as tetraquarks could be easily distinguished from conventional charmonium states as they could have non-zero charge or contain strangeness, for example the $Z(4430)^-$ with a quark content of $(c\bar{c}d\bar{u})$ [24, 80].

A *pentaquark* on the other hand consists of three quarks and one quark-antiquark pair bound together, thus being classified as an exotic baryon. Unfortunately, all pentaquark candidates so-far have been found by high-statistics experiments to be statistical effects rather than true resonances. Despite these null results, as of 2009 LEP results continue to show the existence of a narrow state with a mass of (1524 ± 4) MeV, with a statistical significance of 5.1σ [56] which is considered a pentaquark candidate.

So in principle, combinations such as tetraquark $(q\bar{q}q\bar{q})$ or pentaquark states $(qqq\bar{q}\bar{q})$ could exist, either as bound states in their own right or as hadronic molecules such as $(q\bar{q})-(qqq)$ or $(q\bar{q})-(q\bar{q})$.

Di-Meson Molecular States

In analogy to the formation of deuterons from a proton and a neutron, it is also believed that mesons can as well interact to form molecules. Such a *mesonic molecule* would be a set of two (or more) mesons bound together by the strong force. The interaction within the molecule is thought to be due to the asymptotic and therefore distance-dependent nature of the quark potential: the confined one-gluon exchange interaction among the quarks should dominate at short distances, an interaction via pion exchange at large. A consequence of their loose binding is that they tend to decay as if being free mesons. However, molecular states should result in distinctive decay patterns which would distinguish them from tetraquarks. The difference could possibly be determined from their deviating degrees of freedom and size. Right now, $Z_b(10610)$ and $Z_b(10650)$ seem to be the best candidates for such an observation [76].

The other two approaches to explain exotic states are of a different nature.

Quark-Gluon Hybrids and Glueballs

States with an excited gluon in addition to the quarkonium are referred to as *hybrid mesons*, and are described by many different models, among them the flux-tube model [44]. The lowest excitations of the potential produced by gluons lead to the lowest mass hybrids; of which some show exotic quantum numbers like $J^{PC} = 0^{+-}, 1^{-+}$ or 2^{+-} . Those are not allowed per se in case of conventional charmonium states and their observation would indicate the existence of an exotic resonance.

The lowest charmonium hybrids are predicted by lattice QCD to have masses of about 4200 MeV [53], whereas their dominant decays are expected to be open-charm decays including P -wave mesons in their final states, and hadronic transition to charmonium via emission of light hadrons. In addition, it seems that gluons, the self-interacting mediator particles of the strong interaction, could also form bound states by themselves, so-called *glueballs* [55].

Threshold Effects

Being close to the open-charm threshold can also give rise to structures in cross sections and kinematic distributions. There is in fact a variety of thresholds, depending on the different types of D mesons, e.g. $m_{D^0 D^{*0}} = 3872$ MeV or $m_{D^+ D^-} = 3740$ MeV. S-wave scattering dominates the cross section at the threshold, however in a few cases higher order waves also play a role. Considering that states in a relative S-wave with low relative momentum can live long enough on the timescale of the strong interaction to interact by exchanging pions, a formation of mesonic molecules due to this attractive interaction is thinkable; while any repulsive interaction might suggest a virtual state above threshold [32]. Thus, there can be a structure in the cross section near the kinematical threshold which may or may not be an ordinary, real resonance. In addition, the effect coming from $c\bar{c}$ states near a threshold that can interact with the latter and might result in a mass shift of both, the charmonium resonance and the threshold-related enhancement, could be quite significant in the observed cross section.

3.2.1. The Puzzling $X(3872)$ - An Exotic Charmonium

In the last decade a number of exciting discoveries of new hadron states has challenged our description of hadron spectroscopy. The first and, since its discovery in 2003 by the Belle collaboration, most studied exotic hidden-charm state's existence is the well established, but still mysterious $X(3872)$, see Fig(3.3) [26]. The $X(3872)$ was initially observed as a narrow peak in the $J/\psi\pi^+\pi^-$ invariant mass distribution in the charged B meson decay $B^+ \rightarrow J/\psi\pi^+\pi^-K^+$, and due to the decay to a J/ψ naturally identified as a new charmonium state. Its existence, in inclusive $p\bar{p}$ production, too, was soon confirmed by several other experiments [10, 6, 2]. It is also the only exotic charmonium-like state that has been observed in several decay modes.

The $X(3872)$'s mass is (3871.2 ± 0.5) MeV in the current world average [58] which is very close to the open-charm threshold of $D^0\bar{D}^{*0}$ at (3871.8 ± 0.12) MeV and does not match with any predicted $c\bar{c}$ state. Its exotic nature was in fact first signalled by its unusually narrow width of only $\Gamma < 1.2$ MeV in the best current estimate [58]. This is puzzling as broad structures are expected above threshold which allows the strong decay to a charmed meson pair.

The first step in order to identify the structure of such a state is the determination of its quantum numbers such as total angular momentum J , charge conjugation C and parity P . By now, all early questions concerning quantum numbers and the existence of any charged or neutral partner states have been resolved:

The Belle and Babar collaborations observed the radiative decay $X(3872) \rightarrow J/\psi\gamma$ which determines the C -parity to be positive, $C = +1$ [4, 15]. Two recent searches for a C -odd partner state of $X(3872)$ in the $J/\psi\eta$ and the $\chi_{c1,2}\gamma$ final states were pursued [67, 57]. However, the production of such a partner in two-body B decays and its decay to either $J/\psi\eta$ or $\chi_{c1,2}\gamma$ are found to be considerably suppressed [45, 19].

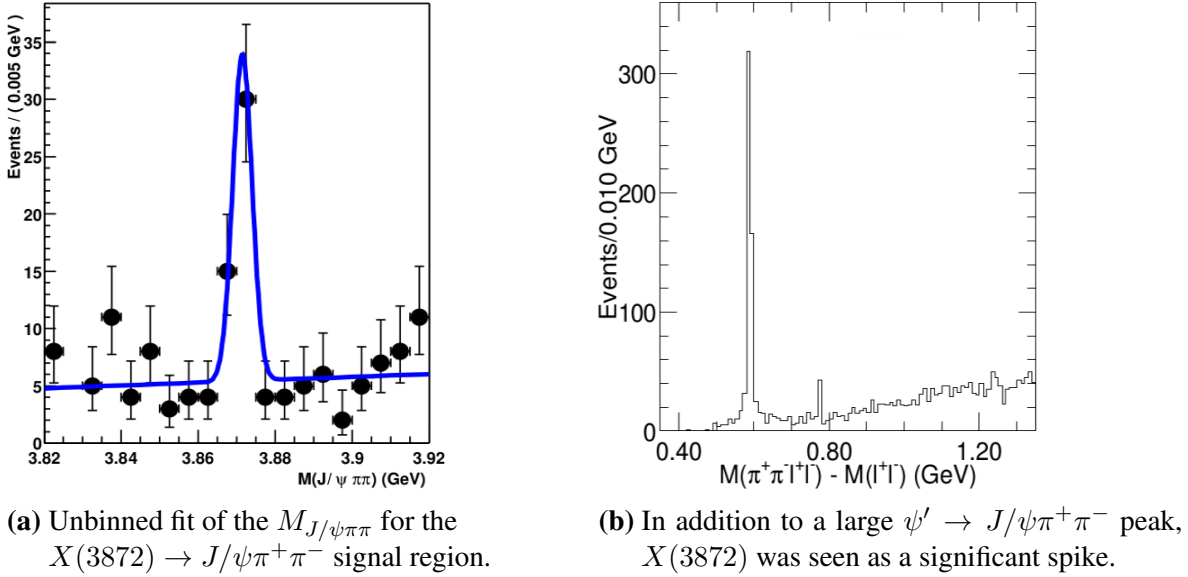


Figure 3.3.: First observation of a narrow charmonium-like state with a mass of $(3872 \pm 0.6 \pm 0.5)$ MeV and a statistical significance in excess of 10σ [26].

The decay angular distributions from $X(3872) \rightarrow J/\psi\pi^+\pi^-$ and the 3π invariant mass spectrum in $J/\psi\pi^+\pi^-\pi^0$ studied as well as the associated pions' invariant mass distributions agree well with expectations for a 1^{++} assignment as proposed by Belle [74], CDF [77] and BaBar [73]. This result has been confirmed and established by the LHCb collaboration in 2013 as can be seen in Fig(3.4).

Currently, $X(3872)$ is only observed in B meson decays and hadron collisions. But ever since there has been conclusive evidence for this now well established state, many hypotheses about its nature have been proposed, especially attempts to treat it as a multiquark state.

The $X(3872)$ has been proposed to be the still undiscovered conventional charmonium state $\chi_{c1}(2P)$ as they are sharing the same quantum numbers of 1^{++} and it displays some characteristics of a charmonium-like state. It is however an unlikely assignment disfavoured by the value of the $X(3872)$ mass leading to a mass difference of ~ 50 MeV [84, 74]. Detailed angular analyses also showed that the decay to $J/\psi\rho^0$ is the dominant one, leading to the conclusion of isospin violation if $X(3872)$ were a conventional charmonium. What was seen in experiments, is that the di-pion mass distribution in $X(3872) \rightarrow J/\psi\pi^+\pi^-$ is consistent with originating from a ρ^0 resonance, while there has been evidence that the tri-pion mass distribution in $X(3872) \rightarrow J/\psi\pi^+\pi^-\pi^0$ favours the decay via a virtual ω resonance.

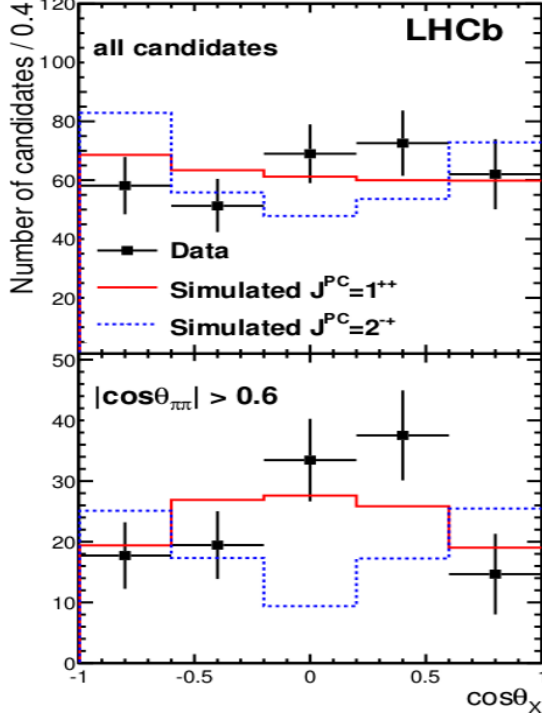


Figure 3.4: Background-subtracted distribution of $\cos \theta_X$ for (top) all candidates and for (bottom) candidates with $|\cos \theta_{\pi\pi}| > 0.6$ for the data (points with error bars) compared to the expected distributions for the $J^{PC} = 1^{++}$ (red solid histogram) and $J^{PC} = 2^{-+}$ hypotheses (blue dashed histogram) at LHCb experiment [1].

The ratio was found to be

$$\frac{\mathcal{B}(X(3872) \rightarrow J/\psi\omega)}{\mathcal{B}(X(3872) \rightarrow J/\psi\rho)} = 1.0 \pm 0.4 \pm 0.3.$$

The sizes of the branching fractions are comparable to each other which makes it necessary to clarify the mechanism to cause such a large isospin violation of the $X(3872)$ [74]. This evidence for isospin breaking contradicts the assignment as $\chi_{c1}(2P)$ is part of an isospin singlet and can therefore not be matched with the isosinglet $X(3872)$.

Isospin violation can also be shown by isospin partners with differing masses, as well as different electric charge: Partner states have been predicted for the $X(3872)$ as a compact four-quark state as it was originally theorised as a tetraquark candidate. This explanation predicts that a neutral doublet should exist corresponding to $[cu][\bar{c}\bar{u}]$ and $[cd][\bar{c}\bar{d}]$. The former would be identified with the $X(3872)$ and produced in the known charged $B^+ \rightarrow J/\psi\pi^+\pi^-K^+$ decay, whereas the additional neutral state should be observed in neutral $B^0 \rightarrow J/\psi\pi^+\pi^-K^0$ decays having a mass differing by a few MeV from the $X(3872)$. However, recent studies have not revealed any significant separation between the masses of the X states produced in charged versus neutral B decays [54, 31, 75]. The ratio of the branching fractions

$$\frac{\mathcal{B}(B^+ \rightarrow X(3872)K^+)}{\mathcal{B}(B^0 \rightarrow X(3872)K^0)} \sim 10\%$$

is predicted, but the experimental value is found to be $0.5 \pm 0.3 \pm 0.05$ [22, 11] speaking in favour of the decay of a single $X(3872)$ state. Also, no evidence for a charged partner of the $X(3872)$ predicted by the tetraquark models in the $J/\psi\pi^+\pi^0$ mode has been seen strongly suggesting isospin zero [9].

As $X(3872)$ shows to be a 1^{++} state and its mass being near the $D^0\bar{D}^{*0}$ mass threshold, it appears as a good candidate for a molecule-like $D^0\bar{D}^{*0}$ bound state [64]. With $L = 0$ it would be a deuteron-like state bound by pion exchange. Supporting this interpretation, the branching fraction of $X(3872) \rightarrow D^0\bar{D}^{*0}$ has been measured to be one order of magnitude larger than that of $X(3872) \rightarrow J/\psi\pi^+\pi^-$ [58, 14].

As the indications for a molecular state keep on accumulating, QCD Sum Rule calculations reported a better agreement with the experimental mass of $X(3872)$ when using a current for the mesonic molecule of the type $(D^{*0}\bar{D}^0 - D^0\bar{D}^{*0})$ than for tetraquark calculations [52].

However, an issue appears when looking at the difference in mass between the $X(3872)$ and the $D^0\bar{D}^{*0}$ threshold which corresponds to the available binding energy in a potential molecule: The $D^0\bar{D}^{*0}$ threshold is at (3871 ± 0.27) MeV, leaving only (0.16 ± 0.31) MeV for an exceptionally weak binding. The binding energy can be translated to the distance between the two D mesons assuming a Yukawa-like potential with pion exchange, resulting in 5 fm in case of $X(3872)$ [23]. Compared to the J/ψ meson's size of about 0.4 fm, the difference in volume is so large that the probability for a c and \bar{c} quark to form a J/ψ and therefore the significant branching to the latter cannot be explained. At last, such a very loosely bound object could hardly be produced in high energy proton-antiproton collisions like they've been observed at Tevatron, making it difficult to explain the $X(3872)$'s production cross section measured by the CDF experiment.

These (pure) molecule interpretations meet some more issues when looking at radiative decays like the heavily suppressed decay to $\psi(2S)\gamma$ which is crucial for understanding the structure of $X(3872)$. BaBar and LHCb found a signal while the Belle experiment did not [15, 20]. This controversial result is reflected in the ratio of the branching fractions

$$\frac{\mathcal{B}(X \rightarrow \psi(2S)\gamma)}{\mathcal{B}(X \rightarrow J/\psi\gamma)} = 2.46 \pm 0.64 \pm 0.29.$$

However, this ratio is predicted to be of order $\times 10^{-3}$ for a $D\bar{D}^*$ molecule [30]. This leads to the conclusion that the relatively large branching fraction for $X(3872) \rightarrow \psi(2S)\gamma$ is generally inconsistent with a pure $\bar{D}^0 D^{*0}$ molecular interpretation of the $X(3872)$, and possibly indicates mixing with a significant $c\bar{c}$ component. [79, 63, 15]

Also in QCD Sum Rules calculations it is possible to explain the properties of the $X(3872)$ assuming it is a mixture between a $c\bar{c}$ state and the $D^0\bar{D}^{*0}$, $D^{*0}\bar{D}^0$, D^+D^{*-} and D^-D^{*+} molecular states [52]. The so-called *coupled channel* approach shows that the $X(3872)$ emerges in a constituent quark model calculation as a mixed state of a DD^* molecule and $\chi_{c1}(2P)$ state. This dual structure may explain simultaneously the isospin violation shown by the experimental data and the radiative decay rates [60].

So, an admixture state of a $D^0\bar{D}^{*0}$ molecule and a conventional charmonium, possibly the still undiscovered $\chi_{c1}(2P)$, seems to be the most plausible hypothesis at the moment [66]. The possibility to find such an intermediate state in multi-body B decays as $B \rightarrow \chi_{c1}\pi^+\pi^-K$ is provided by the so-called B factories and the aim of this thesis.

3.3. B Meson Decays as a Source for Charmonium

In the last decade, both an experimental and a theoretical revival in charmonium physics due to the B factories were seen. In general, e^+e^- colliders are an excellent place to study the heavy quark spectra due to their well-defined production of quarks: the QED process is well-understood, there is no need to know the initial parton structure functions as e^\pm are pointlike particles and the production process is experimentally very clean as there are no remnants as in proton-(anti)proton colliders. Although the B factories were primarily constructed to study the CP -violation in the B meson system and quarkonium studies were not a priority at the start of the running, these facilities have come to function as heavy meson factories collecting large enriched charm samples on spectra and decays. The discovery of a large number of new charmonium-like meson states as described in the previous section became an unexpected bonus. The B factories also provide useful information on charmonium production rates in different processes, as well as kinematic characteristics of produced charmonia, with which models can be tested numerically and charmonium properties be determined. Charmonium states can be produced in numerous production mechanisms:

The simplest B **meson decays** yielding charmonium states are $B \rightarrow KX_{c\bar{c}}$. In two-body B decays the two decay daughters are so quickly getting apart due to the B mesons large mass of 5.28 GeV that very little final state interaction takes place. In such a situation, the decay amplitude can be formulated as the product of two currents into corresponding final state particles. This mechanism is called factorisation. These $B \rightarrow KX_{c\bar{c}}$ decays are described by the Cabibbo-favoured $b \rightarrow c\bar{c}s$ transition, and thus have large branching fractions, $O(10^{-3})$, assuring a high statistics sample. Decays of this type favour production of charmonia bearing $J^{PC} = 0^{-+}, 1^{--}$ and 1^{++} , while known quantum numbers of the parent B meson allow the determination of the spin-parity of the produced $X_{c\bar{c}}$ by performing angular analyses. B mesons can decay into almost all possible charmonium states, with typical inclusive branching fractions $\sim 1\%$, although some states are dynamically suppressed. The first example of charmonium production in B decays was the decay $B \rightarrow J/\psi X$. Two-body decays of the type $B \rightarrow (c\bar{c})K^{(*)}$ have been extensively studied, because of their extremely clean experimental environment and their importance for CP -violation measurements. But even the study of multiple-body decays, like this thesis' target final state $\chi_{c1}\pi^+\pi^-$, is made feasible and benefits from the B factories' environment. There is no additional particle production in $B\bar{B}$ events, thus controlling combinatorial background is manageable.

In resonant direct production in e^+e^- annihilation with **Initial State Radiation** the initial e^\pm radiates one or more photons lowering the centre-of-mass energy accordingly. If the energy of the emitted γ is large enough the charmonium mass range can be reached, allowing the production of charmonia with spin-parity $J^{PC} = 1^{--}$. Being a higher-order QED process suppressed by α_{em} is compensated by very high luminosities. In the special case of both leptons emitting photons that interact, **two-photon collisions** ($\gamma\gamma$ fusion) can give access to states with different quantum numbers. At B factories, two photon collisions produce $J^{PC} = 0^{\pm+}, 2^{\pm+}$ and 3^{++} charmonia.

In hadronisation originating from $c\bar{c}$ pairs produced in e^+e^- annihilation, **prompt charmonium production** was expected to be in $e^+e^- \rightarrow c\bar{c}g(g)$. Here, the gluons carry away enough energy so the mass of the $c\bar{c}$ pair results in the charmonium mass region. Another contribution from $e^+e^- \rightarrow (c\bar{c})(c\bar{c})$ was estimated to be so small, that detection of this process was considered hardly possible. Surprisingly, this **double charmonium production**, $e^+e^- \rightarrow X_{c\bar{c}}Y_{c\bar{c}}$, was observed with a much larger cross section than QCD originally predicted [18].

Thanks to the variety of possible reactions, consequently, the observed spectrum provides a probe of the QCD potential and coupling strength in the non-relativistic limit.

4. The Belle Experiment

This chapter introduces the KEKB accelerator and the Belle experimental apparatus based on standard literature on the topic. More detailed information can be found in references [18, 65, 16].

The Belle experiment is a high energy electron-positron collider experiment and one of two dedicated B physics experiments in the world¹. It is located at the High Energy Accelerator Research Organization (KEK) in Tsukuba, Japan, and conducted by an international collaboration with members from 18 countries. After the first physics run in 1999, the Belle experiment took data mainly for a centre-of-mass energy of 10.58 GeV corresponding to the $\Upsilon(4S)$ resonance. The $\Upsilon(4S)$ decays with a branching fraction $> 96\%$ almost exclusively to charged or neutral B meson pairs [58]. Therefore, e^+e^- experiments operating at this centre-of-mass energy have earned the name of B factories. A total integrated luminosity of 1052 fb^{-1} was accumulated by the Belle detector; operation at the $\Upsilon(4S)$ stopped in 2008, and including runs at other energy points, data taking ceased in 2010. KEKB is now turned off to be upgraded to SuperKEKB which is planned to have a $40\times$ higher luminosity performance.

Belle was primarily designed for a detailed study and test of the Kobayashi-Maskawa mechanism for CP asymmetry in the B meson system and to understand the origin of CP violation. The other physics goals were precise measurements of decays of bottom and charm mesons, τ leptons and the search for rare or forbidden processes in the Standard Model. The baseline requirements for such an experiment were the following:

- high luminosity, namely instantaneous luminosity up to $10^{34} \text{ cm}^{-2}\text{s}^{-1}$,
- $B^0\bar{B}^0$ pairs with a boost factor of the centre-of-mass system relative to the laboratory system sufficient for observing the time evolution of B decays,
- high-resolution and large-coverage detector with excellent particle identification.

Two important findings that then led to the construction of the B factories like the KEKB accelerator were the long lifetime of the B meson and a substantial rate for $B^0\bar{B}^0$ mixing due to the very large top quark mass. Furthermore, extraordinary advancements in the performance of e^+e^- storage rings with order-of-magnitude luminosity improvements contributed. Progress in the capabilities of large solid-angle detectors, especially considering performance of data acquisition systems to handle the huge event rates associated with the available luminosities, precision tracking and vertexing devices was made. Last but not least, the advancement in software and storage technologies required to deal with these large data samples permitted the realisation of the B factories.

¹The other experiment is BaBar at SLAC in Stanford, USA.

4.1. The KEKB Accelerator

KEKB is an asymmetric energy accelerator colliding 8 GeV electron and 3.5 GeV positron beams. It was designed to produce B mesons with a lab-frame boost sufficient to enable decay-time-dependent measurements; therefore the $\Upsilon(4S)$ resonance at 10.58 GeV, on which KEKB was mostly running, was boosted by $\beta\gamma = 0.425$.

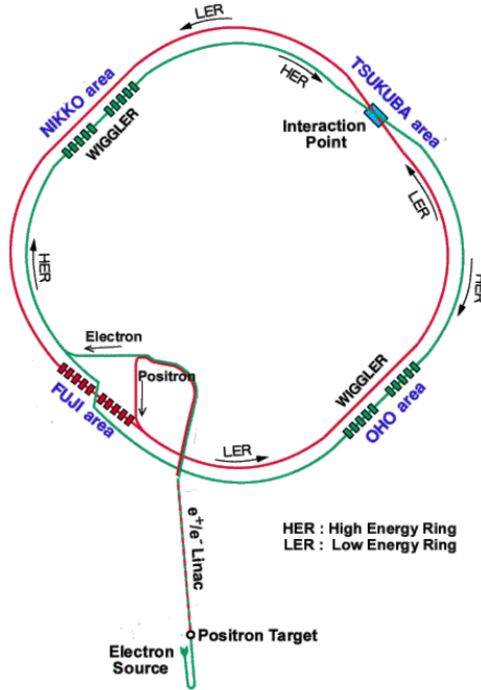


Figure 4.1: Schematic view of the KEKB ring at KEK in Tsukuba, Japan [18].

On the accelerator side the biggest challenge was how to reach the necessary high luminosity. It was decided on a setup in which the two beams collide with a small but finite crossing angle of 22 mrad in the horizontal plane at the beam collision point.

Characteristic	Value
Beam energy [GeV]	8.0 (e^-), 3.5 (e^+)
Beam current [A]	1.2 (e^-), 1.6 (e^+)
Beam size at IP	
x [μm]	80
y [μm]	1
z [mm]	5
Luminosity [$\text{cm}^{-2}\text{s}^{-1}$]	2.1×10^{34}
Number of beam bunches	1584
Bunch spacing [m]	1.84
Beam crossing angle [mrad]	22

Table 4.1.: Machine parameters of KEKB during the last stage of operation [18].

In this collision scheme, the beams are naturally apart after the beam bunch crossing, thus no additional magnet is necessary to let beams reenter and circulate two proper rings. In 2007, the superconducting crab cavity was installed. It realigns the directions of the beam bunches so they pass through each other head-on, leading to a higher beam-beam interaction resulting in higher specific luminosity. This treatment eliminates parasitic collisions and reduces synchrotron radiation around the beam collision point. Also shorter bunch spacing is allowed in principle and there is more available space for the detector components near the interaction point. KEKB eventually reached a peak luminosity of $2.1 \times 10^{34} \text{cm}^{-2} \text{s}^{-1}$, more than twice as large as the design luminosity.

4.2. The Belle Detector

Belle is a large solid angle spectrometer. It shows a compact design with a cylindrical symmetry around the beam axis surrounding the beam crossing point. Its size was optimised to realise a large enough tracking system volume and to make the volume of the calorimeter reasonable. Due to the asymmetric collider the detector is arranged asymmetrically along the direction of the boost to maximise acceptance. By convention, the forward and backward sides are defined relative to the high energy beam. With the boost, more particles are produced on average in the forward direction.

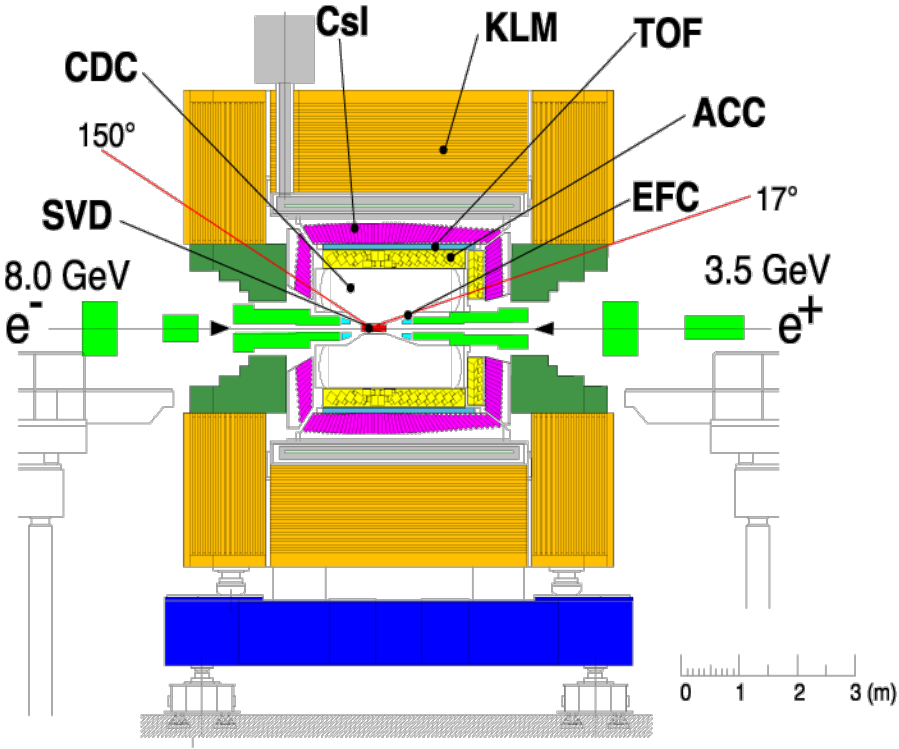


Figure 4.2.: The Belle detector [17].

The forward and backward acceptances are constrained by the beamline geometry. The field strength of the superconducting solenoid magnet is 1.5 T with the field uniformity better than 4% in the central tracking volume.

The main requirements for such a detector were a composition of light material for the inner detector and very good vertexing capability. Also good particle identification over a broad range of momentum was important, especially $\pi - K$ separation which is mandatory for CP studies. Electromagnetic calorimetry to precisely measure the energy of both electrons and photons is also essentially important. A good K_L and muon identification was significant for CP violation measurements as well. Regarding the huge amount of events produced by the high luminosity machine, data handling capabilities from the detector system front-end, classified by a trigger system, and storing for subsequent processing were a challenge as well.

An overview of the Belle detector with its major components can be seen in Fig(4.2). Below, a brief description of specifications of the Belle sub-detectors can be found with a summarising table at the end of this chapter:

The Silicon Vertex Detector SVD

During the first three years, the so-called SVD1 detector was used. Its design consisted of three layers of AC coupled double-sided silicon-strip detectors and covered the $23^\circ < \theta < 140^\circ$ part of the Belle detector acceptance. It was adequate at the beginning of the experiment. However, it was foreseen that limited radiation hardness of the chip and its long shaping time among other issues with connected Belle read-out electronics made it difficult to keep up with the performance improvements of the KEKB collider. Consequently, efforts to upgrade the SVD started before KEKB began operation. The second generation silicon vertex detector, SVD2 was installed in summer 2003. It consists of four layers of double-sided silicon-strip detectors. It covered the full angular acceptance of $17^\circ < \theta < 150^\circ$, showed improved radiation tolerance and used a newly developed read-out chip. The radii of the SVD2 layers range from 20 mm to 88 mm. For this upgrade, the inner radius of the beam pipe was reduced to 15 mm. The SVD is mechanically supported by the central drift chamber, CDC. This contributes to a minimal material accumulation inside the inner radius of the CDC.

The Central Drift Chamber CDC

Several important roles are assigned to the CDC. In the first place, it performs the reconstruction of charged particle tracks and the precise measurement of their hit coordinates in the detector volume. Together with the magnetic field provided by the superconducting solenoid, particle momenta can be measured. The reconstructed tracks in the CDC are extrapolated to the SVD to pick up associated hits in order to precisely determine the event vertex as well as the B meson vertices. This tracking system combination provides good momentum resolution without problematic deterioration for low-momentum tracks. Tracks with $p_T > 70$ MeV can be reconstructed where p_T is the transverse momentum with respect to the beam axis.

The resolution for tracking by SVD and CDC is measured to be $\sigma_{p_T}/p_T = (0.0030/\beta \oplus 0.0019p_T)$, where p_T is in GeV. Finally, using dE/dx measurements within the gas volume enables particle identification. A helium-ethane (50 : 50) gas mixture was chosen to minimise multiple scattering. The CDC also provides efficient and reliable trigger signals for charged particles. The innermost part of the CDC was modified in 2003 to accommodate for the SVD2. Since the majority of the particles in B meson decays have momenta < 1 GeV, minimising the material when building a tracking detector is important.

The CDC is built asymmetrically along the beam direction with an angular coverage of $17^\circ \leq \theta \leq 150^\circ$. Its outer radius is 880 mm and it has 50 cylindrical layers. The chamber has a total of 8400 drift cells. The maximum wire length is 2400 mm. In all layers, except the three innermost that correspond to the cathode part, the maximum drift distance is between 8 and 10 mm. The maximum drift time is < 300 ns. Detailed alignment and calibration led to an overall spatial resolution of $\sim 130 \mu\text{m}$ and a dE/dx resolution of 7% for minimum-ionizing particles, which is important for particle identification.

The Time-of-Flight Counter _{TOF}

A barrel of 128 plastic scintillation counters makes up the time-of-flight system, where one module consists of two counters and one thin trigger counter. This configuration includes an air gap to remove false triggers from photon-conversion which is coming from a large photon background due to scattering in the beam pipe. The detector's acceptance is $33^\circ < \theta < 121^\circ$ where the minimum transverse momentum to reach a TOF counter is 0.28 GeV. The system measures the time of flight for charged particles whose tracks have been reconstructed by the CDC distinguishing between kaons and pions for tracks with momenta < 1.2 GeV.

The Aerogel Cherenkov Counter _{ACC}

The detector is built from aerogel modules of several distinct types, varying in refractive index, number and size of photomultipliers used to detect photons, according to their position in polar angle. The modules are filled with a silica aerogel radiator and covered with a reflector of high reflectivity. The barrel part is divided into 60 identical sectors in the φ direction where there are 16 modules arranged in each sector. The polar angle acceptance of the forward end cap part is $13.6^\circ < \theta < 33.4^\circ$. This device consists of 12 identical sectors in the φ direction with 19 modules in each sector. The polar angle coverage in the barrel is $33.3^\circ < \theta < 127.9^\circ$. The ACC also helps to achieve the necessary $K - \pi$ separation for tracks with momenta > 1.5 GeV which are not covered by the TOF.

The Electromagnetic Calorimeter _{ECL}

The ECL is located inside the solenoid coil. It consists of a barrel section and two end caps made of finely segmented arrays of 8736 CsI(Tl) crystals in total.

Each tower-like shaped crystal is 30 cm long with the scintillation light detected with two pieces of silicon photodiodes. The crystals point towards the interaction point but are tilted by a small angle in the θ and φ directions to prevent photons escaping through the gaps between them. The barrel part is 3.0 m in length and has an inner radius of 1.25 m, while the end caps are located at $z = +2.0$ m and $z = -1.0$ m. This scheme results in a total angular coverage of $12.4^\circ < \theta < 155.1^\circ$. Calorimeter calibration is performed using cosmic rays, Bhabha scattering and $e^+e^- \rightarrow \gamma\gamma$ events. The ECL energy resolution varies from 4% for 100 MeV particles to about 1.6% at 8 GeV. For low energies, the angular resolution is about 13 mrad and for high energies 3 mrad. This system also provides the E/p ratio of shower energy to track momentum which represents the main parameter for electron-hadron separation.

In addition, the ECL determines both online and offline luminosity by measuring the rate of Bhabha events using geometrical coincidences of high energy deposits in the forward and backward parts.

The K_L^0 and Muon Detector KLM

The iron flux-return yoke outside the solenoid magnet is instrumented with layers of active detector material. There are 15 detector layers of double-gap glass-electrodes-based resistive plate counters, and 14 layers of 4.7 cm thick iron plates alternating in the barrel region. Each end cap is made of 14 detector layers and 14 iron layers. A traversing ionising particle results in a local discharge in the 2 mm gas gap and initiates a signal in the electrodes. They identify K_L mesons and muons with momenta > 600 MeV with high efficiency. The polar angle coverage is $45^\circ < \theta < 125^\circ$ for the octagonal barrel part, while the forward and backward end caps extend this range to $20^\circ < \theta < 155^\circ$. The direction of a K_L can be determined from its hadronic shower where we assume the kaon to originate from the e^+e^- interaction point. A discrimination between muons and hadrons, namely π^\pm or K^\pm , becomes possible through the differing range and transverse deflection of non-showering charged particles. Hit position is resolved to about 1.1 cm and results in an angular resolution of under 10 mrad.

Trigger and Data Acquisition

The trigger system consists of sub-triggers that are provided by CDC, ECL, TOF, and KLM signals and the global decision logic (GDL) which makes a logical combination of summarised information from the sub-triggers. The GDL triggers on hadronic, Bhabha and $\mu^+\mu^-$ pair events, etc. These make up the so-called Level1 (L1) hardware trigger and are not processed by the Level3 (L3) software trigger run on the online computer farm. Here, good charged particle tracks are selected to reduce the size of raw data that will be recorded. The typical trigger rate is about 300 Hz at beam currents of 200 mA for LER and 100 mA for HER. Later, a coincidence with sub-triggers from TOF hits or ECL isolated clusters was required as well to reduce such a high trigger rate while maintaining an appropriate efficiency for physics events. In the final state, the timing of the Belle detector was dependent on the KEKB Radio Frequency that controlled the bunch crossing rate of ~ 509 MHz corresponding to ~ 2 ns

intervals. With the TOF information available, it is capable of picking up the proper beam crossing signal. By the ECL trigger alone, a timing resolution of 20 ns is achieved and it is sufficient to perform an energy measurement for pure neutral events such as $e^+e^- \rightarrow \gamma\gamma$.

Sub-detector	Detector type	θ coverage
SVD	3 – 4 double-sided Si detectors	[17°; 150°]
CDC	Drift chamber	[17°; 150°]
TOF	Scintillator tubes	[34°; 130°]
ACC	Cherenkov counter with aerogel	[13.6°; 127.9°]
ECL	CsI(Tl)	[12.4°; 155.1°]
KLM	Resistive plate counters	[20°; 155°]
L1	Hardware	full Belle acceptance
L3	Software	full Belle acceptance

Table 4.2.: Main characteristics of the Belle detector [18].

The Belle Data Acquisition (DAQ) was originally required to read out the eight sub-detectors at a design trigger rate of 500 Hz. It was built in order to record the data read by VME processors after a Belle specific event builder and the L3 data reduction by real time processing. As an increasing trigger rate was necessary to keep up with the expected luminosity increase, Belle DAQ systems were continuously upgraded.

Physics process	Cross section (nb)	Trigger rate (Hz)
$\Upsilon(4S) \rightarrow B\bar{B}$	1.2	12
Hadron production from continuum	2.8	28
$\mu^+\mu^- + \tau^+\tau^-$	1.6	16
Bhabha ($\theta \leq 17^\circ$, prescaled by 100)	44	4.4
$\gamma\gamma$ ($\theta > 17^\circ$, prescaled by 100)	2.4	0.24
two-photon ($\theta > 17^\circ$, $p_T \leq 0.1$ GeV/c)	~ 15	~ 35
Total	~ 67	~ 96

Table 4.3.: Total cross-section and trigger rates with a luminosity $L = 10^{34} \text{ cm}^{-2}\text{s}^{-1}$ for some physics processes at 10.58 GeV [35].

Improvement of the FASTBUS readout and upgrades of five detector sub-systems resulted in a reduction in dead time to less than 1%. The event builder and VME based online computer farm performing the L3 trigger were replaced with the so-called EFARM and connected via Fast Ethernet providing sufficient bandwidth. A large scale PC farm for real time full event reconstruction directly fed by the event builder, the so-called RFARM, was introduced as well using parallel processing of events offering processing power for the back-end system to cope with the expected increase in luminosity.

The processing results such as the reconstructed IP position were also fed back to the accelerator control, which greatly contributed to realize proper accelerator parameters tuning.

4.3. Particle Identification

Charged hadron identification is accomplished by a so-called *likelihood method*. Here, the available information from detector response is composed from probability density functions (PDF) and is used to give a likelihood. The total likelihood for a given particle type is obtained by combining the sub-detectors' likelihoods. Information is collected from the silica aerogel Cherenkov counters ACC giving the number of Cherenkov photons, the time-of-flight measurements from the TOF counters and a specific ionization measurement dE/dx in the CDC together with the measured momentum. The product of likelihoods for the particle being of type i , \mathcal{L}_i ($i = K, \pi$), is then calculated as $\mathcal{L}_i = \mathcal{L}_{\text{CDC}} \times \mathcal{L}_{\text{TOF}} \times \mathcal{L}_{\text{ACC}}$.

Charged pions and kaons are distinguished and selected by their ratio being defined as

$$\mathcal{L}\left(\frac{K}{\pi}\right) = \frac{\mathcal{L}(K)}{\mathcal{L}(\pi) + \mathcal{L}(K)},$$

for kaons and correspondingly $\mathcal{L}(\pi/K)$ for pions. The finally applied cut value is optimized depending on the analysis.

For lepton identification, a combination of the following parameters is arranged into a likelihood: dE/dx in the CDC, E/p ratio (E being the energy deposited in the ECL and p the momentum measured in the CDC and SVD), shower shape in the ECL and the number of Cherenkov photons in the ACC. In case of electron identification, performance is slightly lower at around $\theta \sim 125^\circ$ due to a small gap between the barrel and backward endcap ECL. Muons are identified based on track penetration depth and hit scatter pattern in the KLM system. Their reconstructed hits in the KLM are compared to the extrapolation of CDC tracks. The likelihood ratio

$$\mathcal{L} = \frac{\mathcal{L}_\mu}{\mathcal{L}_\mu + \mathcal{L}_\pi + \mathcal{L}_K}$$

based on the muon, pion and kaon hypotheses is used as a discriminating variable.

As the photon is an electrically neutral particle, it can not be identified directly. For photon selection, the electromagnetic interaction in the ECL is studied in form of the resultant shower production. A 5×5 crystal matrix surrounding the seed crystal is defined, where the seed is determined as the one crystal with the highest energy deposit among neighbouring crystals which has to be at least > 10 MeV. In order to retrieve the incident particle energy, the crystal matrix's contributions are summed up if they exceed a threshold of typically 0.5 MeV. The position of such a particle is found through an energy-weightage of the energies of each contributing crystal. Still remaining biases for both reconstructed energy and incident position are corrected by dedicated Monte Carlo studies due to electromagnetic shower behaviour being a QED process and therefore predictable. Finally, showers without associated charged tracks

reconstructed as explained above and extrapolated to the ECL are sought to distinguish photon from charged particle candidates.

4.4. Data Sample

The Belle data consists of a large number of events which not only come from $e^+e^- \rightarrow \Upsilon(4S) \rightarrow B\bar{B}$ but also from several other processes. In fact, non- $B\bar{B}$ events show a large cross section in electron-positron colliders operating at the $\Upsilon(4S)$ resonance. The most common is e^+e^- elastic scattering known as Bhabha scattering. But also radiative Bhabha reactions, continuum events from $e^+e^- \rightarrow q\bar{q}$ (where q stands for u, d, s and c), two-photon processes $e^+e^- \rightarrow \gamma\gamma$, lepton pair production $e^+e^- \rightarrow \ell^+\ell^-$ (where ℓ stands for μ or τ) and beam-gas interactions contribute. The total number of $B\bar{B}$ pairs in the used high statistics sample of $e^+e^- \rightarrow \Upsilon(4S) \rightarrow B\bar{B}$, making up the foundation of this thesis, is $(771.6 \pm 10.6) \times 10^6$ with a total integrated luminosity of 703 fb^{-1} .

Hadronic events are selected (skimming) by requiring at least three reconstructed charged tracks with a transverse momentum $p_T > 0.1 \text{ GeV}$ originating in the vicinity of the interaction point. The total visible energy from charged tracks and reconstructed photons in the ECL in the centre-of-mass system (cms) must exceed 20% of the total cms energy \sqrt{s} . Hadronic events furthermore have to show two or more large-angle clusters ($-0.7 < \cos\theta < 0.9$ in the laboratory frame), with an average cluster energy $< 1 \text{ GeV}$ and a total cluster energy $0.18 - 0.8 \times \sqrt{s}$. This way τ -pair, beam gas and two-photon events as well as radiative Bhabha and higher multiplicity QED processes are suppressed. Also, an absolute value of the z component of the cms momentum $< 50\% \sqrt{s}$, and a reconstructed primary vertex that is consistent with the known location of the interaction point have to be satisfied. By establishing these criteria the selection of hadronic events is found to be 99% efficient for B meson signal events determined by Monte Carlo simulation.

In this study, we are interested in events coming from those $B\bar{B}$ events in which one of the B mesons has $J/\psi \rightarrow \ell^+\ell^-$ (ℓ being e or μ) in the final state of its decay. As some of the hadronic event skim's selection criteria are not favourable to inclusive ψ events, events with J/ψ and $\psi(2S)$ candidates are explicitly added. One lepton track is required to have a probability > 0.01 of being an electron or > 0.1 of being a muon and the di-lepton system has to pass a tight mass cut within $2780 \text{ MeV} \leq M_{\ell\ell} \leq 3820 \text{ MeV}$. To suppress continuum two-jet non- $\Upsilon(4S)$ background relative to $B\bar{B}$ events, the ratio of second to zeroth Fox-Wolfram moments, $R_2 = H_2/H_0$, is required to be < 0.5 [37]. Badly measured charged particle tracks or those that are not coming from the interaction point are removed by requiring a distance of closest approach to the interaction point (impact parameters) along the beam direction $z < 50 \text{ mm}$ and $r < 15 \text{ mm}$ in the transverse xy -plane.

5. Event Selection

The B meson decay studied in this thesis, $B^\pm \rightarrow \chi_{c1} \pi^+ \pi^- K^\pm$, is reconstructed by combining the final state particles. While the pions and the charged kaon are stable, the proper secondary decays of χ_{c1} and its daughters have to be considered. Monte Carlo simulations are used to optimise the event selection and reconstruction process.

5.1. Monte Carlo Simulation Dataset

In order to build a reconstruction routine for $B \rightarrow \chi_{c1} \pi^+ \pi^- K$ and to estimate the reconstruction efficiency for a decay signal and the possible background contamination, we need to understand acceptance and performance of the detector. For this purpose an adequate Monte Carlo simulation (MC) is performed with an event generator designed for the simulation of physics of B decays. The *EvtGen* program [51] is used to generate the $B \rightarrow \chi_{c1} \pi^+ \pi^- K$ decay signal events as well as possible background events. This program is capable to handle the key kinematics and angular distributions of the resultant decay products. It uses a generic and an analysis specific decay table as its main input. This way specifically defined B meson decays can be generated, not only according to the available phase space but also as decay processes through particular intermediate states. For the description and modeling of the detector material and interactions of particles during their passage through the detector, a Belle specific *GEANT3*-based [8] software is used. This simulation contains the particles' energy loss in active material, detector response as well as readout electronics and digitisation effects.

Signal MC samples of 0.5 million events have been generated for each of the following categories:

- $B^\pm \rightarrow \chi_{c1} \pi^+ \pi^- K^\pm$ obeying the available phase space for a four-body decay,
- $B^\pm \rightarrow X(3872) K^\pm$ followed by the hypothetical decay of $X(3872) \rightarrow \chi_{c1} \pi^+ \pi^-$,
- $B^\pm \rightarrow \chi_{c1}(2P) K^\pm$ followed by the hypothetical decay of $\chi_{c1}(2P) \rightarrow \chi_{c1}(1P) \pi^+ \pi^-$.

In the two latter cases, the first two-body B decay and the $X(3872)$ and $\chi_{c1}(2P)$ decays, respectively, are treated by phase space decay (PHSP) while taking final state radiation into account. Also, in the quasi two-body B decay case, two more signal MC samples have been prepared setting the intermediate state mass to 3900 MeV and 3950 MeV to further understand the reconstruction efficiency as a function of the $\chi_{c1} \pi^+ \pi^-$ invariant mass as discussed in detail later in Sec(6.2).

5.2. Reconstruction of χ_{c1} Candidates

χ_{c1} meson candidates are reconstructed by combining a J/ψ candidate with a photon.

The J/ψ meson is reconstructed from oppositely charged lepton pairs via its decay mode $J/\psi \rightarrow \ell^+\ell^-$, where ℓ stands for e^\pm or μ^\pm . Charged tracks are identified as muons if they satisfy a muon likelihood > 0.1 or as electrons if the electron likelihood is > 0.01 .

A correction for final state radiation or bremsstrahlung in the inner parts of the detector is applied by including the four-momentum of every photon detected within 0.05 radians of the original electron or positron direction in the e^+e^- invariant mass calculation.

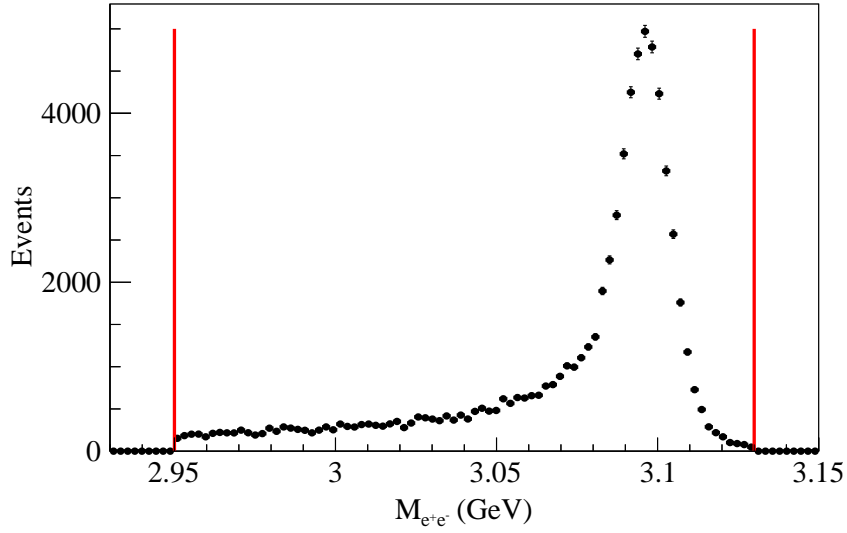
Taking into account the still existing small radiative tails, an asymmetric invariant mass requirement of $2950(3030) \text{ MeV} \leq M_{ee(\mu\mu)} \leq 3130 \text{ MeV}$ is chosen to define a J/ψ candidate in the electron (muon) channel.

A vertex and a mass-constrained fit are applied to the selected J/ψ candidates. The application of kinematic fits reduces the effects of limited detector resolution and improves the mass or momentum resolutions to determine the decay vertex of a particle candidate. There are two types of kinematic fitting used in this analysis:

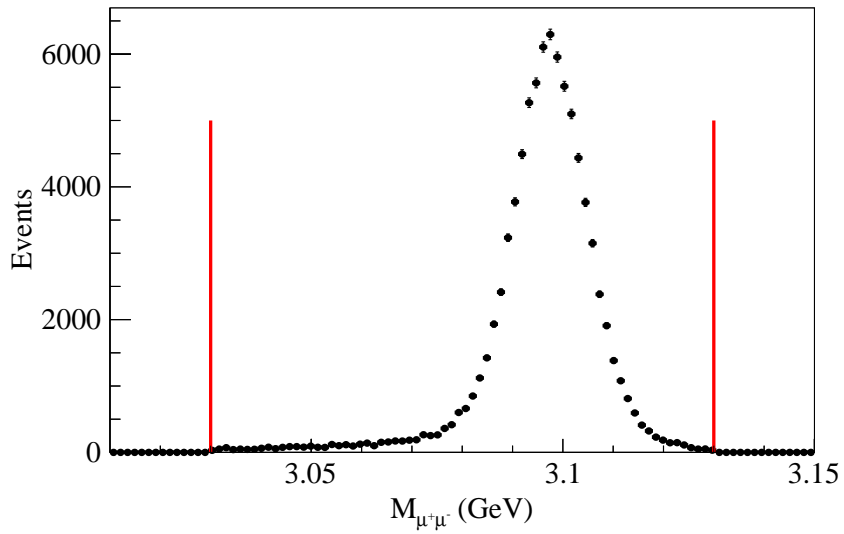
- The invariant mass of the candidate is fixed to the known, nominal mass and the momenta of its daughters are re-calculated in the *mass-constrained fit*. This approach can be applied when the reconstructed state has a narrow width and the observed invariant mass distribution is dominated by detector resolution.
- In case of the *vertex-constrained fit* tracks used to reconstruct a candidate may not converge in the same point. By tuning the momentum and position of each daughter particle according to its measurement errors the candidate particle's decay vertex is obtained so that all tracks pass through a single point. This tuning of momentum or position is done by a minimisation of the χ^2 , using a Lagrange multiplier approach.

A cms momentum cut of $p_{\ell\ell}^* < 2.0 \text{ GeV}$ rejects J/ψ mesons not coming from B decays. Fig(5.1) shows the di-lepton invariant mass distribution in phase space signal MC, cut requirements are indicated by vertical red lines.

To identify χ_{c1} the invariant $J/\psi\gamma$ mass is used in a mass window of $3467 \text{ MeV} \leq M_{J/\psi\gamma} \leq 3535 \text{ MeV}$, see Fig(5.2). Photon selection is requiring $E_\gamma > 100 \text{ MeV}$ to reduce combinatorial background. Also, a veto on photons coming from π^0 is applied by rejecting photons if their combined invariant mass with another randomly picked photon in the same event is within $117 \text{ MeV} \leq M_{\gamma\gamma} \leq 153 \text{ MeV}$ [49]. From the invariant mass of the combined system with another photon and the energy and polar angle of the photon of interest, a probability is calculated for the latter photon to come from a π^0 and we require this parameter to be $< 80\%$ to still accept the photon for χ_{c1} reconstruction. A figure of merit study was performed to find the best cut and can be found in App(A). A mass-constrained fit is performed on the χ_{c1} candidates in order to improve momentum resolution.



(a) Di-electron mass with selection windows indicated by red lines.



(b) Di-muon mass with selection windows indicated by red lines.

Figure 5.1.: Invariant di-lepton mass spectrum to select a J/ψ candidate in phase space MC.

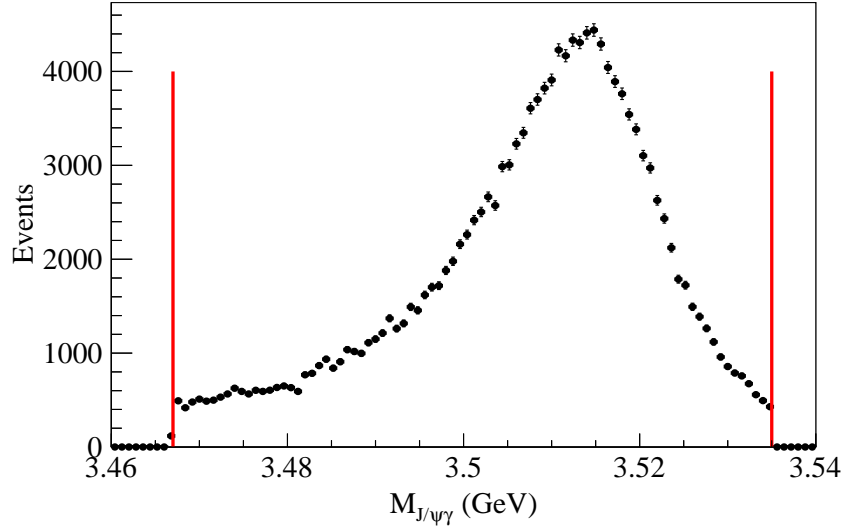


Figure 5.2.: Invariant $J/\psi\gamma$ mass spectrum to select a χ_{c1} candidate in phase space MC with selection window indicated by red lines.

In the next step, reconstructing the final B candidate requires the selection of an oppositely charged pion pair. Then, a charged kaon will be added. In the event selection itself no explicit requirements are applied for a possible intermediate state decaying to $\chi_{c1}\pi^+\pi^-$; the possibility of a resonance in the $\chi_{c1}\pi^+\pi^-$ spectrum is only implemented in the respective quasi two-body decay MC datasets.

5.3. Selection of Light Meson Candidates

For charged pions the likelihood ratio is required to be $\mathcal{L}(\pi/K) > 0.6$ as well as for charged kaons $\mathcal{L}(K/\pi) > 0.6$. Looking at the invariant di-pion mass, there is no obvious background coming from $\gamma \rightarrow e^+e^-$ where e^\pm are misidentified as pions, and therefore no need to apply a mass cut, see Fig(5.3). Still, a vertex-constrained fit is applied to the pion pair and its convergence is required.

5.3.1. Low Transverse Momentum Pion Selection

In case of the $X(3872) \rightarrow \chi_{c1}\pi^+\pi^-$ mode, the pions' transverse momenta with respect to the beam axis, p_T , are low. This is because only a small Q-value is available, $m_{X(3872)} - m_\chi - 2 \times m_\pi \approx 80$ MeV, and reconstruction efficiency is limited by the Belle detector's acceptance for low p_T tracks [82]. Such particles curl up in the Central Drift Chamber CDC and can eventually be reconstructed multiple times, ending up forming excess B candidates. This effect results in pions that appear to have same charge with nearly identical three-momenta, or oppositely-charged pions with nearly opposite three-momenta, as illustrated in Fig(5.4). Similar considerations can be made for the $\chi_{c1}(2P)$ case.

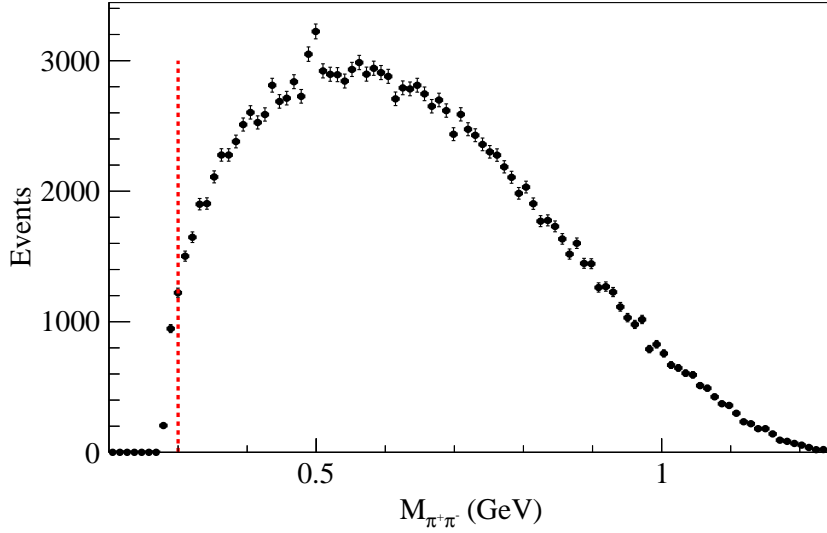


Figure 5.3.: Invariant di-pion mass spectrum in B candidate reconstruction, the red dashed line hints the possible cut.

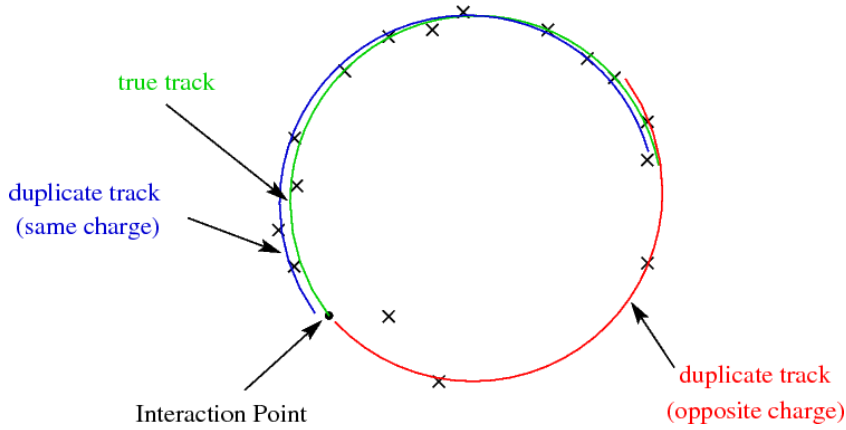


Figure 5.4.: Curl up of low p_T pions.

For pions with $p_T < 0.25$ GeV, tracks are paired to check if the following criteria is satisfied: if $|p_{\pi_1} - p_{\pi_2}| < 0.1$ GeV the opening angle between those tracks is checked. Duplicated reconstruction should appear for angles $\sim 0^\circ$ and $\sim 180^\circ$. MC shows that these tracks are in fact concentrated around $|\cos(\theta_{\text{open}})| \approx 1$, see Fig(5.5). Focusing on $\cos(\theta_{\text{open}}) > 0.95$ for same-charged tracks and $\cos(\theta_{\text{open}}) < -0.95$ for oppositely-charged tracks, only one of them is regarded as the real and correctly reconstructed track.

Comparing these pion tracks, the one closest to the interaction point is chosen: The particle with the smaller value of

$$\left| \frac{dr}{15\text{mm}} \right|^2 + \left| \frac{dz}{50\text{mm}} \right|^2$$

where dr and dz are the impact parameters in mm, is selected based on the knowledge established by previous Belle studies [38, 47].

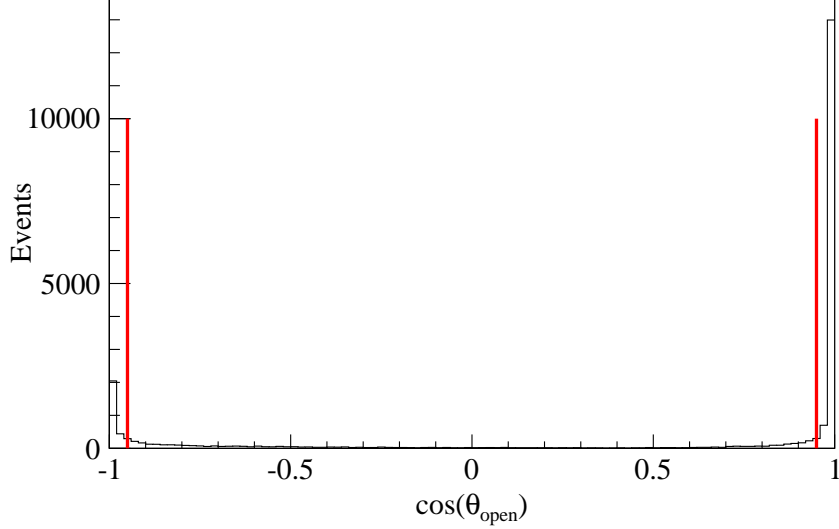


Figure 5.5.: $\cos(\theta_{\text{open}})$ for multiply reconstructed pions in $|\cos(\theta_{\text{open}})| \approx 1$.

Applying this method, misidentification of a pion as a kaon can be reduced to 5% and multiplicity of B candidates is improved. The pion and kaon selection efficiency is 94% each.

5.4. Reconstruction of B Candidates

The reconstruction of B meson candidates is completed by combining the $\chi_{c1}\pi^+\pi^-$ system with a charged kaon; the inclusion of the charge conjugate state is from here-on implied. We make full use of the two-body kinematics of the $\Upsilon(4S) \rightarrow B\bar{B}$ decay in the cms by considering that the reconstructed B 's energy must consequently be half of the total energy of the e^+e^- system. The kinematic variables of interest to identify a B meson candidate are the *beam-constrained mass* M_{bc} and the *difference-to-beam energy* ΔE :

$$M_{\text{bc}} = \sqrt{E_{\text{beam}}^2 - (p_{\chi_{c1}\pi\pi} + p_K)^2}$$

$$\Delta E = (E_{\chi_{c1}\pi\pi} + E_K) - E_{\text{beam}},$$

where E_{beam} is half the e^+e^- system (beam) energy, p the momenta and E the energies of the particle candidates in the cms of $\Upsilon(4S)$.

5.5. Properties of the reconstructed B Candidate

M_{bc} peaks at the nominal B meson mass for correctly reconstructed B candidates and has a much better resolution than the bare reconstructed mass, hence providing a better separation of signal and background. In an ideal case, ΔE is supposed to peak at zero for properly reconstructed B mesons.

The multiplicity is defined as the fraction of the events with more than one B candidate out of the total number of events having B candidates. So far, multiplicity is at 39.7% for multiple reconstructed candidates per phase space event found in the signal region. This seems relatively high but is expected for a four-body final state. Multiplicity is increasing in case of the quasi two-body decays and also with increasing mass.

Decay mode	Multiplicity
$B^\pm \rightarrow \chi_{c1}\pi^+\pi^-K^\pm$ (PHSP)	39.7%
$B^\pm \rightarrow X(3872)K^\pm$	45.6%
$B^\pm \rightarrow \chi_{c1}(2P)K^\pm$	48.2%

Table 5.1.: Multiplicity in $|\Delta E| < 0.12$ GeV for Monte Carlo datasets.

This can be understood when looking at the very limited phase space left for pions in the decay $B \rightarrow X(3872)(\rightarrow \chi_{c1}\pi^+\pi^-)K$ or $B \rightarrow \chi_{c1}(2P)(\rightarrow \chi_{c1}\pi^+\pi^-)K$: The kaons have high momentum but the pions are rather slow, in contrary to the $B \rightarrow \chi_{c1}\pi^+\pi^-K$ phase space case where a more kinematically symmetric event topology of kaons and pions can be allowed. As the detection efficiency for charged particles is a function of the particle's momentum p_T , it becomes more difficult to only select the proper low p_T pions for an event, leading to a higher probability of wrong combination and consequently higher multiplicity.

Looking at the ΔE distributions, the signal peaks at $\Delta E = 0$ are exhibiting similar resolutions for all three cases. This is an effect of employing a mass-constrained fit to the χ_{c1} candidate which includes a photon. A tail appears in the positive ΔE region in the quasi two-body decays which is not visible in the phase space case. It is due to a difference in reconstruction efficiency as explained above. Since both, $X(3872)$ and $\chi_{c1}(2P)$ at 3920 MeV are still close to the kinematic threshold. Wrongly picked up pions are mainly having higher momenta than true ones. On the other hand, all the available kinematical region is averaged in the phase space case thus no such tendency shows in the ΔE projection.

If more than one B meson candidate is found in an event, the best candidate is selected as the one having the closest beam-constrained mass M_{bc} compared to the nominal B mass. With this best candidate selection, BCS, 87.4% of the correctly combined B meson candidates are selected in the phase space signal MC case.

The ΔE and M_{bc} distributions for all three MC datasets are shown in Fig(5.6) and Fig(5.7) for comparison. As the ΔE distributions are showing the desired behaviour of peaking at zero, the invariant mass spectra of $\chi_{c1}\pi^+\pi^-$ are presented in the B candidate signal enhanced region¹. They can be seen in Fig(5.8). The manageable amount of events in the $M(\chi_{c1}\pi^+\pi^-)$ tail in signal MC is due to wrong combination. A clear peak around 3.87 GeV indicates the reconstructed $X(3872)$ and the $\chi_{c1}(2P)$ is visible at its predicted mass at 3.92 GeV. In phase space MC the spectrum is distributed over the entire possible range, as expected.

These plotted distributions verify the proper functionality of the reconstruction routine.

¹see next Chapter for Figure of Merit study and deduction of the signal window and signal enhanced region.

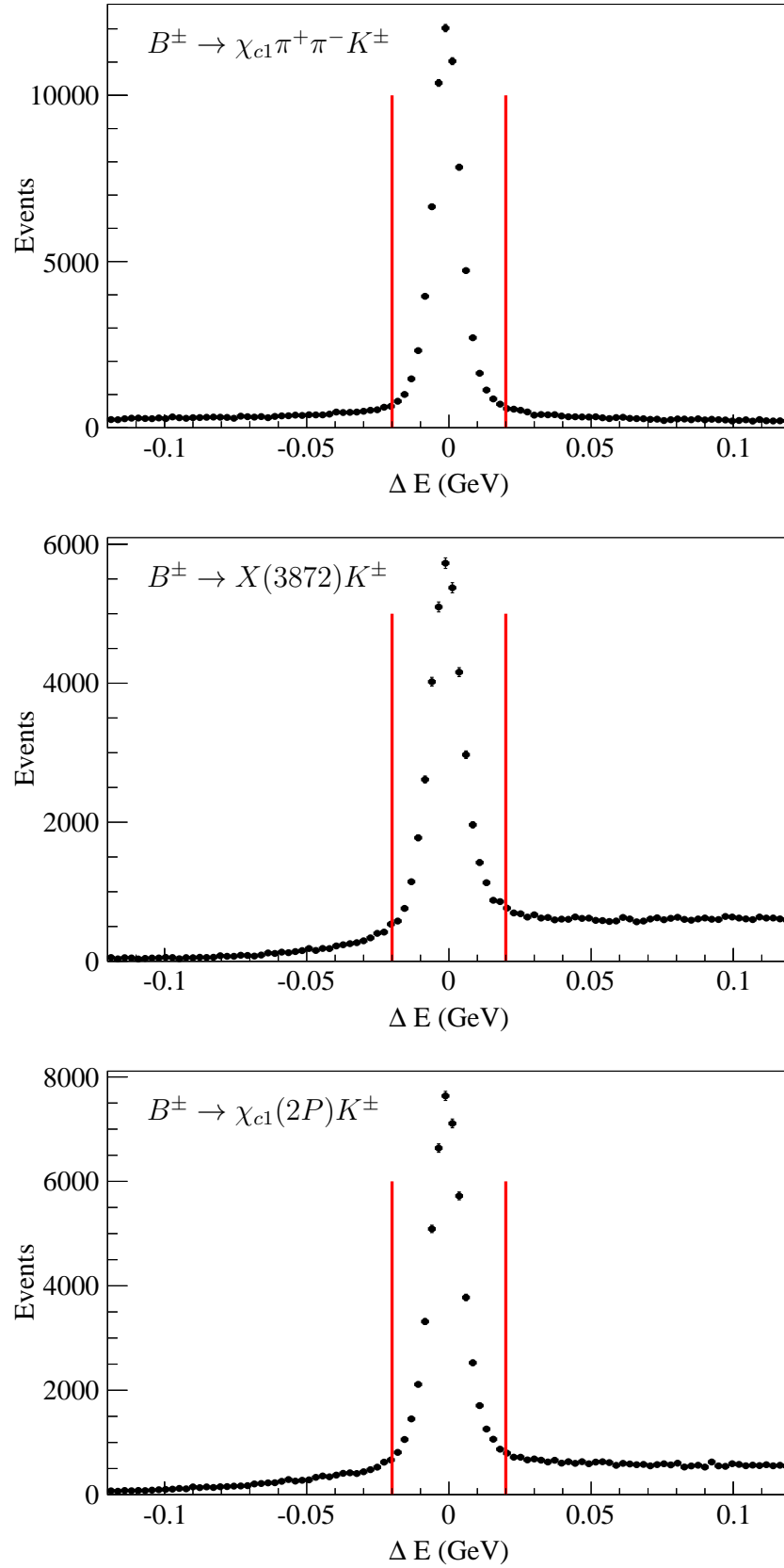


Figure 5.6.: ΔE distribution for all three MC datasets; $M_{bc} > 5.27$ GeV, BCS applied.

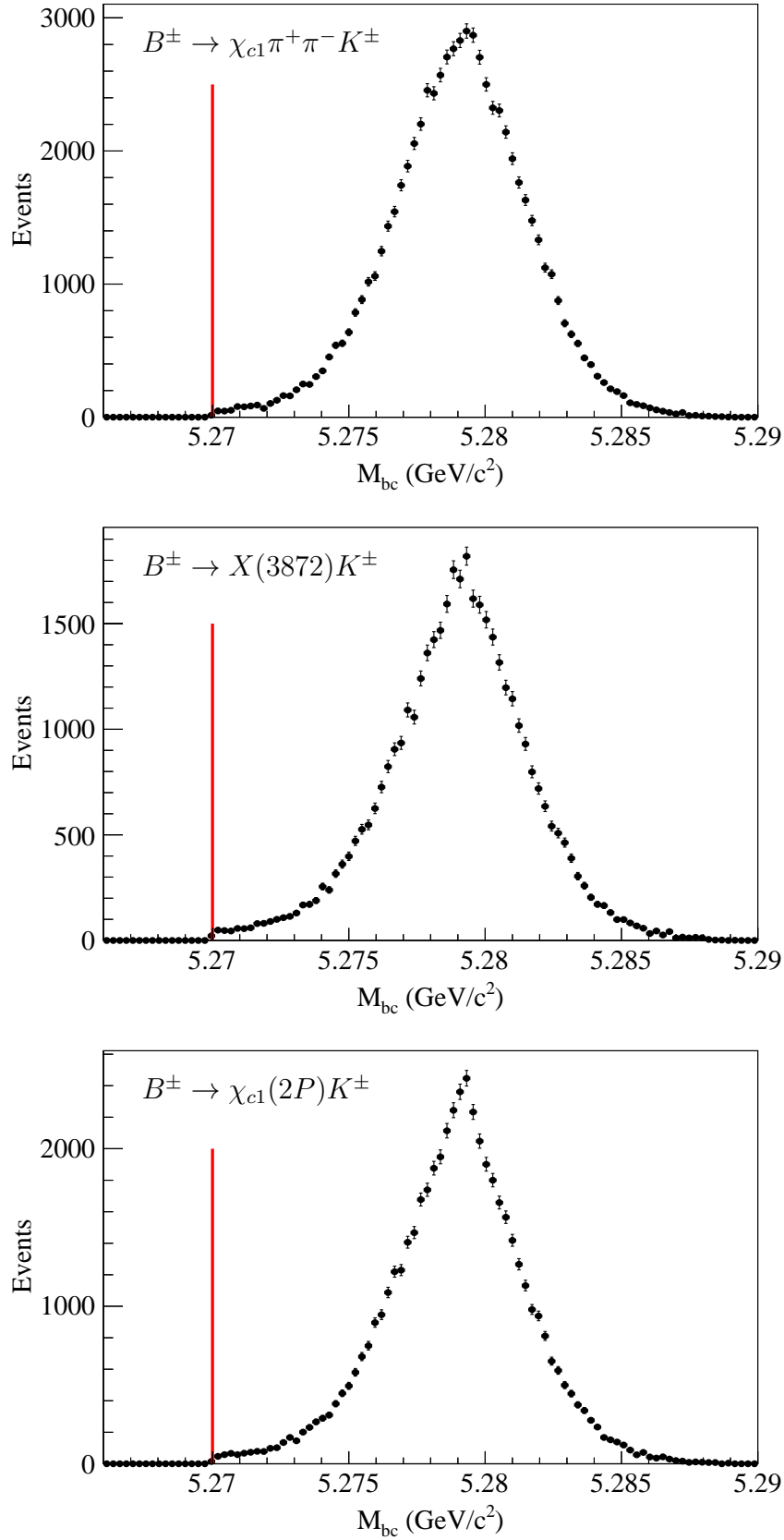


Figure 5.7.: M_{bc} distribution for all three MC datasets; $|\Delta E| < 0.12$ GeV, BCS applied.

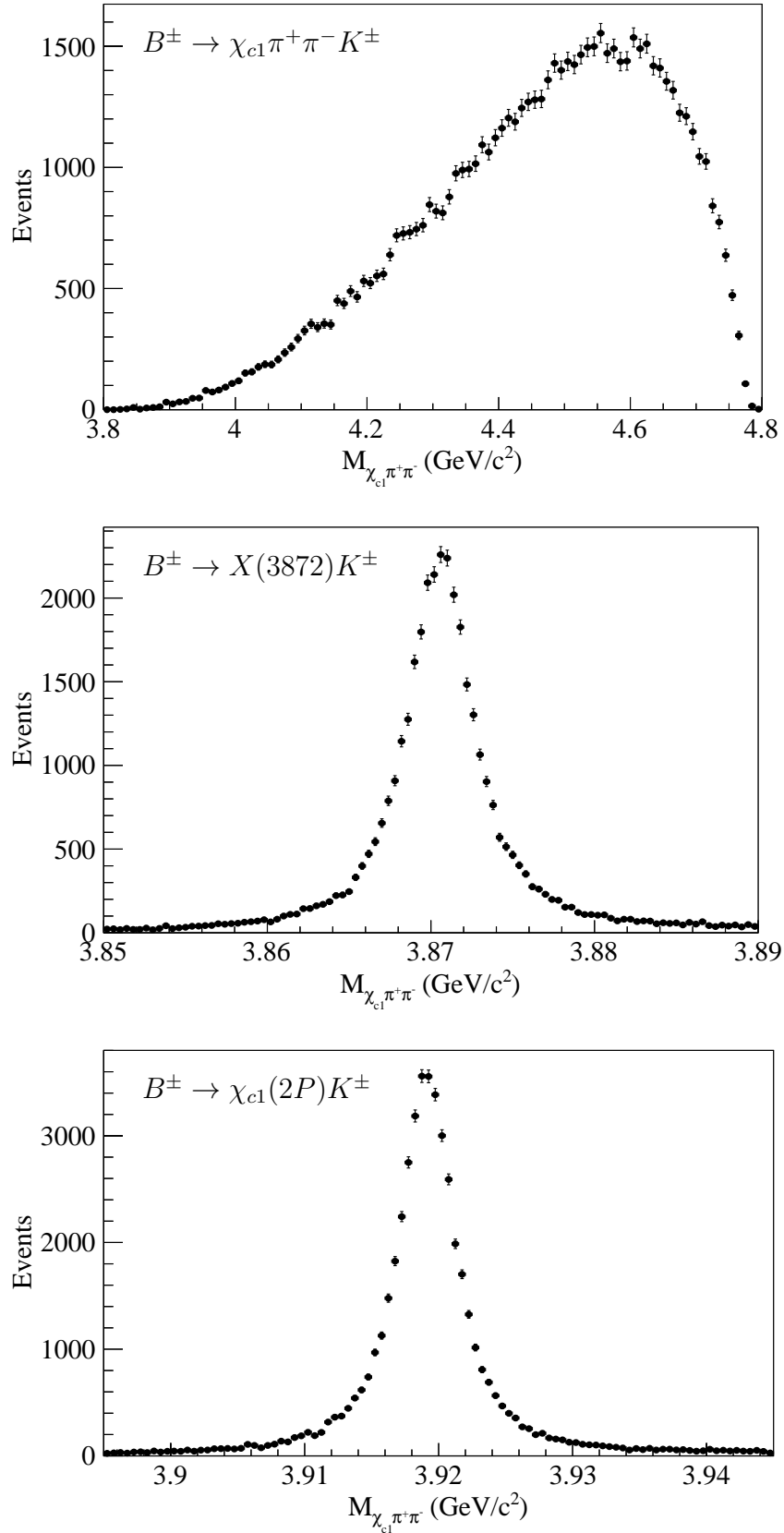


Figure 5.8.: $M_{\chi_{c1}\pi\pi}$ invariant mass distribution for all three MC datasets; $|\Delta E| < 0.12$ GeV, $M_{bc} > 5.27$ GeV, BCS applied.

6. Monte Carlo Studies

For the reconstruction procedure to get B^\pm meson candidates from $\chi_{c1}\pi^+\pi^-K^\pm$, the background contamination modes have to be identified and their contributions to be estimated. The ΔE signal is then fitted to study the line shape in order to extract a probability density function, and ultimately calculate a branching fraction. For this, the reconstruction efficiency is needed and estimated as a function of the invariant mass of the $\chi_{c1}\pi^+\pi^-$ intermediate state ($M_{\chi_{c1}\pi\pi}$). Finally, the $M_{\chi_{c1}\pi\pi}$ spectrum is studied and a fitting probability density function is obtained to hunt for a resonance.

6.1. Background Estimation

We expect the dominant background for the $B^\pm \rightarrow \chi_{c1}(\rightarrow J/\psi\gamma)\pi^+\pi^-K^\pm$ final state to come from those B decays that have a real $J/\psi \rightarrow e^+e^-$ or $J/\psi \rightarrow \mu^+\mu^-$ in their final state. Therefore, a large $B \rightarrow J/\psi X$ MC sample has been prepared to estimate the major background modes, where X denotes one or more decay products. Decays of higher charmonium states such as $\psi(2S)$, χ_{c0} , χ_{c1} , χ_{c2} with a J/ψ in the final state are also taken into account. It provides a $B \rightarrow J/\psi X$ dataset that is $100\times$ larger than the later used Belle data sample and includes all known and kinematically allowed decay modes having J/ψ in the final state.

6.1.1. Expected Background in ΔE

Fig(6.1) shows the possible contributions to background estimated from the $B \rightarrow J/\psi X$ MC sample. There is only one mode to point out, all other backgrounds have shown to be smooth in their ΔE distributions in the $|\Delta E| < 0.12$ GeV window.

The structures in this distribution can be divided in the signal part, $B \rightarrow \chi_{c1}X_{\bar{s}u}$, where $\pi^+\pi^-K$ can be formed from $X_{\bar{s}u}$ which is the \bar{s} and u quark system to be hadronised according to the PYTHIA/JETSET string fragmentation model. It results in the desired signal final state indicated by ΔE peaking at zero. The other contribution is coming from $B^\pm \rightarrow \chi_{c2}\pi^+\pi^-K^\pm$ and represents the background. A small peak can be seen, shifted to the negative ΔE region because of the χ_{c2} 's slightly higher mass at 3556 MeV which is being mass-constrained to the χ_{c1} mass of 3510 MeV.

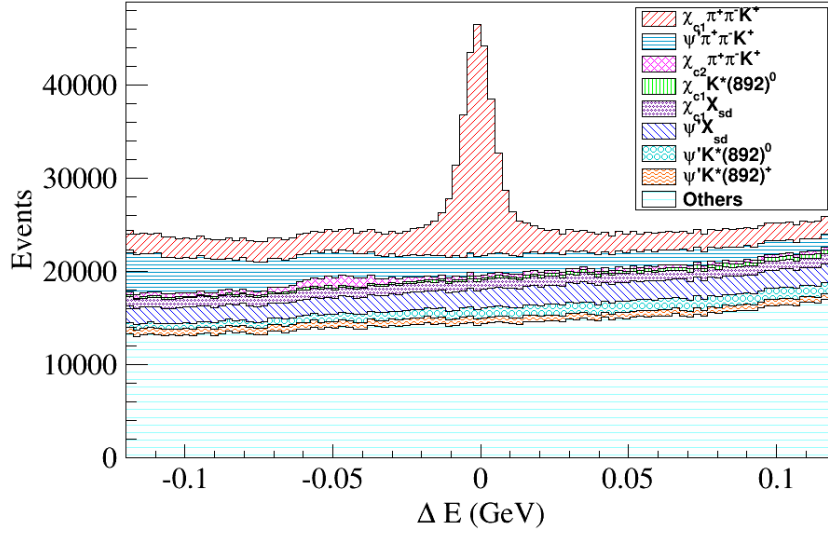


Figure 6.1.: ΔE distribution on $B \rightarrow J/\psi X$ MC sample; $M_{bc} > 5.27$ GeV and BCS applied.

6.1.2. Figure of Merit

Candidates satisfying $M_{bc} > 5.27$ GeV and $|\Delta E| < 0.12$ GeV are considered for extracting a B decay signal as shown in Fig(6.1). Due to this ΔE window choice, the obtained ΔE distribution is adjusted to not include the intricately shaped background coming from B decays with five-body final states. These backgrounds tend to cluster at -0.14 GeV or $+0.14$ GeV for five- or three-body modes, respectively, as a result of an ignored or additional pion.

In order to study the $\chi_{c1}\pi^+\pi^-$ mass spectrum, the B decay candidates are taken from the tight signal enhanced window. To validate this requirement, a Figure of Merit study was performed. Using phase space signal MC and the $B \rightarrow J/\psi X$ MC sample for background we assume that the branching of $B^\pm \rightarrow \chi_{c1}\pi^+\pi^- K^\pm$ is comparable to $B^\pm \rightarrow J/\psi\pi^+\pi^- K^\pm$ with 4×10^{-4} (see below), and estimate the signal yield.

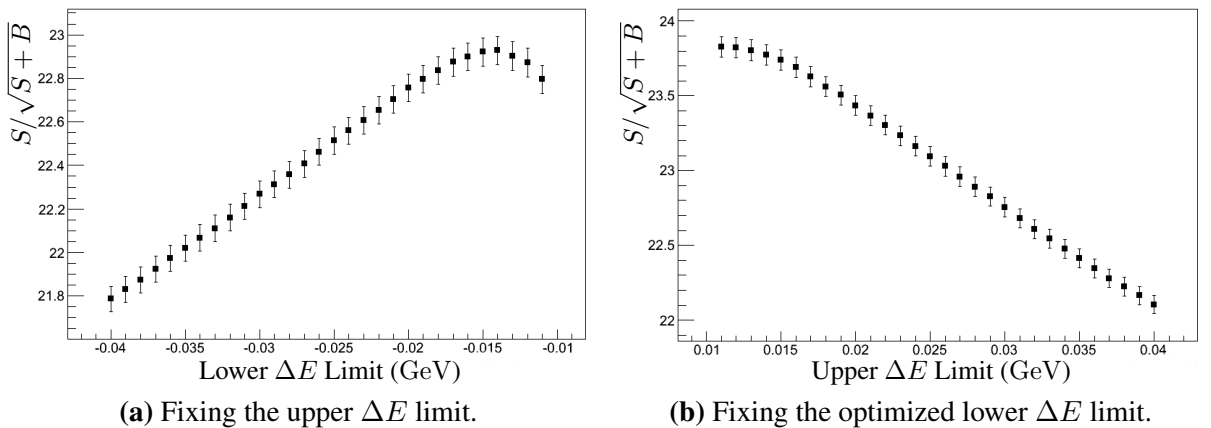


Figure 6.2.: Figure of merit study to optimise the ΔE window for the signal enhanced region.

The upper ΔE limit is fixed while ramping the lower limit. This way the ratio of signal and background $S/\sqrt{S+B}$, where S is the expected signal yield and B the expected background, is checked. After finding the lower limit for ΔE to be -0.02 GeV considering the error, to give the best result, the procedure is repeated for the upper limit. Looking for the signal enhanced region, the decision falls on a symmetric ΔE window, fixing the upper and lower limit to ± 0.02 GeV to cope with a potential ΔE resolution difference between data and MC.

A two-dimensional illustration of the signal enhanced region is shown in Fig(6.3).

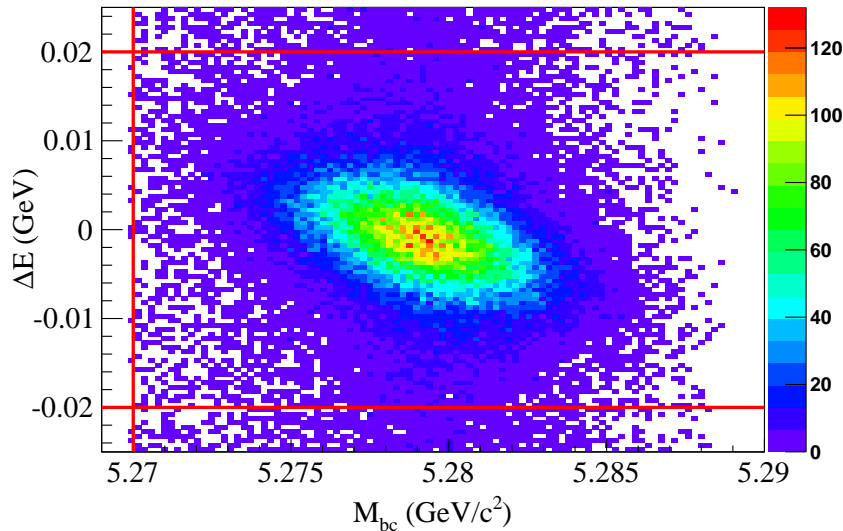


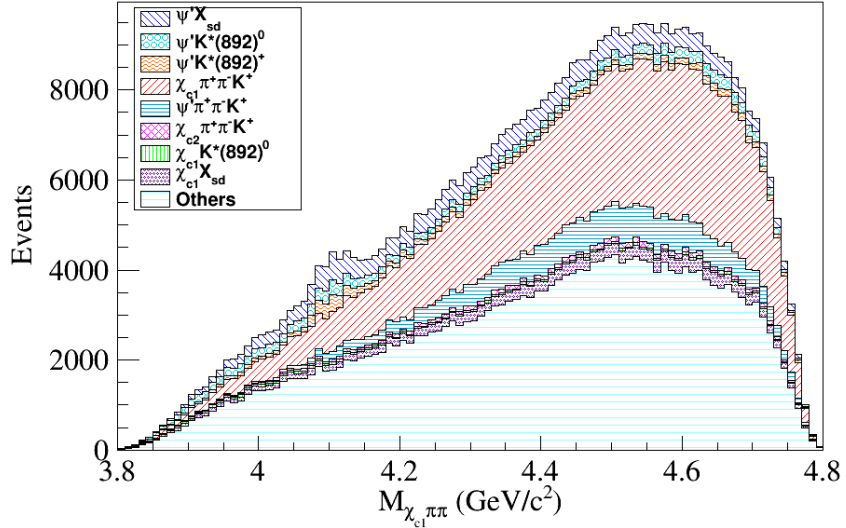
Figure 6.3.: Two-dimensional illustration of the signal enhanced region in ΔE and M_{bc} with cuts indicated by red lines.

The ΔE distribution in the formerly chosen larger window can be seen in App(B).

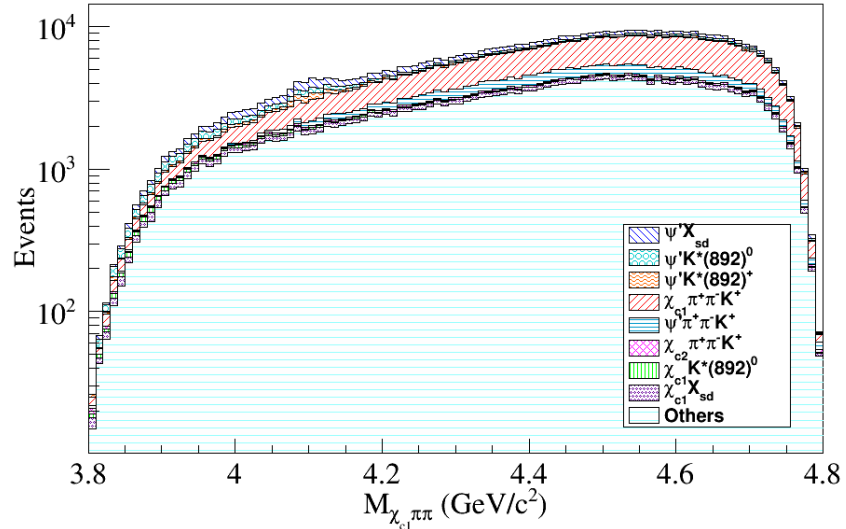
6.1.3. Expected Background in $M_{\chi_{c1}\pi\pi}$

Looking at the invariant mass spectrum of $\chi_{c1}\pi^+\pi^-$ using the $B \rightarrow J/\psi X$ MC sample, the only peaking component is a reflection from ψ' that appears at 4.1 GeV as shown in Fig(6.4a).

If, in the event, a ψ' decays to $J/\psi\pi^+\pi^-$ and an additional, unrelated photon is picked up, a fake χ_{c1} candidate can be formed. Because of the mass-constrained fit applied to the χ_{c1} candidates, combining this fake χ_{c1} with the pion pair coming from ψ' results in a peak at 4.1 GeV. To have a closer look at the bump in the expected invariant mass spectrum of $\chi_{c1}\pi^+\pi^-$, it was also plotted on a logarithmic scale as shown in Fig(6.4b). A ψ' -veto was developed in order to suppress this peaking background but found to create an artificial dip and is therefore being ineffective. As this peak is not interfering with the mass region of interest, which is the $\chi_{c1}(2P)$ mass prediction or the $X(3872)$ mass (between 3.89 – 3.95 GeV), we leave this reflection untreated.



(a) $M_{\chi_{c1}\pi\pi}$ distribution on $B \rightarrow J/\psi X$ MC.



(b) $M_{\chi_{c1}\pi\pi}$ distribution on logarithmic scale.

Figure 6.4.: Expected $M_{\chi_{c1}\pi\pi}$ distribution on the $B \rightarrow J/\psi X$ MC sample; $M_{bc} > 5.27$ GeV, $|\Delta E| < 0.02$ GeV and BCS applied.

In connection with the $\chi_{c1}\pi^+\pi^-$ invariant mass, it was further verified that, concerning the background, a cut on the di-pion mass is not necessary. There is close to no contamination below 0.3 GeV. The invariant mass of $\pi^+\pi^-$ was plotted with the $B \rightarrow J/\psi X$ MC sample and can be seen in Fig(6.5). As the $B \rightarrow J/\psi X$ MC sample consists of all known modes with a J/ψ in the final state, including the signal decay $B^\pm \rightarrow \chi_{c1}\pi^+\pi^-K^\pm$, $\pi^+\pi^-$ might originate from π^-K^* , K^* , K_S^0 or ρK^\pm . These modes are handled as fragmentation processes.

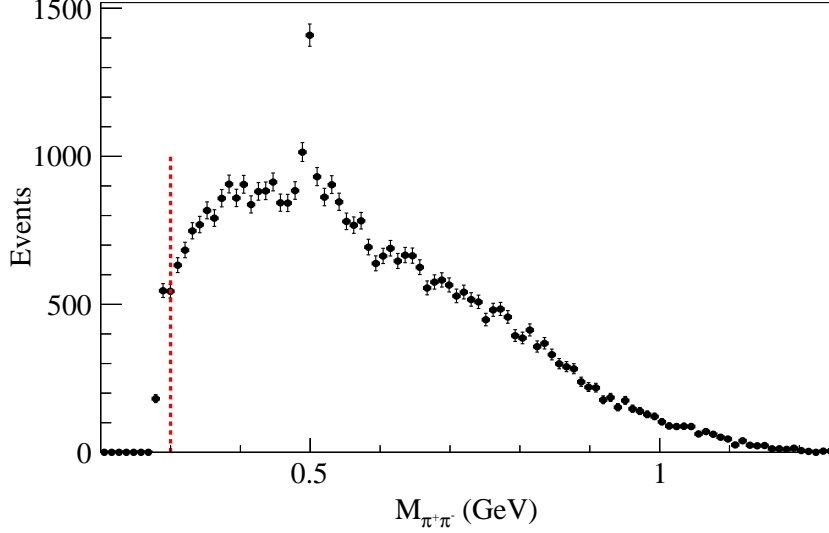


Figure 6.5.: $M_{\pi^+\pi^-}$ on the $B \rightarrow J/\psi X$ MC sample scaled to data.

6.2. Fitting Strategy and Observable Extraction

For both, the ΔE and $M_{\chi_{c1}\pi\pi}$ spectra, the line shapes are studied. A fitting routine is compiled leading to Probability Density Functions (PDF) which will be used to extract the $B \rightarrow \chi_{c1}\pi^+\pi^-K$ signal yield from the Belle data (see next chapter). In order to make assumptions about the expected signal yield, the reconstruction efficiency is estimated as a function of the mass of an intermediate state for different mass hypotheses. Finally, toy studies verify the choice of PDFs.

6.2.1. ΔE Fit and Efficiency Estimation

ΔE Signal PDF

For the extraction of the signal yield, an unbinned maximum likelihood (UML) fit is used on a 0.5 million events sample for $B^\pm \rightarrow \chi_{c1}\pi^+\pi^-K^\pm$ (PHSP). The probability density function (PDF) to describe this B decay signal is composed by summing the following two components:

- the peak is parametrised using a sum of two Gaussians $P_{\text{peak}}(\Delta E_i)$ and
- the outlier (OL) is described by a second order Chebyshev polynomial $P_{\text{OL}}(\Delta E_i)$.

Thus the likelihood function to be maximised is

$$\mathcal{L} = \frac{e^{-N}}{N!} \prod_{i=1}^N [n_{\text{OL}} \cdot P_{\text{OL}}(\Delta E_i) + n_{\text{peak}} \cdot P_{\text{peak}}(\Delta E_i)]. \quad (6.1)$$

Here

$$P_{\text{peak}}(\Delta E_i) = (1 - f_{\text{tail}}) \frac{1}{\sigma_1 \sqrt{2\pi}} e^{-\frac{(\Delta E_i - \mu_1)^2}{2\sigma_1^2}} + f_{\text{tail}} \frac{1}{\sigma_2 \sqrt{2\pi}} e^{-\frac{(\Delta E_i - \mu_2)^2}{2\sigma_2^2}} \quad (6.2)$$

where N is the total number of candidate events, n_{peak} and n_{OL} denote the number of peak and outlier events, respectively. f_{tail} is the fraction of the second Gaussian, μ_1, μ_2 and σ_1, σ_2 are the mean values and standard deviations for the corresponding Gaussians. In all fits, $\mu_1 = \mu_2$ is assumed throughout this analysis.

Fig(6.6) shows the fitted distribution. The Chebyshev polynomial describing the outlier is not counted as part of the signal as it is thought to be absorbed as a part of combinatorial background.

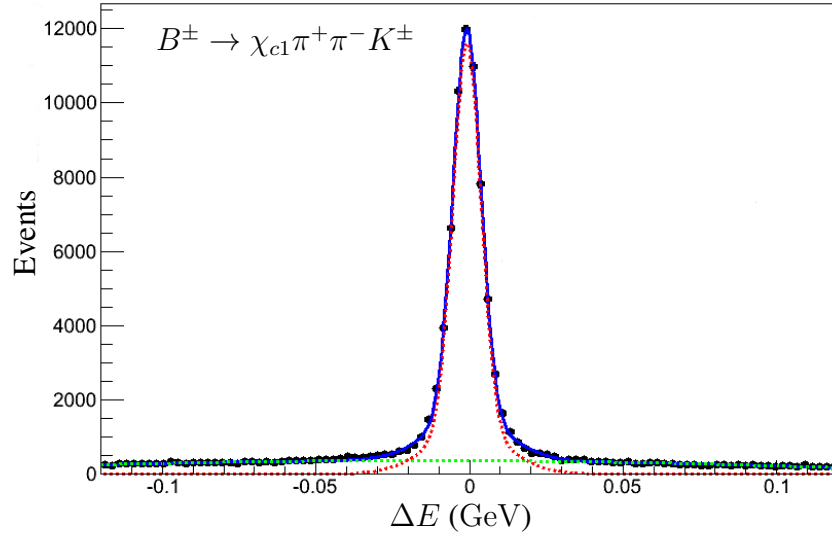


Figure 6.6.: Fitted ΔE distribution for $B^\pm \rightarrow \chi_{c1}\pi^+\pi^-K^\pm$ in signal phase space MC (blue), signal part (red) and combinatorial background (green); $M_{bc} > 5.27$ GeV and BCS applied.

The ΔE distribution peaks at zero showing a standard deviation of 4.6 MeV, the outlier is due to wrong combination coming from misreconstruction. A peak yield of 65255 ± 339 is extract out of 0.5 million generated events.

In all three signal MC cases the same fitting function Eqn(6.1) is used. As expected for signal MC, also the distributions for $X(3872)$ and $\chi_{c1}(2P)$ as intermediate states of the main B meson decay peak at zero as shown in Fig(6.7).

A signal yield of 32222 ± 259 is extract with a standard deviation of 5.3 MeV for the $X(3872)$ case. In the $\chi_{c1}(2P)$ signal MC, the peak yield is found to be 52258 ± 337 with a standard deviation of 5.6 MeV. Chebyshev polynomials were used to describe the combinatorial background in both cases.

These peak yields will be of interest when calculating the reconstruction efficiency for the different intermediate states.

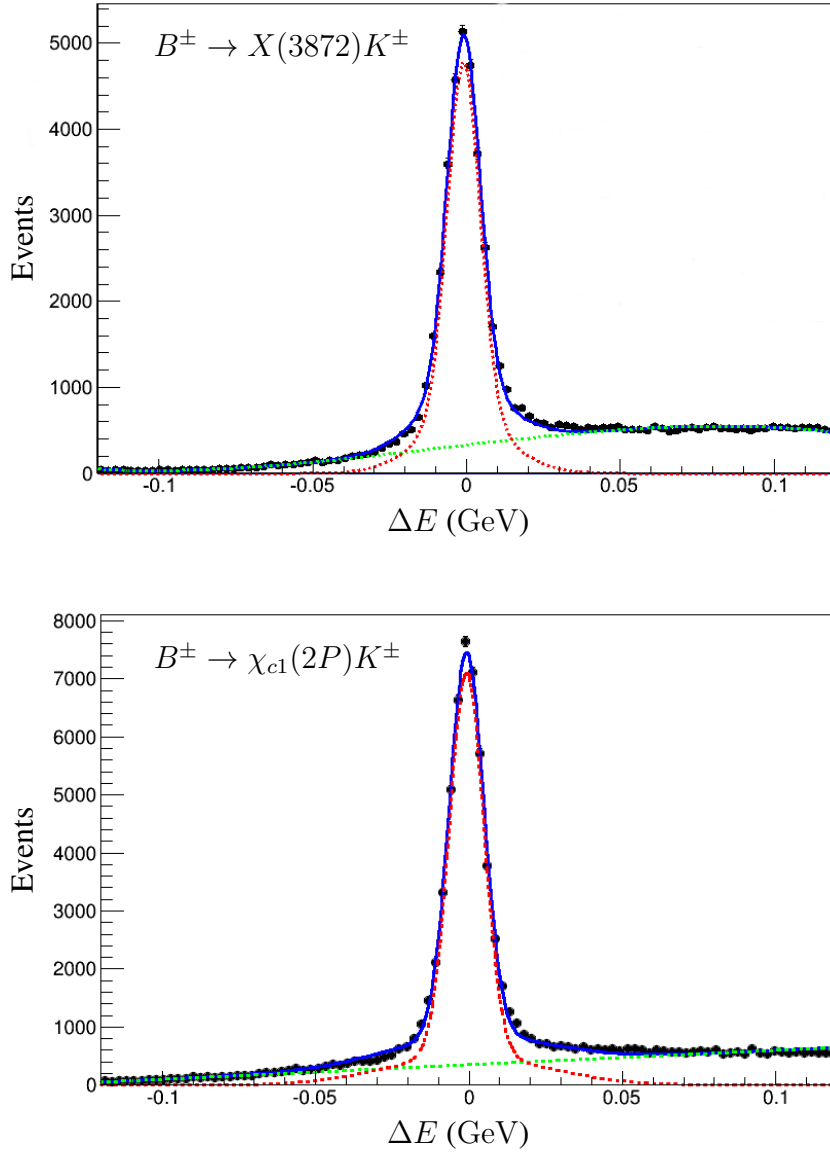
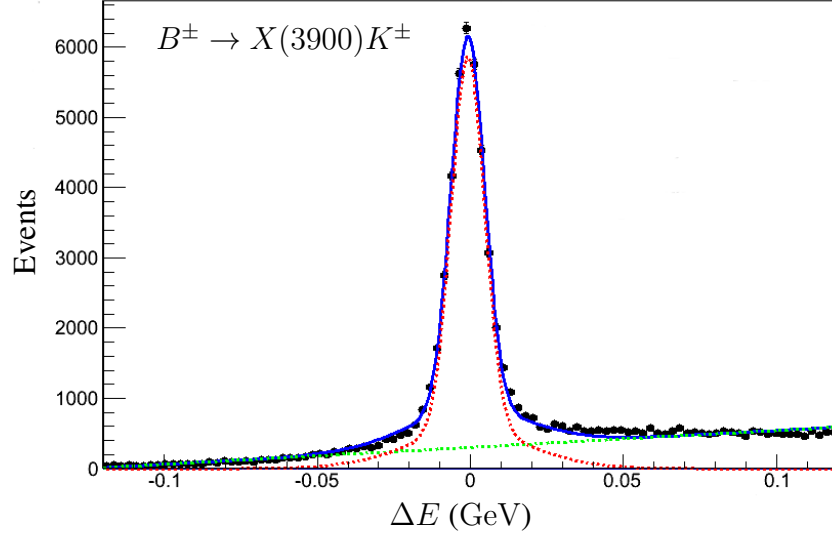


Figure 6.7.: Fitted ΔE distribution for $B^\pm \rightarrow X(3872)K^\pm$ and $B^\pm \rightarrow \chi_{c1}(2P)K^\pm$ in their respective signal MC (blue), signal part (red) and combinatorial background (green); $M_{bc} > 5.27$ GeV and BCS applied.

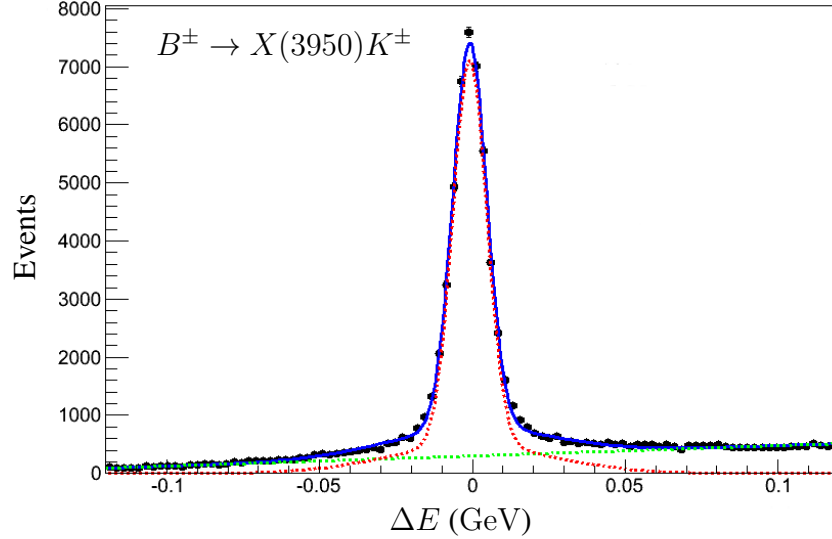
Efficiency Estimation for different Masses of an Intermediate State

Here, efficiency is defined as the peak yield extracted from the signal MC fit divided by the number of generated events. Hence, the reconstruction efficiency estimated for signal extraction in the phase space is $\varepsilon = 13.05\%$. However, the reconstruction efficiency would depend on the mass of an intermediate state.

And as this study's goal is to search for such a resonance we are especially looking at $X(3872)$ and $\chi_{c1}(2P)$ in their decays to $\chi_{c1}\pi^+\pi^-$. Respective signal MC samples have been prepared for the quasi two-body decay processes and in order for a general search for resonances, 3900, 3920 and 3950 MeV have been generated in addition to $X(3872)$. The fits to the ΔE distributions for the two other mass hypotheses, namely 3900 and 3950 MeV, can be seen in Fig(6.8).



(a) Fit of the ΔE distribution for $m_X = 3900$ MeV yields 41361 ± 271 peak events.



(b) Fit of the ΔE distribution for $m_X = 3950$ MeV yields 51841 ± 343 peak events.

Figure 6.8.: Individual fits for ΔE for masses 3900 MeV and 3950 MeV of the $\chi_{c1}\pi^+\pi^-$ system in the respective signal MC (blue), signal part (red) and combinatorial background (green); $M_{bc} > 5.27$ GeV, $|\Delta E| < 0.02$ GeV and BCS applied .

The reconstruction efficiencies are summarised in Tab(6.1). As expected, efficiency increases with the mass of the intermediate state: as the $X(3872)$ is very close to the kinematical threshold in $B^\pm \rightarrow \chi_{c1}\pi^+\pi^-K^\pm$ the Q-value is limited and therefore the transverse momentum of the pions is so small that a sizable amount of the pions are missed to be detected. As the mass of the $\chi_{c1}\pi^+\pi^-$ system increases, the pions' p_T becomes larger and thus easier to be reconstructed.

Assumed mass for X (MeV)	Efficiency (%)
3872	6.44
3900	8.27
3920	10.45
3950	10.37
PHSP	13.05

Table 6.1.: Efficiencies for phase space decay and different mass assumptions of the $\chi_{c1}\pi^+\pi^-$ system in $B \rightarrow X(\rightarrow \chi_{c1}\pi^+\pi^-)K$ extracted from their respective ΔE distributions.

This feature is taken into account to obtain the B decay branching fraction from the data as described later in Sec(7.2).

Background ΔE PDF

As seen in the previous section, only $B^\pm \rightarrow \chi_{c2}\pi^+\pi^-K^\pm$ decays form a peak in the ΔE background distribution. For this contribution, an individual fit is performed to obtain a probability density function to describe its line shape.

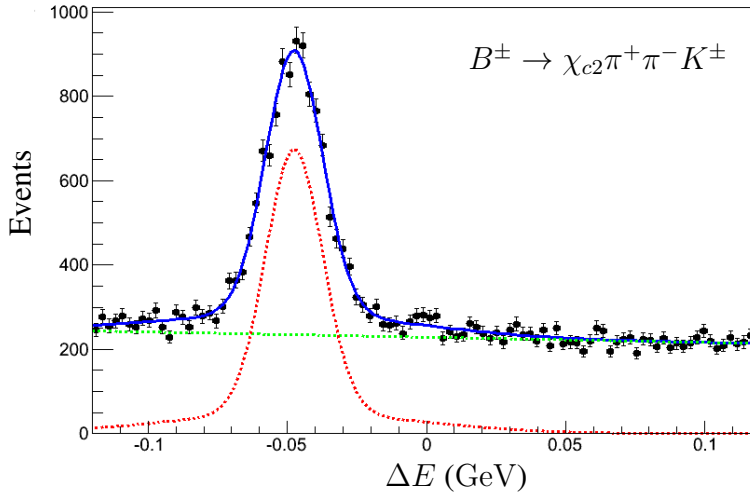


Figure 6.9.: Fit of $B \rightarrow \chi_{c2}\pi^+\pi^-K$ in the $B \rightarrow J/\psi X$ MC sample (blue), signal part (red) and combinatorial background (green); $M_{bc} > 5.27$ GeV, $|\Delta E| < 0.02$ GeV and BCS applied.

Thus the total background ΔE PDF is given by summing the following two components:

- $B \rightarrow \chi_{c2}\pi^+\pi^-K$ is parameterized by a sum of two Gaussians, see Fig(6.9),
- all other background modes have shown to be smoothly distributed in the ΔE spectrum and will be described by a first order polynomial.

The same fitting method is applied as described for the signal part of the ΔE spectrum above, compare Eqn(6.1). The optimum line shape parameters, namely the ratio of the areas of the two Gaussians as well as the ratio of their sigmas and mean and sigma, are selected.

Total PDF for the ΔE Distribution

Combining the signal and the background PDFs, the likelihood function \mathcal{L} for the fit to the ΔE distribution is expressed as:

$$\mathcal{L} = \frac{e^{-(n_{\text{peak}_1} + n_{\text{peak}_2} + n_{\text{OL}})}}{N!} \prod_{i=1}^N [n_{\text{OL}} \cdot P_{\text{OL}}(\Delta E_i) n_{\text{peak}_1} \cdot P_{\text{peak}_1}(\Delta E_i) + n_{\text{peak}_2} \cdot P_{\text{peak}_2}(\Delta E_i)]. \quad (6.3)$$

where n_{OL} and $P_{\text{OL}}(\Delta E_i)$ are the normalisation and PDF for the outlier component to express combinatorial background and misreconstructed signal due to picking up a wrong final state particle combination, n_{peak_1} and $P_{\text{peak}_1}(\Delta E_i)$ are signal yield and PDF of the peak component for the $B^\pm \rightarrow \chi_{c1}\pi^+\pi^-K^\pm$ signal, and n_{peak_2} and $P_{\text{peak}_2}(\Delta E_i)$ are the normalisation and PDF of the peaking component for the $B^\pm \rightarrow \chi_{c2}\pi^+\pi^-K^\pm$ background. As already described, $P_{\text{OL}}(\Delta E_i)$ is expressed as a first order Chebyshev polynomial and both $P_{\text{peak}_1}(\Delta E_i)$ and $P_{\text{peak}_2}(\Delta E_i)$ are formulated by a sum of two Gaussians. During the fit with this PDF to describe the overall distribution, the mean and sigma as well as signal yield of the signal peak component are floated. At the same time, all parameters are fixed for the peaking background of $B^\pm \rightarrow \chi_{c2}\pi^+\pi^-K^\pm$ except for its normalisation. The result of the final fit by MC can be seen in Fig(6.10) as a typical pseudo-experiment.

6.2.2. Fitting of the Invariant Mass Spectrum $M_{\chi_{c1}\pi\pi}$

A fitting routine for the $M_{\chi_{c1}\pi\pi}$ spectrum is prepared to search for any narrow resonance in the $\chi_{c1}\pi^+\pi^-$ final state.

$M_{\chi_{c1}\pi\pi}$ Signal Fit

The invariant mass spectrum in the $B^\pm \rightarrow X(3872)K^\pm$ signal MC is fitted with a PDF composed of

- a sum of two Gaussians for the peaking component and
- a second order Chebyshev polynomial to describe the outlier component.

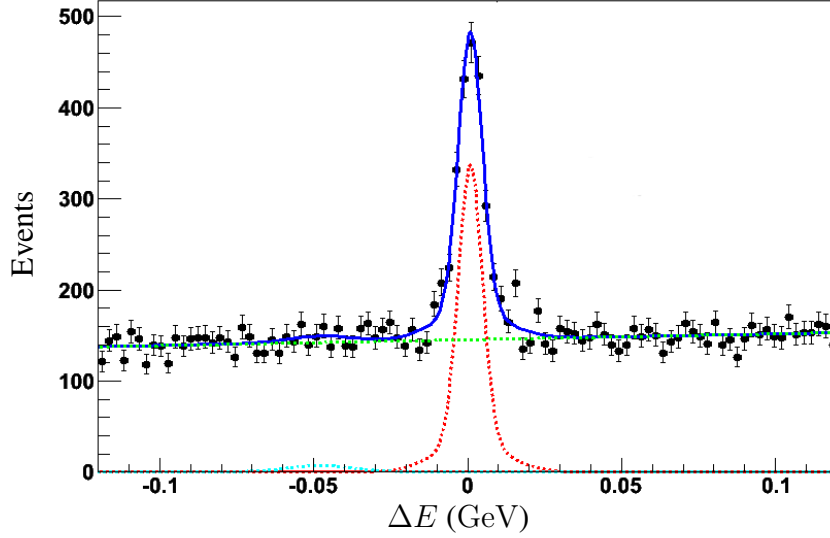


Figure 6.10.: One typical pseudo-experiment to test the complete PDF for the phase space case (blue) of ΔE distribution with mean and sigma of the $\chi_{c1}\pi^+\pi^-$ signal as well as fractions of the backgrounds floated. Each component is shown as: $B \rightarrow \chi_{c2}\pi^+\pi^-K$ (cyan), signal (red), flat background (lightgreen).

Looking at the signal enhanced region in $M_{bc} > 5.27$ GeV and $|\Delta E| < 0.02$ GeV a signal yield of 29062 ± 215 events can be extracted and translated to a reconstruction efficiency $\varepsilon = 5.81\%$ for $X(3872)$ as the intermediate state. Its signal is found at mean = 3.871 GeV with a standard deviation of 1.8MeV. A second order Chebyshev polynomial was used to describe the combinatorial background.

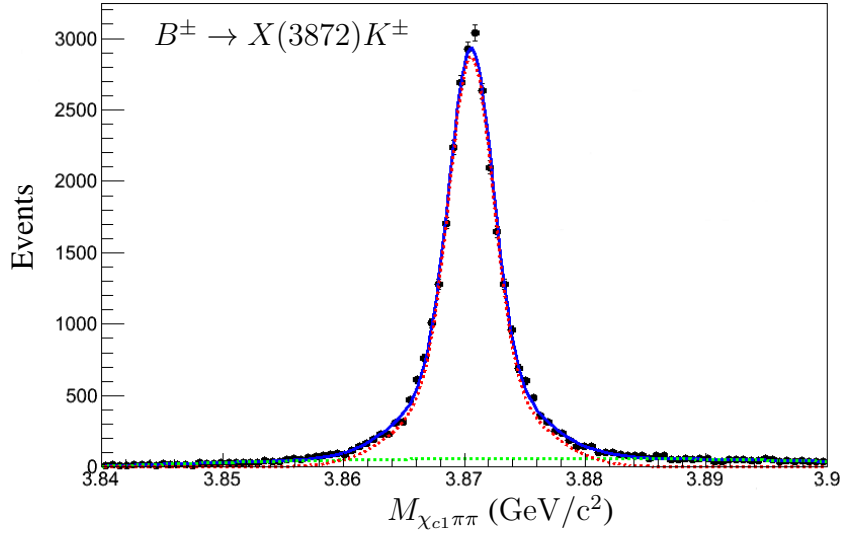


Figure 6.11.: Fitted $M_{\chi_{c1}\pi\pi}$ distribution in the $X(3872)$ signal MC (blue), signal part (red) and combinatorial background (green); $M_{bc} > 5.27$ GeV, $|\Delta E| < 0.02$ GeV and BCS applied.

Fitting the invariant mass spectrum with the $\chi_{c1}(2P)$ hypothesis, the peak component of the signal is found to be 9.31% with 46527 ± 226 signal events based on the 0.5 million generated events. The outlier component is thought to be absorbed into combinatorial background and described with a first order Chebyshev polynomial.

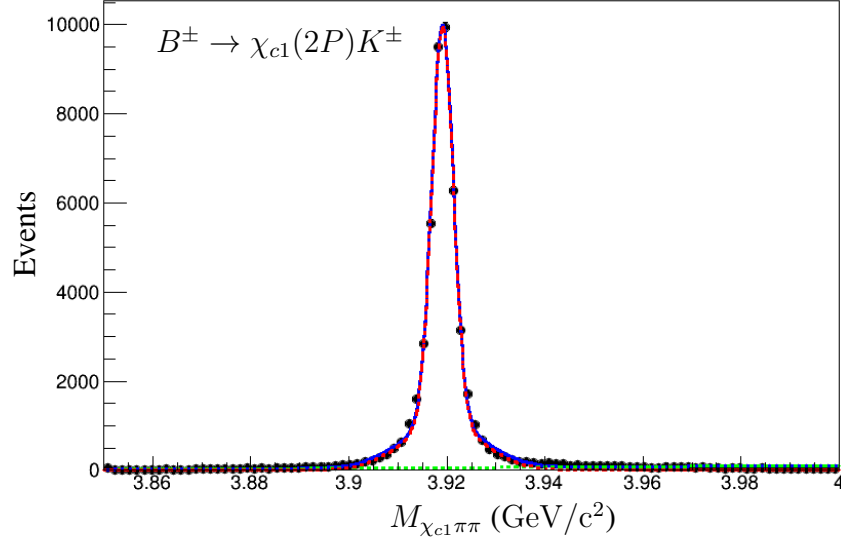


Figure 6.12.: Fitted $M_{\chi_{c1}\pi\pi}$ distribution in the $\chi_{c1}(2P)$ signal MC (blue), signal part (red) and combinatorial background (green); $M_{bc} > 5.27$ GeV, $|\Delta E| < 0.02$ GeV and BCS applied.

The reconstruction efficiencies in the $M_{\chi_{c1}\pi\pi}$ spectrum as a function of the intermediate state's mass are summarised in Tab(6.2).

Assumed $M_{\chi_{c1}\pi\pi}$ (MeV)	Efficiency (%)
3872	5.81
3920	9.31

Table 6.2.: Efficiencies for phase space decay and different mass assumptions of the $\chi_{c1}\pi^+\pi^-$ system in $B \rightarrow X(\rightarrow \chi_{c1}\pi^+\pi^-)K$ extracted from their respective $M_{\chi_{c1}\pi^+\pi^-}$ distributions.

Expected Signal Yield in the $M_{\chi_{c1}\pi\pi}$ Distribution in the $X(3872)$ Case

To make an estimation for how many events can be expected under the $X(3872)$ hypothesis, we assume the branching ratio $\mathcal{B}(X(3872) \rightarrow \chi_{c1}\pi^+\pi^-)$ to be similar to the branching $\mathcal{B}(X(3872) \rightarrow J/\psi\pi^+\pi^-)$, then roughly 15 events can be expected in data.

$$\begin{aligned}
& N_{B\bar{B}} \times \mathcal{B}(B \rightarrow X(3872)(\rightarrow \chi_{c1}\pi^+\pi^-)K) \times \mathcal{B}(\chi_{c1} \rightarrow J/\psi\gamma) \times \mathcal{B}(J/\psi \rightarrow l^+l^-) \times \varepsilon \\
&= 771.581 \cdot 10^6 \times 8 \cdot 10^{-6} \times 0.344 \times (0.0593 + 0.0594) \times 0.0581 \\
&\approx 15 \text{ events}
\end{aligned}$$

Background Fit for $M_{\chi_{c1}\pi\pi}$

The background distribution for the invariant mass spectrum of $\chi_{c1}\pi^+\pi^-$ is obtained from the $B \rightarrow J/\psi X$ MC sample. It is described best by a third order threshold function, where m_{Th} is the threshold and m_x the value of $M_{\chi_{c1}\pi\pi}$,

$$a \cdot (m_x - m_{Th})^{\frac{1}{2}} + b \cdot (m_x - m_{Th})^{\frac{3}{2}} + c \cdot (m_x - m_{Th})^{\frac{5}{2}}.$$

As shown in Fig(6.13), this parametrisation is found to be capable to describe the $M_{\chi_{c1}\pi\pi}$ distribution in a non-resonant case.

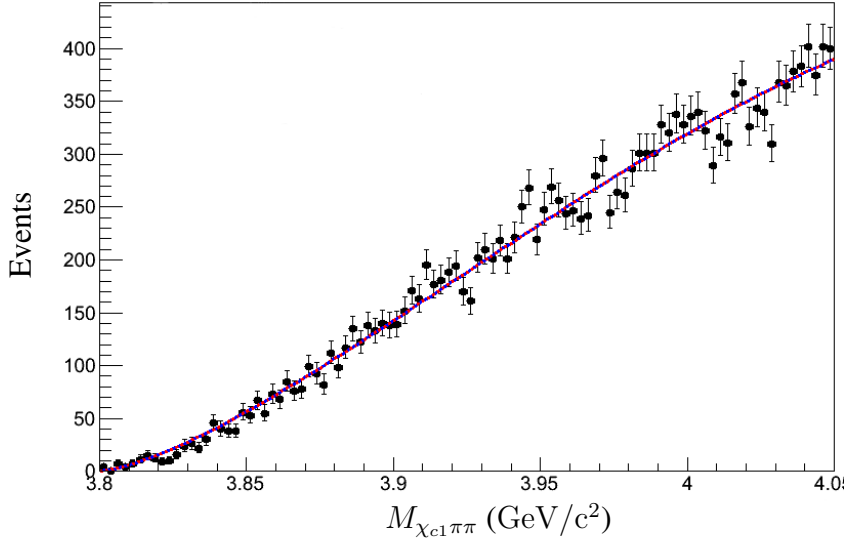


Figure 6.13.: Fit of $M_{\chi_{c1}\pi\pi}$ in the $B \rightarrow J/\psi X$ MC sample (blue) and signal part (red); $M_{bc} > 5.27$ GeV, $|\Delta E| < 0.02$ GeV and BCS applied.

Total Probability Density Function for the $M_{\chi_{c1}\pi\pi}$ Distribution in the $X(3872)$ Case

To describe the overall distribution we use a PDF where the signal part is modelled by the sum of two Gaussians with the mean and standard deviation fixed due to the small expected signal yield. The signal yield itself is floated though. All parameters for the background which is described by a third order threshold function are floated as well.

The number of background events from the $B \rightarrow J/\psi X$ MC sample has been scaled down to match data - the original $B \rightarrow J/\psi X$ MC sample contains $100\times$ the amount of data events. The result of the final fit can be seen in Fig(6.14).

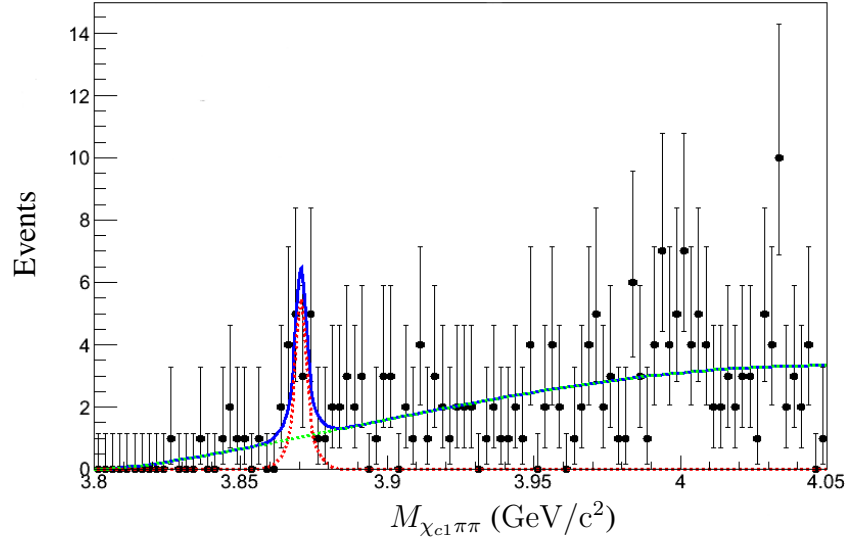


Figure 6.14.: One typical pseudo-experiment assuming that $\mathcal{B}(X(3872) \rightarrow J/\psi\pi^+\pi^-) = \mathcal{B}(X(3872) \rightarrow \chi_{c1}\pi^+\pi^-)$ to test the complete PDF for the $X(3872)$ case (blue) of $M_{\chi_{c1}\pi\pi}$ distribution with fractions of the signal and all background parameters floated. The components are shown as signal (red) and flat background (lightgreen).

The reliability of the fitting procedure for both, the ΔE and $M_{\chi_{c1}\pi\pi}$ distributions has been confirmed in a linearity test using a Toy MC sample. For ΔE , 2000 pseudo-experiments were generated for each dataset at seven different input signal yields between 800 and 2100. For $M_{\chi_{c1}\pi\pi}$, six datasets of 2000 samples each were generated with different signal yields ranging from 0 to 25. In both cases, good linearity and stability of the fitting routine was observed.

7. Results and Discussion

The fit procedure to extract a signal yield from the ΔE distribution for $B^\pm \rightarrow \chi_{c1}\pi^+\pi^-K^\pm$ has been composed and tested in Monte Carlo datasets. Applying the fit to the data sample allows to look for the existence of this decay and if found, to obtain the branching fraction. The invariant mass spectrum is studied in the data sample and by applying the derived fitting procedures, the decays $X(3872) \rightarrow \chi_{c1}\pi^+\pi^-$ and $\chi_{c1}(2P) \rightarrow \chi_{c1}(1P)\pi^+\pi^-$ are looked for, with the goal to clarify the existence of the decays of such resonances.

7.1. ΔE Distribution

The Belle data is analysed for a sample as described in Section(4.4) and a fit to extract a B decay signal in the ΔE spectrum is performed. A sum of two Gaussians is used for the signal part. Its tail part Gaussian's shape and fraction are fixed according to the MC study PDF but the core part Gaussian's mean and sigma of the signal as well as the signal yield are floated. The background is described by a first order Chebyshev polynomial, its normalisation is floated. The possible $B^\pm \rightarrow \chi_{c2}\pi^+\pi^-K^\pm$ contamination which clusters at $\Delta E = -0.05$ GeV is also considered; the shape of this component is fixed by the MC and normalisation is floated.

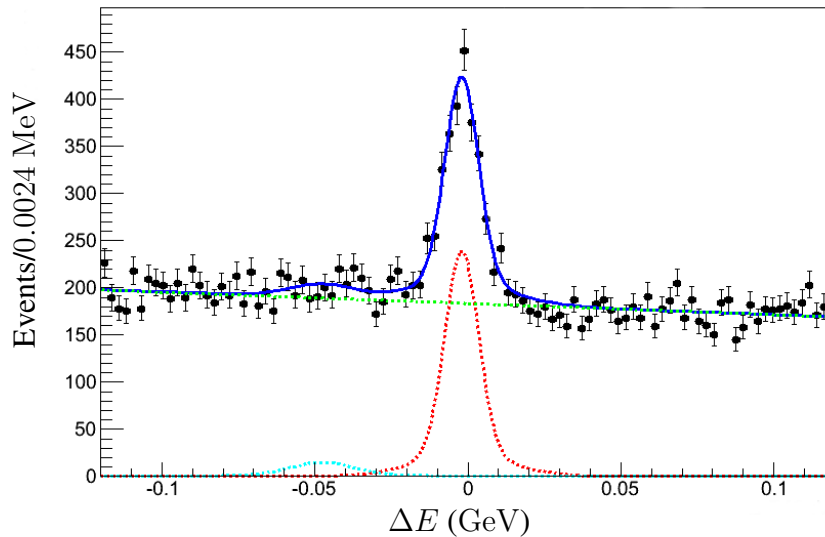


Figure 7.1.: Fit of ΔE distribution on data (blue), signal part (red) and $\chi_{c2}\pi^+\pi^-$ peaking background (cyan), combinatorial background (green); $M_{bc} > 5.27$ GeV, $|\Delta E| < 0.12$ GeV and BCS applied.

The $B^\pm \rightarrow \chi_{c1}\pi^+\pi^-K^\pm$ decay signal yield is found to be 1597 ± 76 events. The statistical significance is 29.6σ . It was obtained in a likelihood ratio test that is used to compare the fit of two models: the null model is a special case and assumes no signal, while the alternative model is represented by the fit above. The fit's quality is represented by the likelihood ratio which expresses how much more likely the data is for one model than for the other. Thereby this result is consistent with the assumption about the expected signal yield made in App(C). Comparing ΔE resolutions in MC and data, they are found to be consistent within 10%: $\sigma_{data}/\sigma_{MC} = 1.18 \pm 0.068$. The $\chi_{c2}\pi^+\pi^-K$ background contributes with 196 ± 80 events.

7.2. Weighted Detection Efficiency Estimation

Now, that it is obvious that the reconstruction efficiency is a function of the invariant mass of $\chi_{c1}\pi^+\pi^-$, using a less straightforward approach to tackle the phase space decay of $B^\pm \rightarrow \chi_{c1}\pi^+\pi^-K^\pm$ becomes mandatory. The net ΔE signal yield that will be extracted from a fit to the Belle data N_{obs} is a product of the actual signal yield N_{phys} and the detection efficiency of the detector and particle identification ε :

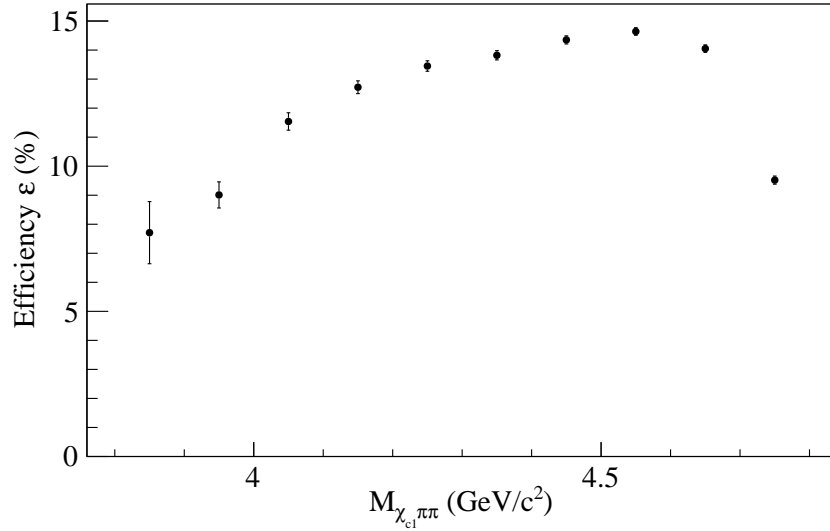
$$N_{\text{obs}} = N_{\text{phys}} \cdot \varepsilon.$$

In order to give a proper branching fraction in the long term, the number of physical events N_{phys} is desired. With the reconstruction efficiency being a function of the $\chi_{c1}\pi^+\pi^-$ invariant mass, we will weight the efficiency per mass bin $\varepsilon(i)$ with the ΔE signal yield in data per mass bin $N_{\text{obs}}(i)$ in the following way:

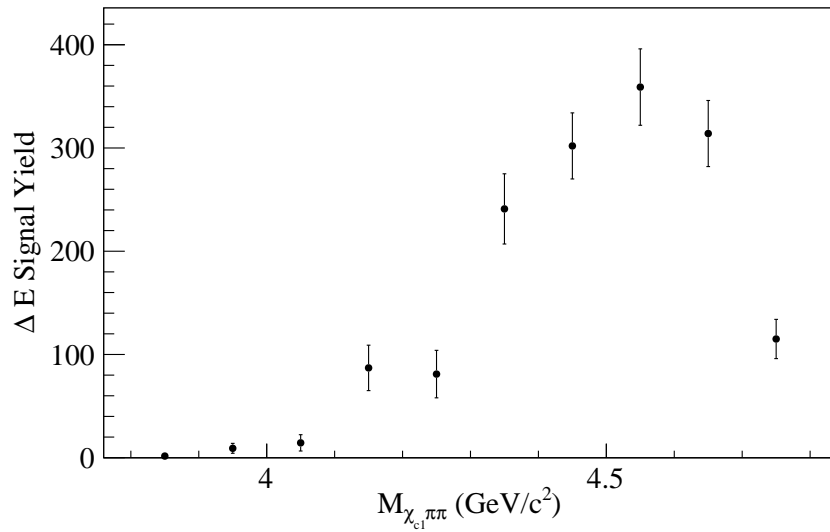
$$\varepsilon = \frac{\sum_{i=1}^{10} \varepsilon(i) \cdot N_{\text{obs}}(i)}{\sum_{i=1}^{10} N_{\text{obs}}(i)} \quad (7.1)$$

First, the signal yield in ten 100 MeV mass bins in the $M_{\chi_{c1}\pi\pi}$ spectrum in phase space signal MC is calculated. From that, the respective efficiencies $\varepsilon(i)$ are determined. Finally, a total reconstruction efficiency can be obtained by weighting with the signal yield N_{obs} in data in the same mass bins. The result for the efficiencies per mass bin can be seen in Fig(7.2a), the ΔE signal yields used for weighting in Fig(7.2b).

Through this method a resultant reconstruction efficiency of $\varepsilon = 13.41\%$ is obtained for the phase space case, compared to the formerly gained 13.05% without weighting.



(a) Reconstruction efficiencies from phase space signal MC.



(b) ΔE signal yield in data.

Figure 7.2.: Weighted detection efficiency for ten bins of $M_{\chi_{c1}\pi\pi}$.

7.3. Efficiency Correction and Systematic Uncertainty

Systematic uncertainty needs to be considered when one does not exactly know the dimensions of the errors that come along with the use of Monte Carlo datasets, imperfect particle identification on other typical measurements. The following methods describe the estimation of the correction to the reconstruction efficiency caused by this kind of possible differences, for example between data and MC.

Number of B Mesons

The official number of B mesons coming from the decay of $\Upsilon(4S)$ recorded by Belle is given with $(771.581 \pm 10.566) \times 10^6$. It is determined by counting the recorded hadronic events and the event shape variables' distributions to separate continuum and $B\bar{B}$ events. Due to the uncertainty on this number a systematic uncertainty of 1.37% is taken into account.

Tracking Efficiency

Track finding efficiency has been measured by the number of partially and fully reconstructed D^* decays in $D^* \rightarrow \pi D^0$, with $D^0 \rightarrow \pi\pi K_S^0$ and $K_S^0 \rightarrow \pi^+\pi^-$. By calculating the ratio of tracking efficiency in data and MC, the systematic uncertainty associated with tracking has also been evaluated. That study's results present $(-0.13 \pm 0.30 \pm 0.10)\%$ per track [21], where a systematic uncertainty of 0.10% is given for particles with momentum higher than 200 MeV. It was also found that tracking charge asymmetry is negligible in data while giving $(-0.52 \pm 0.20)\%$ in MC. In this analysis, we do not apply a correction to the reconstruction efficiency as the deviation is small. As a conservative estimation, the central value and the statistical and systematic errors are summed in quadrature to be 0.342% per track. This thesis' targeted final state contains five charged particles, and as the tracks are correlated the uncertainties from each track are added linearly. Consequently, $0.342 \times 5 = 1.71\%$ is assigned.

Electron ID Efficiency

The electron identification efficiency correction which can arise as a potential difference between data and MC needs to be estimated. The efficiency correction and its uncertainty have been determined by investigating the ratio of single and double tag yields in data and MC using a $J/\psi \rightarrow e^+e^-$ mode. The correction is estimated to be 0.9755, with an uncertainty of 0.0042 which will be considered as 0.43% per $J/\psi \rightarrow e^+e^-$ decay in the systematic uncertainty.

Muon ID Efficiency

To determine the muon identification efficiency correction and its contribution to the systematic uncertainty, $e^+e^- \rightarrow e^+e^-\mu^+\mu^-$ events as well as $J/\psi \rightarrow \mu^+\mu^-$ decays are used. The efficiency correction and its uncertainty are separately checked for positively and negatively charged muons and the variation depending on the experimental periods are considered. A weighted average of those results gives 0.9654 as the efficiency correction and 0.0299 as its uncertainty per $J/\psi \rightarrow \mu^+\mu^-$ decay.

The contribution from electrons and muons is averaged. In conclusion, the combined lepton identification systematic uncertainty is 1.77%.

Kaon and Pion ID Efficiency

For kaon and pion identification efficiency corrections due to differences between data and MC, estimations are made based on a $D^{*+} \rightarrow D^0(K^-\pi^+)\pi_{\text{slow}}^+$ process. Similar to the muon identification case, variation depending on experimental periods are checked and the weighted average gives 1.0119 ± 0.0124 for kaon identification correction and its error which will be considered as 1.23% in the systematic uncertainties.

For pions, the identification efficiency correction and its error are determined by the same process as kaons. As a $\pi^+\pi^-$ pair has to be considered in the final state, the efficiency correction is 0.9798 with its error being 0.0192 per $\pi^+\pi^-$ pair. This corresponds to a systematic uncertainty of 1.96%.

π^0 Veto

In the event selection for the reconstruction of χ_{c1} candidates a π^0 veto is used in order to reject background photons coming from π^0 decays. This systematic uncertainty is estimated by obtaining the ratio of ΔE signal yield when using the cut, Y_w , and without using the cut, Y_{wo} , for data and Monte Carlo, and then dividing those in a double ratio:

$$R\left(\frac{\text{data}}{\text{MC}}\right) = \frac{(Y_w/Y_{wo})^{\text{data}}}{(Y_w/Y_{wo})^{\text{MC}}}.$$

Based on this conservative approach, the difference between the efficiency in data and MC due to the π^0 veto has been estimated to be 1.22%.

Probability Density Functions

When extracting the signal yield, a fit to the data is performed which is described by a set of parameters. The possible influence of this modeling can be estimated by varying the fixed parameters by $\pm 1\sigma$. The resultant variation of the respective ΔE signal yield of each parameter change is added in quadrature. This systematic uncertainty for the B decay branching fraction is estimated to be 2.96%.

Signal MC Sample Statistics

The extraction of the uncorrected detection efficiency ε by fitting the ΔE distribution in signal MC bears a systematic uncertainty due to the finite number of statistical generated events. This contribution is found to be 0.51%.

Secondary Branching Fraction

For calculating the branching fraction of $B \rightarrow \chi_{c1}\pi^+\pi^-K$ branching fractions of secondary decays as $\chi_{c1} \rightarrow J/\psi\gamma$ and $J/\psi \rightarrow \ell^+\ell^-$ given by the PDG are used [58]. Those secondary decays' uncertainties are considered as part of the systematic uncertainty in obtaining $\mathcal{B}(B^+ \rightarrow \chi_{c1}\pi^+\pi^-K^+)$: $\mathcal{B}(\chi_{c1} \rightarrow J/\psi\gamma) = (34.8 \pm 1.5)\%$ and $\mathcal{B}(J/\psi \rightarrow \ell^+\ell^-) = (11.87 \pm 0.08)\%$ show an uncertainty themselves. Adding them in quadrature amounts to 1.50%.

The total correction to the efficiency is given as $corr(\varepsilon) = \prod_n corr_n$, with averaged lepton ID, kaon and pion ID contributing, and will be considered with a factor 0.9622.

Therefore, the efficiency difference between data and the MC simulation is less than 4.0%. A corrected resultant reconstruction efficiency of $13.41\% \times 0.9622 = 12.90\%$ is acquired for $B^\pm \rightarrow \chi_{c1}\pi^+\pi^-K^\pm$.

The systematic uncertainty from each source sums up in quadrature to its final total value of 5.10%. Tab(7.1a) summarises all contributions to the systematic uncertainty estimated by the methods described above.

variable	uncertainty (%)	Parameter	Value
PDF	2.96	N_{sig}	1597 ± 76
pion ID	1.96	ε_{det}	12.90%
lepton ID	1.77	$\mathcal{B}(\chi_{c1} \rightarrow J/\psi\gamma)$	$(34.8 \pm 1.5)\%$
tracking	1.71	$\mathcal{B}(J/\psi \rightarrow e^+e^-)$	$(5.94 \pm 0.06)\%$
2ndary BF	1.50	$\mathcal{B}(J/\psi \rightarrow \mu^+\mu^-)$	$(5.93 \pm 0.06)\%$
$N_{B\bar{B}}$	1.37	$N_{B\bar{B}}$	$(772 \pm 11) \times 10^6$
kaon ID	1.23		
π^0 veto	1.22		
signal MC	0.52		
total	5.10		

(a) Summary of systematic uncertainties. (b) Summary of values used in calculating the branching ratio.

Table 7.1.: Parameters and their values.

7.4. Branching Fraction of $B^\pm \rightarrow \chi_{c1}\pi^+\pi^-K^\pm$

The branching fraction of the decay is then calculated as follows:

$$\mathcal{B}(B^+ \rightarrow \chi_{c1}\pi^+\pi^-K^+) = \frac{N_{\text{sig}}}{\varepsilon_{\text{det}} \times \mathcal{B}(\chi_{c1} \rightarrow J/\psi\gamma) \times \mathcal{B}(J/\psi \rightarrow \ell^+\ell^-) \times N_{B\bar{B}}},$$

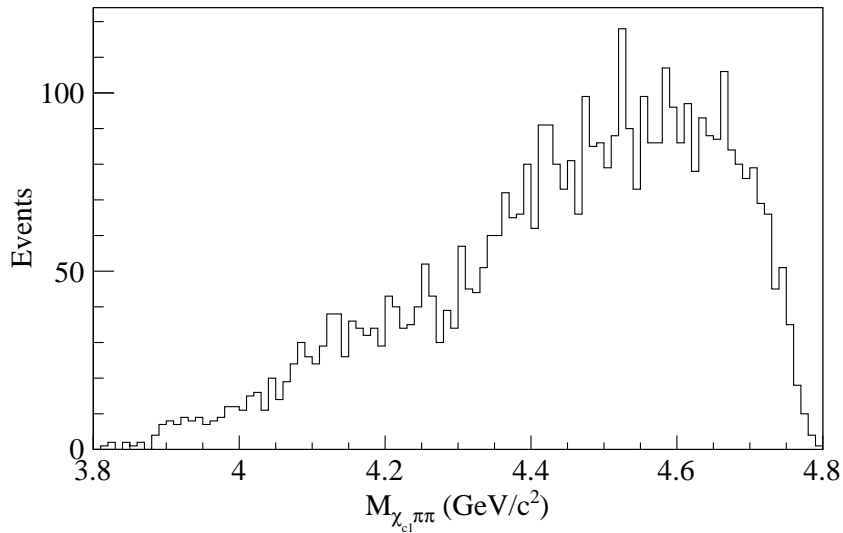
where N_{sig} is the signal yield, $N_{B\bar{B}}$ the number of $B\bar{B}$ pairs and \mathcal{B} the secondary branching ratios including $\mathcal{B}(J/\psi \rightarrow \ell^+\ell^-) = [\mathcal{B}(J/\psi \rightarrow e^+e^-) + \mathcal{B}(J/\psi \rightarrow \mu^+\mu^-)]$. The respective values used in calculating the branching fraction are summarised in Tab(7.1b).

We find the branching ratio of $B^\pm \rightarrow \chi_{c1}\pi^+\pi^-K^\pm$ to be 3.89×10^{-4} ; including statistical and systematic uncertainties, as derived in Sec(7.3), the final result is:

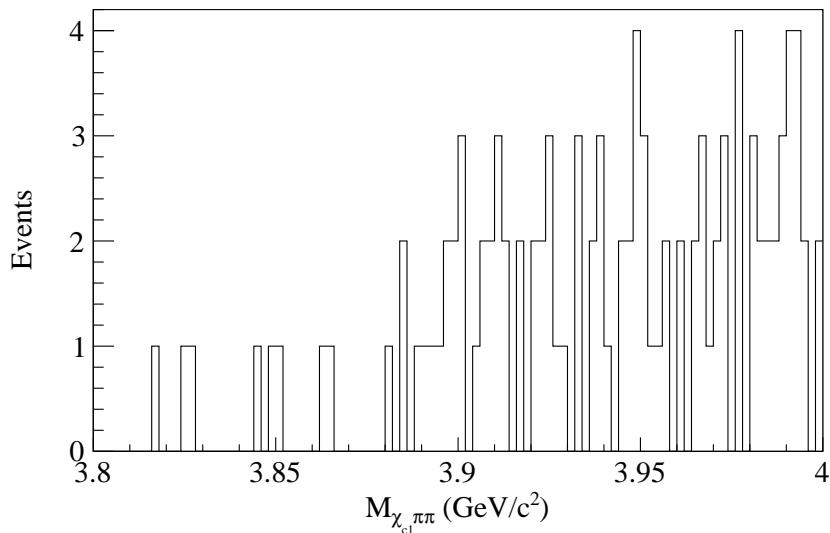
$$\mathcal{B}(B^+ \rightarrow \chi_{c1}\pi^+\pi^-K^+) = (3.89 \pm 0.19 \text{ (stat)} \pm 0.20 \text{ (syst)}) \times 10^{-4}.$$

7.5. $\chi_{c1}\pi^+\pi^-$ Invariant Mass Spectrum

The invariant mass of $\chi_{c1}\pi^+\pi^-$ is studied with the data sample and an intermediate charmonium-like state is looked for. In the signal enhanced window of $M_{bc} > 5.27$ GeV and $|\Delta E| < 0.02$ GeV no distinguished structure is showing at the masses of interest, 3872 MeV for the $X(3872)$ or 3920 MeV for the $\chi_{c1}(2P)$.



(a) $M_{\chi_{c1}\pi^+\pi^-}$ on data; whole kinematic range.



(b) $M_{\chi_{c1}\pi^+\pi^-}$ on data; region of interest.

Figure 7.3.: Invariant mass distribution of $\chi_{c1}\pi^+\pi^-$ on data; $M_{bc} > 5.27$ GeV, $|\Delta E| < 0.02$ GeV and BCS applied.

7.6. Upper Limit for $X(3872)$ decaying to $\chi_{c1}\pi^+\pi^-$

The relevant $\chi_{c1}\pi^+\pi^-$ invariant mass spectrum around 3871 MeV is shown in Fig(7.4). A 3σ region is defined from the $X(3872) \rightarrow \chi_{c1}\pi^+\pi^-$ signal MC and in this signal region we find zero events. Including sideband regions, we found 60 events from 3.8 to 4.0 GeV.

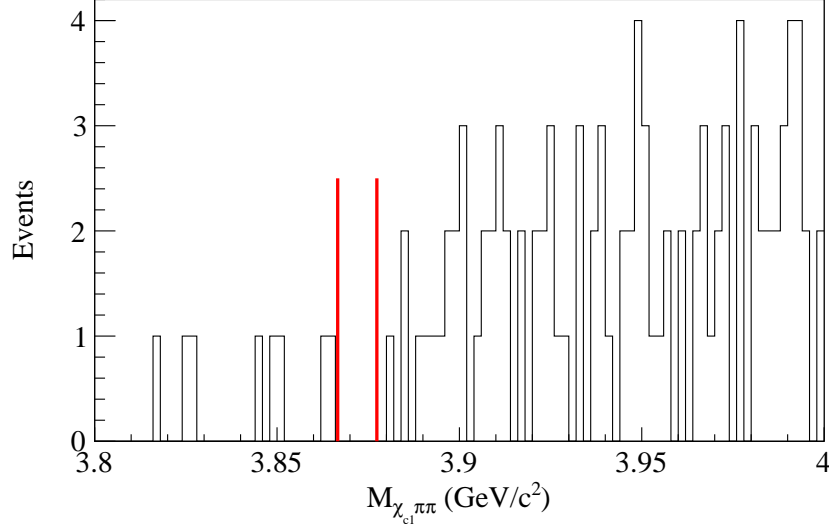


Figure 7.4.: Invariant mass distribution of $\chi_{c1}\pi^+\pi^-$ in data with 3σ signal region marked by the red lines; $M_{bc} > 5.27$ GeV, $|\Delta E| < 0.02$ GeV and BCS applied.

Because of the very limited statistics around the search window, proper convergence of the UML fit could not be realized in the $M_{\chi_{c1}\pi\pi}$ distribution to look for a potential $X(3872)$ contribution. Instead, the signal yield upper limit is estimated by counting events with featuring an approach based on the work of Feldman and Cousins [36]. As there is no signal, the number of background events in the signal region is assumed to be zero as well. From the Figure and Table provided by [36] that can be found in App(D), one obtains 2.44 events as an upper limit at 90% C.L.. Taking into account the 5.1% systematic uncertainty, 2.56 events are regarded as the proper upper limit.

Thus an upper limit of the product of branching fractions, including both statistical and systematic uncertainties is found to be

$$\mathcal{B}(B^\pm \rightarrow X(3872) K^\pm) \times \mathcal{B}(X(3872) \rightarrow \chi_{c1}(1P)\pi^+\pi^-) < 1.4 \times 10^{-6} @ 90\% \text{ C.L..}$$

The values used in calculating the branching fraction are the same as in Tab(7.1b) but for the number of signal events $N_{\text{sig}} = 2.56$ and the efficiency $\varepsilon_{\text{det}} = 5.59\%$.

7.7. Upper Limit for $\chi_{c1}(2P)$ decaying to $\chi_{c1}(1P)\pi^+\pi^-$

In case of a possible decay of $\chi_{c1}(2P) \rightarrow \chi_{c1}(1P)\pi^+\pi^-$ the invariant mass spectrum of $\chi_{c1}(1P)\pi^+\pi^-$ is searched for a signature around the predicted $\chi_{c1}(2P)$ mass at 3920 MeV.

The $\chi_{c1}(2P)$ signal in the $M_{\chi_{c1}\pi\pi}$ spectrum is expressed by a PDF composed as a convolution of a Breit-Wigner function with a Gaussian. The width of the Breit-Wigner is chosen as 20 MeV based on the assumptions made in Sec(3.1.1) when comparing with the already discovered $\chi_{c0}(2P)$ and $\chi_{c2}(2P)$ states. 2 MeV are assumed for the Gaussian's standard deviation to represent detector mass resolution; they were obtained from the signal MC fits with a very narrow resonance at 3920 MeV.

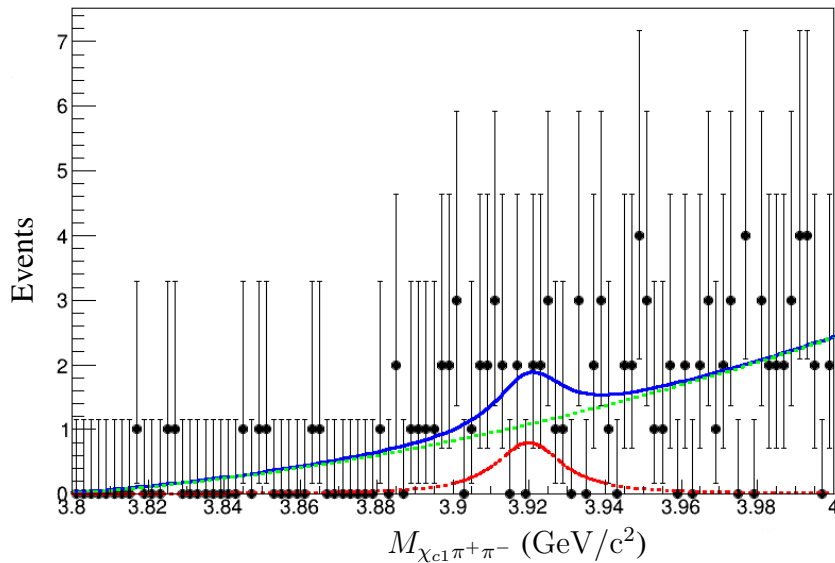


Figure 7.5.: Fit of the invariant mass distribution of $\chi_{c1}\pi^+\pi^-$ on data (blue), signal part (red) and combinatorial background (green); $M_{bc} > 5.27$ GeV, $|\Delta E| < 0.02$ GeV and BCS applied.

The fit result to the experimental data can be seen in Fig(7.5). A signal yield of 12.2 ± 9.1 events can be extracted. As the significance is not sufficient to quote an evidence, a product branching fraction upper limit is presented. Including statistical and systematic uncertainties as well as considering the 90% confidence level, the number of observed signal events amounts to 30.34 events. The derived upper limit is found to be:

$$\mathcal{B}(B^\pm \rightarrow \chi_{c1}(2P)K^\pm) \times \mathcal{B}(\chi_{c1}(2P) \rightarrow \chi_{c1}(1P)\pi^+\pi^-) < 1.1 \times 10^{-5} @ 90\% \text{ C.L.}$$

The values used in calculating the branching fraction are the same as in Tab(7.1b) but for the number of signal events $N_{\text{sig}} = 30.34$ and the efficiency $\varepsilon_{\text{det}} = 8.91\%$.

8. Conclusion

The exploration of the quark potential led us to study the spectra of heavy quarkonia, especially the charmonium system $c\bar{c}$. While many states have been measured with high precision and were found to obey the Standard Model predictions, some states above the open-charm threshold could not yet be seen. Furthermore, new resonances with unusual exotic quantum numbers have shown up and are waiting to be studied for their structure and nature to become known.

The Belle experiment at the KEK B factory discovered many of those charmonium-like exotic hadrons. Among those, the exotic $X(3872)$ was first observed in the charged B meson decay $B^+ \rightarrow X(3872)K^+$ followed by $X(3872) \rightarrow J/\psi\pi^+\pi^-$ by the Belle Collaboration in 2003. This resonance has a much smaller width, $\Gamma < 1.2$ MeV at 90% C.L., than other charmonia above the open-charm threshold. Its mass is very close to the threshold of the charmed meson pair $D^0\bar{D}^{*0}$ and its quantum numbers were finally pinned down to be $J^{PC} = 1^{++}$. Furthermore, not finding a charged partner suggests isospin zero. All this concluded in many speculations about the nature of this well established but puzzling state. By now, an admixture of a $D^0\bar{D}^{*0}$ molecule and a conventional charmonium, most likely the still undiscovered $\chi_{c1}(2P)$, is one of the most plausible hypotheses. However, the little energy that is left for the molecule's binding energy can be translated to a distance between the two D mesons and implies a size of about a few fm. This seems too large to explain the significant branching to J/ψ . The mass prediction for $\chi_{c1}(2P)$ is around 3920 MeV and this member of the $\chi_{cJ}(2P)$ spin triplet has yet to be seen. Even if $X(3872)$ does not contain a $\chi_{c1}(2P)$ component, a significant branching of $\chi_{c1}(2P)$ to the $\chi_{c1}\pi^+\pi^-$ final state can be expected, just like $\psi' \rightarrow J/\psi\pi^+\pi^-$ is one of the major decay modes. Considerations as to its width by comparing with the recently established $\chi_{c0}(2P)$ and $\chi_{c2}(2P)$ states leads to assuming a possibly relatively broad resonance with $\Gamma \approx 20$ MeV. Summarising the statements above, the $M_{\chi_{c1}\pi\pi}$ distribution in still to be measured $B^\pm \rightarrow \chi_{c1}\pi^+\pi^-K^\pm$ decay is also a suitable source to look for a signature and clarify the existence of the decays of such resonances.

The results presented in this thesis are based on a total of 772×10^6 $B\bar{B}$ events accumulated at the $\Upsilon(4S)$ resonance collected by the Belle detector at the KEKB asymmetric-energy e^+e^- collider. Charged pions and kaons were selected using the combined information from tracking and particle identification sub-detectors. Their identification is based upon a likelihood ratio. Due to the small Q-value in case of $X(3872)$ and $\chi_{c1}(2P)$ decaying to $\chi_{c1}\pi^+\pi^-$ additional selection criteria for pions with low transverse momentum became necessary to reduce fake tracks and improve multiplicity. J/ψ candidates were reconstructed from their di-lepton decay mode and paired with a photon to form χ_{c1} . By combining the $\chi_{c1}\pi^+\pi^-$ system with a charged kaon, B meson candidates were reconstructed.

The kinematic variables of interest, the beam-constrained mass M_{bc} and the difference-to-beam energy ΔE are defined in the $\Upsilon(4S)$ rest frame. The signal extraction region was determined to be in $|\Delta E| < 0.12$ GeV and $M_{bc} > 5.27$ GeV. A best candidate selection was applied in case of multiple B candidates per event based on closest mass compared to the nominal B mass.

Using Monte Carlo samples of 0.5 million events each for the four-body phase space case and the quasi two-body cases with hypothetical intermediate states decaying to $\chi_{c1}\pi^+\pi^-$ possible contributions to the background have been estimated. The dominant background for $B^\pm \rightarrow \chi_{c1}\pi^+\pi^-K^\pm$ decays was expected to come from those B decays with a real $J/\psi \rightarrow \ell^+\ell^-$ in their final state. A large $B \rightarrow J/\psi X$ Monte Carlo sample exposed that $B^\pm \rightarrow \chi_{c2}\pi^+\pi^-K^\pm$ only has a small contribution to form a peak in the ΔE projection; all other backgrounds have shown to be smooth. In the invariant mass spectrum of $\chi_{c1}\pi^+\pi^-$ the only peaking component is found to be a reflection from ψ' which was left untreated since ψ' is not interfering with the mass region of interest corresponding to the $X(3872)$ mass or the $\chi_{c1}(2P)$ mass at 3920 MeV. A fitting routine for ΔE and $M_{\chi_{c1}\pi\pi}$ has been obtained by composing the respective Probability Density Functions and was tested in toy Monte Carlo studies. The reconstruction efficiency has been calculated as a function of the invariant mass of the intermediate state and probable signal yields have been estimated. These and the study about contributions to the systematic uncertainty were used to obtain a branching ratio and upper limits.

The $B^\pm \rightarrow \chi_{c1}\pi^+\pi^-K^\pm$ signal yield is extracted from an unbinned maximum likelihood fit to the ΔE distribution. We made a first observation of the decay $B^\pm \rightarrow \chi_{c1}\pi^+\pi^-K^\pm$ with a statistical significance of 29.6σ . The signal yield reconstructed in data is 1597 ± 76 events and very well comparable to the expected signal yield of 1700 events. We find the ΔE resolution to be consistent with the Monte Carlo expectation. The B decay branching fraction has been measured to be

$$\mathcal{B}(B^+ \rightarrow \chi_{c1}\pi^+\pi^-K^+) = (3.89 \pm 0.19 \text{ (stat)} \pm 0.20 \text{ (syst)}) \times 10^{-4}.$$

In order to identify a new $X(3872)$ decay mode and a still unseen $\chi_{c1}(2P)$, the $\chi_{c1}\pi^+\pi^-$ invariant mass spectrum has been studied. Under a plausible assumption concerning branching ratios, the signal was expected to be in this study's sensitivity range about 15 or more events. However, the data exhibits no signature.

Consequently, an upper limit for the exotic $X(3872)$ charmonium-like state to decay to $\chi_{c1}\pi^+\pi^-$ has been calculated for the first time using the method of Feldman and Cousins including both statistical and systematic uncertainties which we report with

$$\mathcal{B}(B^\pm \rightarrow X(3872)K^\pm) \times \mathcal{B}(X(3872) \rightarrow \chi_{c1}(1P)\pi^+\pi^-) < 1.4 \times 10^{-6} @ 90\% \text{ C.L.},$$

Comparison with its sibling triplet states and well thought out assumptions about the properties of the still undiscovered conventional charmonium $\chi_{c1}(2P)$ following a mass assumption of 3920 MeV led to a preliminary upper limit with

$$\mathcal{B}(B^\pm \rightarrow \chi_{c1}(2P)K^\pm) \times \mathcal{B}(\chi_{c1}(2P) \rightarrow \chi_{c1}(1P)\pi^+\pi^-) < 1.1 \times 10^{-5} @ 90\% \text{ C.L..}$$

These results are compatible with and favour the interpretation of $X(3872)$ as an admixture state of a $D^0\bar{D}^{*0}$ molecule and a conventional state which might be the suspicious and maybe not so conventional $\chi_{c1}(2P)$. In [66], Takizawa et al. investigate $X(3872)$ as a charmonium-hadronic molecule hybrid suggesting a scenario of a $c\bar{c}$ core state coupling to the $D^0\bar{D}^{*0}$ and D^+D^{*-} molecular states. This model is capable of explaining many of the observed properties of the $X(3872)$, such as its large isospin symmetry breaking, the strangely high production rate in $p\bar{p}$ collisions when considering the size of the molecule, and the absence of a charged partner. The non-observation of the $\chi_{c1}(2P)$ resonance predicted by the quark model is explained by a strong coupling to $D\bar{D}^*$ two-meson state which results in a resonance with a very broad width - being consistent with our assumptions.

The admixture scenario for $X(3872)$ predicts other probable final states to look for a partner states. To properly see the signature of a broad admixed $X(3872)$ state, search for partner states and to fully understand its nature more statistics are needed. They will be provided by the Belle2 experiment at the next-generation flavour-factory SuperKEKB, a collider with a design luminosity of $8 \times 10^{35} \text{ cm}^{-2}\text{s}^{-1}$ which is around 50 times as large as the peak luminosity achieved by the KEKB collider. The Belle2 detector is a general purpose spectrometer to efficiently collect data of e^+e^- collisions and consists of several sub-detector components where the Time-of-Propagation counters and the ring-imaging Cherenkov counters are will replace the TOF and ACC [5,62]. The physics reach was investigated and studies at the Belle2 experiment will focus on flavour physics and CP violation measurements [7].

A. Cut Selection for π^0 Veto

A figure of merit study was performed to select the most appropriate cut value for the π^0 veto. 0.8 was chosen meaning all photons that have a probability $> 80\%$ to originate from a π^0 will be rejected and not used in the reconstruction of χ_{c1} candidates from $J/\psi\gamma$.

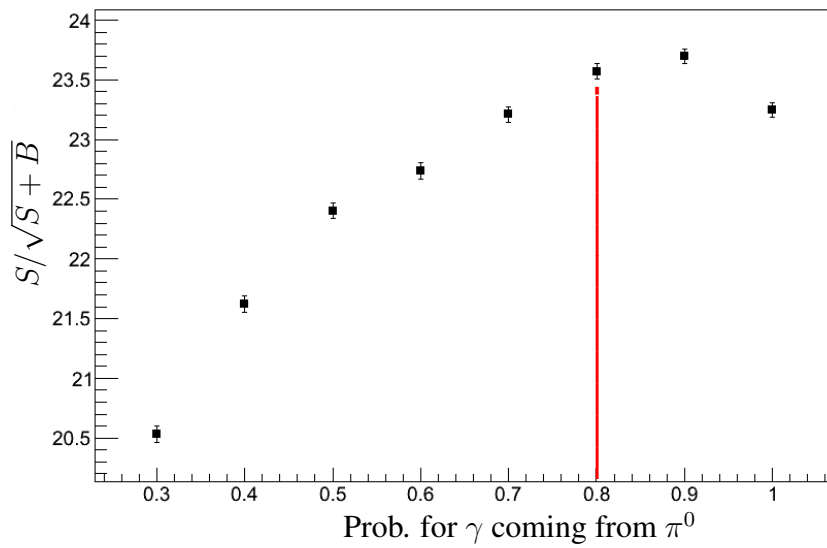


Figure A.1.: Figure of merit study to select a veto for photons coming from π^0 in the χ_{c1} candidate reconstruction.

B. Estimated ΔE Distribution in the Larger Window

There are five modes to point out when looking at $|\Delta E| < 0.2$ GeV which can be divided as follows:

- Signal: $B^\pm \rightarrow \chi_{c1} X_{\bar{s}u}$, where $X_{\bar{s}u}$ can form $\pi^+\pi^-K^\pm$ and result in the signal final state. In this case ΔE peaks at zero.
- Background: $B^\pm \rightarrow \psi' \pi^+\pi^-K^\pm$, where $\psi' \rightarrow \chi_{c1}\gamma$. The missing energy from the ψ' decay photon, compared to the signal final state, is 80 to 280 MeV, resulting in a broad bump in the negative ΔE region.
- Background: $B^\pm \rightarrow \chi_{c2} X_{\bar{s}u}$, where $X_{\bar{s}u} \rightarrow \pi^+\pi^-K^\pm$. A small peak can be seen, shifted to the negative ΔE region because of the χ_{c2} 's slightly higher mass ($\Delta m \approx 50$ MeV).
- Background: $B^\pm \rightarrow \chi_{c1} K^*$ and $B \rightarrow \chi_{c1} X_{\bar{s}d}$. If one additional, unrelated pion is added, the signal final state is faked. Here, ΔE is shifted to values > 0.15 GeV. $B^0 \rightarrow \chi_{c1} X_{\bar{s}d}$ is kinematically the same as $\chi_{c1} K^*$ when $X_{\bar{s}d} \rightarrow \pi^\mp K^\pm$ happens.

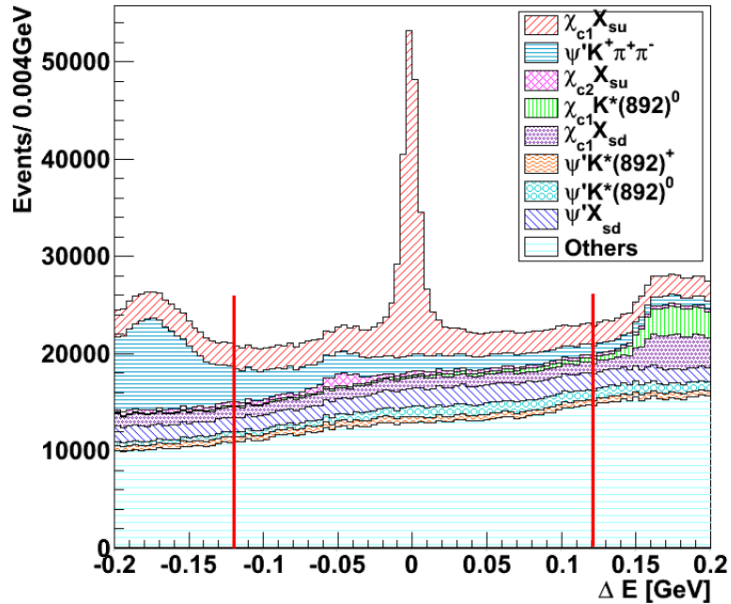


Figure B.1.: ΔE distribution on the $B \rightarrow J/\psi X$ MC sample; $M_{bc} > 5.27$ GeV and BCS applied.

C. Expected Signal Yield in the ΔE Distribution in the Phase Space

Based on the estimated efficiency ε an expected peak yield for the yet unseen $B^\pm \rightarrow \chi_{c1}\pi^+\pi^-K^\pm$ decay can be calculated assuming that it is obeying a phase space distribution:

$$\begin{aligned} N_{B\bar{B}} \times \mathcal{B}(B \rightarrow \chi_{c1}\pi^+\pi^-K) \times \mathcal{B}(\chi_{c1} \rightarrow J/\psi\gamma) \times \mathcal{B}(J/\psi \rightarrow l^+l^-) \times \varepsilon \\ = 771.6 \cdot 10^6 \times 4 \cdot 10^{-4} \times 0.344 \times (0.0593 + 0.0594) \times 0.1341 \\ \approx 1700 \text{ events} \end{aligned}$$

where, taking possible decay dynamics into account, the assumed branching fraction of $B \rightarrow \chi_{c1}\pi^+\pi^-K$ was derived from the decay of $B \rightarrow J/\psi\pi^+\pi^-K$ [58] as follows:

$$\begin{aligned} \mathcal{B}(B \rightarrow \chi_{c1}\pi^+\pi^-K) &= \mathcal{B}(B \rightarrow J/\psi\pi^+\pi^-K) \cdot \frac{\mathcal{B}(B \rightarrow \chi_{c1}K)}{\mathcal{B}(B \rightarrow J/\psi K)} \\ &= 8.1 \cdot 10^{-4} \cdot \frac{4.79 \cdot 10^{-4}}{1.02 \cdot 10^{-3}} \\ &\approx 4 \cdot 10^{-4} \end{aligned}$$

About 1700 events are expected in data when looking for the $B^\pm \rightarrow \chi_{c1}\pi^+\pi^-K^\pm$ decay in its ΔE distribution.

D. Upper Limit Calculation

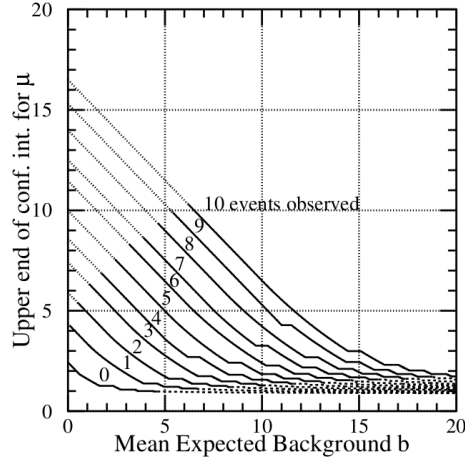


Figure D.1.: Upper end μ_2 of our 90% C.L. confidence intervals $[\mu_1, \mu_2]$, for unknown Poisson signal mean μ in the presence of expected Poisson background with known mean b . The curves for the cases n_0 from zero through ten are plotted. Dotted portions on the upper left indicate regions where μ_1 is non-zero. Dashed portions in the lower right indicate regions where the probability of obtaining the number of events observed or fewer is less than 1%, even if $\mu = 0$. [36]

$n_0 \backslash b$	0.0	0.5	1.0	1.5	2.0	2.5	3.0	3.5	4.0	5.0
0	0.00, 2.44	0.00, 1.94	0.00, 1.61	0.00, 1.33	0.00, 1.26	0.00, 1.18	0.00, 1.08	0.00, 1.06	0.00, 1.01	0.00, 0.98
1	0.11, 4.36	0.00, 3.86	0.00, 3.36	0.00, 2.91	0.00, 2.53	0.00, 2.19	0.00, 1.88	0.00, 1.59	0.00, 1.39	0.00, 1.22
2	0.53, 5.91	0.03, 5.41	0.00, 4.91	0.00, 4.41	0.00, 3.91	0.00, 3.45	0.00, 3.04	0.00, 2.67	0.00, 2.33	0.00, 1.73
3	1.10, 7.42	0.60, 6.92	0.10, 6.42	0.00, 5.92	0.00, 5.42	0.00, 4.92	0.00, 4.42	0.00, 3.95	0.00, 3.53	0.00, 2.78
4	1.47, 8.60	1.17, 8.10	0.74, 7.60	0.24, 7.10	0.00, 6.60	0.00, 6.10	0.00, 5.60	0.00, 5.10	0.00, 4.60	0.00, 3.60
5	1.84, 9.99	1.53, 9.49	1.25, 8.99	0.93, 8.49	0.43, 7.99	0.00, 7.49	0.00, 6.99	0.00, 6.49	0.00, 5.99	0.00, 4.99
6	2.21, 11.47	1.90, 10.97	1.61, 10.47	1.33, 9.97	1.08, 9.47	0.65, 8.97	0.15, 8.47	0.00, 7.97	0.00, 7.47	0.00, 6.47
7	3.56, 12.53	3.06, 12.03	2.56, 11.53	2.09, 11.03	1.59, 10.53	1.18, 10.03	0.89, 9.53	0.39, 9.03	0.00, 8.53	0.00, 7.53
8	3.96, 13.99	3.46, 13.49	2.96, 12.99	2.51, 12.49	2.14, 11.99	1.81, 11.49	1.51, 10.99	1.06, 10.49	0.66, 9.99	0.00, 8.99
9	4.36, 15.30	3.86, 14.80	3.36, 14.30	2.91, 13.80	2.53, 13.30	2.19, 12.80	1.88, 12.30	1.59, 11.80	1.33, 11.30	0.43, 10.30
10	5.50, 16.50	5.00, 16.00	4.50, 15.50	4.00, 15.00	3.50, 14.50	3.04, 14.00	2.63, 13.50	2.27, 13.00	1.94, 12.50	1.19, 11.50
11	5.91, 17.81	5.41, 17.31	4.91, 16.81	4.41, 16.31	3.91, 15.81	3.45, 15.31	3.04, 14.81	2.67, 14.31	2.33, 13.81	1.73, 12.81
12	7.01, 19.00	6.51, 18.50	6.01, 18.00	5.51, 17.50	5.01, 17.00	4.51, 16.50	4.01, 16.00	3.54, 15.50	3.12, 15.00	2.38, 14.00
13	7.42, 20.05	6.92, 19.55	6.42, 19.05	5.92, 18.55	5.42, 18.05	4.92, 17.55	4.42, 17.05	3.95, 16.55	3.53, 16.05	2.78, 15.05
14	8.50, 21.50	8.00, 21.00	7.50, 20.50	7.00, 20.00	6.50, 19.50	6.00, 19.00	5.50, 18.50	5.00, 18.00	4.50, 17.50	3.59, 16.50
15	9.48, 22.52	8.98, 22.02	8.48, 21.52	7.98, 21.02	7.48, 20.52	6.98, 20.02	6.48, 19.52	5.98, 19.02	5.48, 18.52	4.48, 17.52
16	9.99, 23.99	9.49, 23.49	8.99, 22.99	8.49, 22.49	7.99, 21.99	7.49, 21.49	6.99, 20.99	6.49, 20.49	5.99, 19.99	4.99, 18.99
17	11.04, 25.02	10.54, 24.52	10.04, 24.02	9.54, 23.52	9.04, 23.02	8.54, 22.52	8.04, 22.02	7.54, 21.52	7.04, 21.02	6.04, 20.02
18	11.47, 26.16	10.97, 25.66	10.47, 25.16	9.97, 24.66	9.47, 24.16	8.97, 23.66	8.47, 23.16	7.97, 22.66	7.47, 22.16	6.47, 21.16
19	12.51, 27.51	12.01, 27.01	11.51, 26.51	11.01, 26.01	10.51, 25.51	10.01, 25.01	9.51, 24.51	9.01, 24.01	8.51, 23.51	7.51, 22.51
20	13.55, 28.52	13.05, 28.02	12.55, 27.52	12.05, 27.02	11.55, 26.52	11.05, 26.02	10.55, 25.52	10.05, 25.02	9.55, 24.52	8.55, 23.52

Figure D.2.: 90% C.L. intervals for the Poisson signal mean μ , for total events observed n_0 , for known mean background b ranging from zero to five. [36]

E. Other Invariant Mass Combinations

While one of the main goals of this analysis is the study of any $\chi_{c1}\pi^+\pi^-$ intermediate state, some other invariant mass combinations have been visited as well. However, no unknown structures can be seen in the following invariant mass spectra of χ_{c1} and the higher mass π , the kaon and the lower mass π or the $K\pi^+\pi^-$ system.

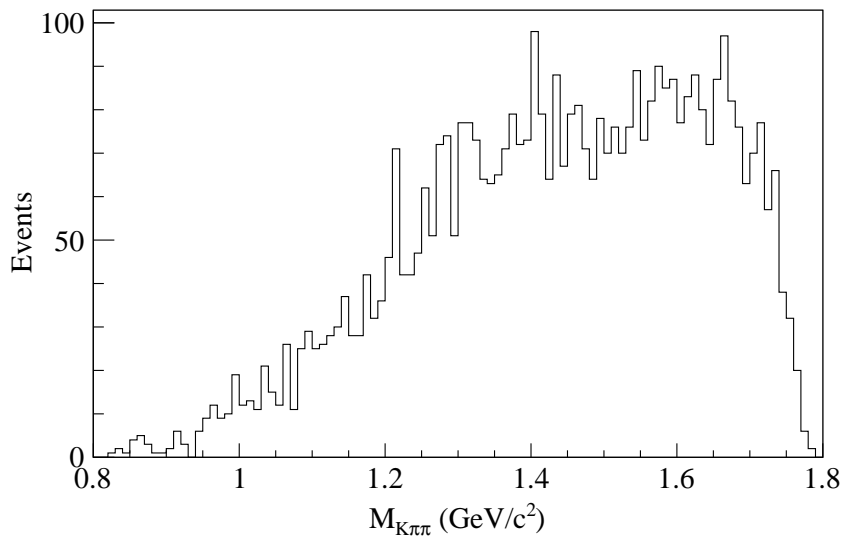
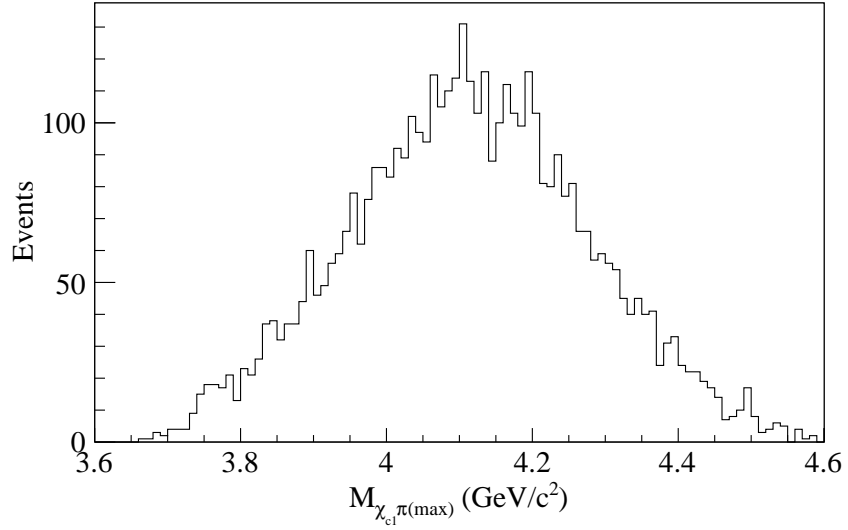
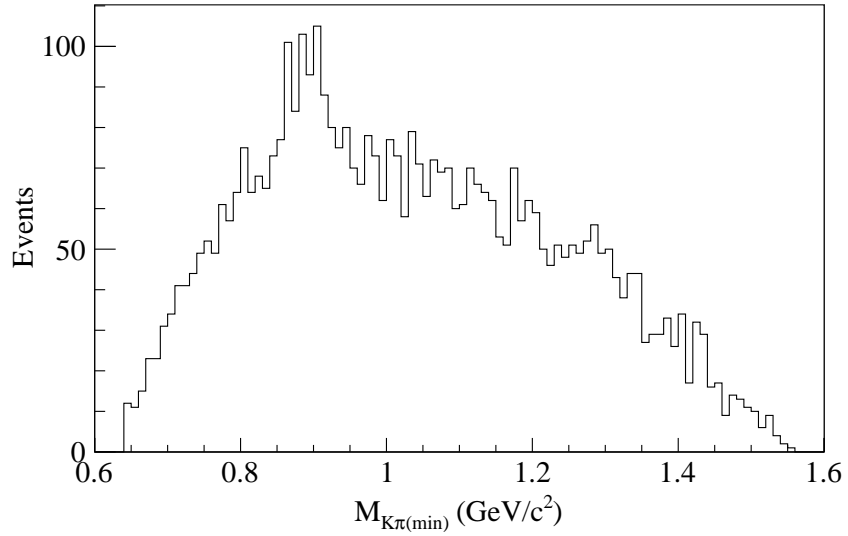


Figure E.1.: Invariant mass distribution of $K\pi\pi$ in data; $M_{bc} > 5.27$ GeV, $|\Delta E| < 0.02$ GeV and BCS applied.



(a) Mass distribution of χ_{c1} and the higher mass π in data.



(b) Mass distribution of K and the lower mass π in data. The peaking structure might be coming from a $K^*(892)$ decay.

Figure E.2.: Invariant mass distributions of correlated final state particles in data; $M_{bc} > 5.27$ GeV, $|\Delta E| < 0.02$ GeV and BCS applied.

Bibliography

- [1] Aaij, R. et al. Determination of the $X(3872)$ Meson Quantum Numbers. *Phys. Rev. Lett.*, 110:222001, May 2013.
- [2] Abazov, V.M. et al. Observation and Properties of the $X(3872)$ Decaying to $J/\psi\pi^+\pi^-$ in $\bar{p}p$ Collisions at $\sqrt{s} = 1.96$ TeV. *Phys. Rev. Lett.*, 93:162002, Oct 2004.
- [3] Abbiendi, G. et al. Search for the Standard Model Higgs Boson at LEP. *arXiv:hep-ex/0306033*, 2003. *Phys. Lett. B*565 (2003) 61-75.
- [4] Abe, K. et al. Evidence for $X(3872) \rightarrow \gamma J/\psi$ and the Sub-Threshold Decay $X(3872) \rightarrow \omega J/\psi$. *arXiv:hep-ex/0505037*, 2005.
- [5] Abe, T. et al. Belle II Technical Design Report. *arXiv:1011.0352*, 2010.
- [6] Acosta, D. et al. Observation of the Narrow State $X(3872) \rightarrow J/\psi\pi^+\pi^-$ in $\bar{p}p$ Collisions at $\sqrt{s} = 1.96$ TeV. *Phys. Rev. Lett.*, 93:072001, Aug 2004.
- [7] Akeroyd, A.G. et al. Physics at Super B Factory. *arXiv:hep-ex/0406071*, 2004.
- [8] Application Software Group. Detector Description and Simulation Tool. *CERN Program Library Long Writeup W5013*, 1995.
- [9] Aubert, B. et al. Search for a Charged Partner of the $X(3872)$ in the B Meson Decay $B \rightarrow X^- K$, $X^- \rightarrow J/\psi\pi^-\pi^0$. *Phys. Rev. D*, 71:031501, Feb 2005.
- [10] Aubert, B. et al. Study of the $B^- \rightarrow J/\psi K^- \pi^+ \pi^-$ Decay and Measurement of the $B^- \rightarrow X(3872) K^-$ Branching Fraction. *Phys. Rev. D*, 71:071103, Apr 2005.
- [11] Aubert, B. et al. Study of the $X(3872)$ and $Y(4260)$ in $B^0 \rightarrow J/\psi\pi^+\pi^- K^0$ and $B^- \rightarrow J/\psi\pi^+\pi^- K^-$ Decays. *Phys. Rev. D*, 73:011101, Jan 2006.
- [12] Aubert, J.J. and Ting, S.C. et al. Experimental Observation of a Heavy Particle J . *Phys. Rev. Lett.*, 33:1404–1406, Dec 1974.
- [13] Augustin, J.E. and Richter, B. et al. Discovery of a Narrow Resonance in e^+e^- Annihilation. *Phys. Rev. Lett.*, 33:1406–1408, Dec 1974.
- [14] Aushev, T. and Zwahlen, N. et al. Study of the $B \rightarrow X(3872)(\rightarrow D^{*0}\bar{D}^0)K$ Decay. *Phys. Rev. D*, 81:031103, Feb 2010.
- [15] BABAR Collaboration. Evidence for $X(3872) \rightarrow \psi(2S)\gamma$ in $B^\pm \rightarrow X(3872)K^\pm$ Decays, and a Study of $B \rightarrow c\bar{c}\gamma K$. *arXiv:0809.0042*, 2008.
- [16] Barletta, W. Detectors for Asymmetric B-factories. *Nuclear Instruments and Methods*

in *Physics Research A*, 479:117–232, 2002.

- [17] Belle Homepage. <http://belle.kek.jp>.
- [18] Bevan, A.J. and Golob, B. and Mannel, Th. and Prell, S. and Yabsley, B.D. Physics of the B Factories. *arXiv:1406.6311*, 2014. submitted to EPJC, SLAC-PUB-15968, KEK Preprint 2014-3.
- [19] Bhardwaj, V. and Miyabayashi, K. et al. Evidence of a New Narrow Resonance decaying to $\chi_{c1}\gamma$ in $B \rightarrow \chi_{c1}\gamma K$. *arXiv:1304.3975*, 2013.
- [20] Bhardwaj, V. et al. Observation of $X(3872) \rightarrow J/\psi\gamma$ and Search for $X(3872) \rightarrow \psi'\gamma$ in B Decays. *Phys. Rev. Lett.*, 107:091803, Aug 2011.
- [21] Bhuyan, B. High p_T Tracking Efficiency Using Partially Reconstructed D^* Decays. *Belle Note*, 1165, 2010.
- [22] Braaten, E. and Kusunoki, M. Exclusive Production of the $X(3872)$ in B Meson Decay. *Phys. Rev. D*, 71:074005, Apr 2005.
- [23] Braaten, E. and Stapleton, J. Analysis of $J/\psi\pi^+\pi^-$ and $D^0\bar{D}^0\pi^0$ Decays of the $X(3872)$. *Phys. Rev. D*, 81:014019, Jan 2010.
- [24] Brambilla, N. and Eidelman, S. Heavy Quarkonium: Progress, Puzzles, and Opportunities. *arXiv:1010.5827*, 2010.
- [25] Cabibbo, N. Unitary Symmetry and Leptonic Decays. *Phys. Rev. Lett.*, 10:531–533, Jun 1963.
- [26] Choi, S.-K. et al. Observation of a Narrow Charmonium-like State in Exclusive $B^\pm \rightarrow K^\pm\pi^+\pi^- J/\psi$ Decays. *Phys. Rev. Lett.*, 91:262001, Dec 2003.
- [27] Choi, S.-K. et al. Observation of a Narrow Charmoniumlike State in Exclusive $B^\pm \rightarrow K^\pm\pi^+\pi^- J/\psi$ Decays. *Phys. Rev. Lett.*, 91:262001, Dec 2003.
- [28] Choi, S.-K. et al. Observation of a Near-Threshold $\omega J/\psi$ Mass Enhancement in Exclusive $B \rightarrow K\omega J/\psi$ Decays. *Phys. Rev. Lett.*, 94:182002, May 2005.
- [29] Christenson, J.H. and Cronin, J.W. and Fitch, V.L. and Turlay, R. Evidence for the 2π Decay of the K_2^0 Meson. *Phys. Rev. Lett.*, 13:138–140, Jul 1964.
- [30] Dong, Y. and Faessler, A. and Gutsche, T. and Lyubovitskij, V.E. $J/\psi\gamma$ and $\psi(2S)\gamma$ Decay Modes of the $X(3872)$. *Journal of Physics G: Nuclear and Particle Physics*, 38(1):015001, 2011.
- [31] Ebert, D. and Faustov, R.N. and Galkin, V.O. Masses of Heavy Tetraquarks in the Relativistic Quark Model. *Phys.Lett. B*, 634:214–219, 2006. *arXiv:hep-ph/0512230*.
- [32] Eichten, E. et al. Charmonium: Comparison with Experiment. *Phys. Rev. D*, 21:203–233, Jan 1980.
- [33] Englert, F. and Brout, R. Broken Symmetry and the Mass of Gauge Vector Mesons. *Phys. Rev. Lett.*, 13:321–323, Aug 1964.

- [34] Epelbaum, E. and Krebs, H. and Lee, D. and Meißner, U.-G. Ab Initio. *Phys. Rev. Lett.*, 106:192501, May 2011.
- [35] Esen, S. *Measurement of $B_s^0 \rightarrow D_s^{(*)-} D_s^{(*)+}$ and Determination of the $B_s - \bar{B}_s$ Width Difference $\Delta\Gamma_s$ Using e^+e^- Collisions*. PhD thesis, University of Cincinnati, 2012.
- [36] Feldman, G.J. and Cousins, R.D. A Unified Approach to the Classical Statistical Analysis of Small Signals. *Phys. Rev. D*, 57:3873–3889, Apr 1998.
- [37] Fox, G. and Wolfram, S. Observables for the Analysis of Event Shapes in e^+e^- Annihilation and Other Processes. *Phys. Rev. Lett.*, 41:1581–1585, Dec 1978.
- [38] Guler, H. An Analysis of the $K^+\pi^+\pi^-$ Final State in $B^+ \rightarrow J/\psi K^+\pi^+\pi^-$ and $B^+ \rightarrow \psi(2S)K^+\pi^+\pi^-$. *Belle Note*, 1048, 2010.
- [39] Guralnik, G.S. and Hagen, C.R. and Kibble, T.W. Global Conservation Laws and Massless Particles. *Phys. Rev. Lett.*, 13:585–587, Nov 1964.
- [40] Herrero, M.J. The Standard Model. *arXiv:hep-ph/9812242*, 1998.
- [41] Higgs, P.W. Broken Symmetries and the Masses of Gauge Bosons. *Phys. Rev. Lett.*, 13:508–509, 1964.
- [42] Higgs, P.W. Broken Symmetries, Massless Particles and Gauge Fields. *Phys. Rev. Lett.*, 12:132–133, 1964.
- [43] Hoyle, F. On Nuclear Reactions Occuring in Very Hot Stars. 1. The Synthesis of Elements from Carbon to Nickel. *Astrophys.J.Suppl.*, Ser. 1:121–146, Sep 1954.
- [44] Isgur, N. and Paton, J.E. Flux-Tube Model for Hadrons in QCD. *Phys. Rev. D*, 31:2910–2929, Jun 1985.
- [45] Iwashita, T. and Miyabayashi, K. and Bhardwaj, V. et al. Measurement of Branching Fractions for $B \rightarrow J/\psi\eta K$ Decays and Search for a Narrow Resonance in the $J/\psi\eta$ Final State. *arXiv:1310.2704*, 2013.
- [46] Jaffe, R.L. Multiquark hadrons. I. Phenomenology of $Q^2\bar{Q}^2$ mesons. *Phys. Rev. D*, 15:267–280, Jan 1977.
- [47] Kakuno, H. Measurement of $\text{Br}(B \rightarrow X_u\ell\nu)$ and $|V_{ub}|$ through M_x Reconstruction with Simulated Annealing Technique. *Belle Note*, 615, 2003.
- [48] Kobayashi, M. and Maskawa, T. CP-Violation in the Renormalizable Theory of Weak Interaction. *Prog. Theor. Phys.*, 49:652–657, 1973.
- [49] Koppenburg, P. An Improved π^0 and η Veto. *Belle Note*, 665, 2004.
- [50] Landau, L. The Moment of a 2-Photon System. *Dokl. Akad. Nauk USSR*, 66:207, 1948.
- [51] Lange, D.J. The EvtGen Particle Decay Simulation Package. *Nucl.Instrum.Meth. A*, 462:152–155, 2001.
- [52] Lee, S.H. and Nielsen, M. and Wiedner, U. $D_s D^*$ Molecule as an Axial Meson. *arXiv:0803.1168*, 2008.

- [53] Liu, L. and Ryan, S.M. and Peardon, M. and Moir, G. and Vilaseca, P. Charmonium Spectroscopy from an Anisotropic Lattice Study. *arXiv:1112.1358*, 2011.
- [54] Maiani, L. and Piccinini, F. and Polosa, A. D. and Riquer, V. et al. Diquark-antidiquark States with Hidden or Open Charm and the Nature of $X(3872)$. *Phys. Rev. D*, 71:014028, Jan 2005.
- [55] Mathieu, V. and Kochelev, N. and Vento, V. The Physics of Glueballs. *arXiv:0810.4453*, 1985.
- [56] Nakano, T. et al. Evidence for a Narrow $S = +1$ Baryon Resonance in Photoproduction from the Neutron. *Phys. Rev. Lett.*, 91:012002, Jul 2003.
- [57] Nieves, J. and Pavón Valderrama, M. Heavy Quark Spin Symmetry Partners of the $X(3872)$. *Phys. Rev. D*, 86:056004, Sep 2012.
- [58] Olive, K.A. et al. The Review of Particle Physics. *Chin. Phys. C*, 38:090001, 2014.
- [59] Olsen, S.L. QCD Exotics. *arXiv:1403.1254*, 2014.
- [60] Ortega, P.G. and Segovia, J. and Entem, D.R. and Fernandez, F. Coupled Channel Approach to the Structure of the $X(3872)$. *arXiv:0907.3997*, 2009.
- [61] Sakharov, A.D. Violation of CP in Variance, C Asymmetry, and Baryon Asymmetry of the Universe. *Soviet Physics Uspekhi*, 34(5):392, 1991.
- [62] SuperKEKB Letter of Intent. <http://superb.kek.jp/documents/loi/loi.html.bak>.
- [63] Swanson, E.S. Diagnostic Decays of the $X(3872)$. *Phys. Rev. B.*, 598:197, 2004.
- [64] Swanson, E.S. The New Heavy Mesons: A Status Report. *Physics Reports*, 429:243–306, Jul 2006. *arXiv:hep-ph/0601110*.
- [65] Takasaki, F. Status of KEKB Accelerator and Detector, BELLE. *arxiv:hep-ex/9912004*, 1999.
- [66] Takizawa, M. and Takeuchi, S. $X(3872)$ as a Hybrid State of Charmonium and the Hadronic Molecule. *Prog. Theor. Exp. Phys.*, 093D01, 2013.
- [67] Terasaki, K. $X(3872)$ and Its Iso-Triplet Partners. *Prog. Theor. Phys.*, 127:577–582, 2012.
- [68] Tevatron New Physics Higgs Working Group and CDF Collaboration and D0 Collaboration. Updated Combination of CDF and D0 Searches for Standard Model Higgs Boson Production with up to 10.0 fb^{-1} of Data. *arXiv:1207.0449*, 2012.
- [69] The ATLAS Collaboration. An Update of Combined Measurements of the new Higgs-like Boson with high Mass Resolution Channels. *Tech. Rep.*, ATLAS-CONF-2012-170, Dec 2012.
- [70] The ATLAS Collaboration. Observation and Study of the Higgs Boson Candidate in the two Photon Decay Channel with the ATLAS Detector at the LHC. *Tech. Rep.*, ATLAS-CONF-2012-168, Dec 2012.

- [71] The ATLAS Collaboration. Observation of a new Particle in the Search for the Standard Model Higgs Boson with the ATLAS Detector at the LHC. *arXiv:1207.7214*, 2012. *Phys.Lett. B*716 (2012) 1-29.
- [72] The ATLAS Collaboration. Measurement of the Higgs Boson Mass from the $H \rightarrow \gamma\gamma$ and $H \rightarrow ZZ^* \rightarrow 4\ell$ Channels in pp Collisions at center-of-mass Energies of 7 and 8 TeV with the ATLAS Detector. *Phys. Rev. D*, 90:052004, Sep 2014.
- [73] The BABAR Collaboration. Evidence for the Decay $X(3872) \rightarrow J/\psi\omega$. *Phys. Rev. D*, 82:011101, Jul 2010.
- [74] The BELLE Collaboration. Experimental Constraints on the possible J^{PC} Quantum Numbers of the $X(3872)$. *arXiv:hep-ex/0505038*, 2005.
- [75] The BELLE Collaboration. Study of $X(3872)$ in B Meson Decays. *arXiv:0809.1224*, 2008.
- [76] The BELLE Collaboration. Observation of two Charged Bottomonium-like Resonances. *arXiv:1105.4583*, 2011.
- [77] The CDF Collaboration. Analysis of the Quantum Numbers J^{PC} of the $X(3872)$ Particle. *Phys. Rev. Lett.*, 98:132002, Mar 2007.
- [78] The CMS Collaboration. Observation of a new Boson at a Mass of 125 GeV with the CMS Experiment at the LHC. *arXiv:1207.7235*, 2012. *Phys.Lett. B*716 (2012) 30-61.
- [79] The LHCb Collaboration. Evidence for the Decay $X(3872) \rightarrow \psi(2S)\gamma$. *arXiv:1404.0275*, 2014.
- [80] The LHCb Collaboration. Observation of the resonant Character of the $Z(4430)^-$ State. *arXiv:1404.1903*, 2014.
- [81] Thomson, M. *Modern Particle Physics*. Cambridge University Press, 2013.
- [82] Trabelsi, K., Mar 2004. Slides at Belle General Meeting.
- [83] Uehara, S. et al. Observation of a χ'_{c2} Candidate in $\gamma\gamma \rightarrow D\bar{D}$ Production at Belle. *Phys. Rev. Lett.*, 96:082003, Mar 2006. *arXiv:hep-ex/0512035*.
- [84] Wang, T.-H. and Wang, G.-L. Radiative $E1$ decays of $X(3872)$. *arXiv:1006.3363*, 2010.
- [85] Weinberg, S. A Model of Leptons. *Phys. Rev. Lett.*, 19:1264–1266, Nov 1967.
- [86] Yang, C.N. Selection Rules for the Dematerialization of a Particle into Two Photons. *Phys. Rev.*, 77:242–245, Jan 1950.

Acknowledgements

There are so many people I would like to thank for helping me being able to finish this "second book of mine". Maybe I start at the beginning when the idea of not just continuing my university studies but also doing so in part in Japan found its way into my head. I was inspired by Miriam Fritsch to take an interest in charmonium spectroscopy. The Belle experiment offered a great opportunity to combine my plans for a dissertation in charmonium analyses and an international exchange with Japan.

Through Miriam I met Soeren Lange, a colleague from the PANDA collaboration who also happens to be a Belle member, who then introduced me to Ariane Frey in Göttingen and Kenkichi Miyabayashi in Nara. They have been my supervisors and most respected role models for the last four years. Both have been unbelievably supportive of the still not common concept of a binational joint doctoral supervision. I would not have been able to do my doctorate under these excellent conditions without their help. Also many others on the administrative level have been contributing to negotiate and set up contracts, making sure both universities' requirements will be satisfied for the award of a doctor's degree, especially Stefan Häußler and all the officials of Nara Women's University taking care of formalities.

Even before I started in Göttingen in January 2011, Wolfgang Gradl took me to one of the *B* factory legacy book meetings held at the University of Mainz and I met some future Belle colleagues for the first time which left me very excited to become a part of such an inspiring collaboration. I am much indebted to my German supervisor Ariane Frey for her warm welcome, support and assistance at any time. She has been a reliable pillar of good will and care throughout this time. Also a special thank you goes to Philipp Hamer for many hours of patiently introducing me to the art of C++ and the Belle experiment's analysis framework BASF. I thank my colleagues and fellow PhD students in the II. Institute, past and present, for their support and encouragement, especially Julia Rieger, Martina Schulte-Borchers, Jens Weingarten und Jörn Große-Knetter.

At Nara Women's University I would like to thank the staff of the international office for their help with all the small things and formalities. My thanks go to all colleagues for useful discussions and to my fellow students in the high energy physics lab for many smiles and cheerfulness. But the biggest impact had the incredible and never-ending support and assistance, patience and motivation I received from my Japanese supervisor Kenkichi Miyabayashi who I owe my deepest gratitude. His enthusiasm and dedication have been a great motivation. I am further indebted to Miyabayashi-san for valuable discussions and help in the preparation of this thesis. For a lot of discussions, explanations and advice, and not to forget constant encouragement and guidance through all the different phases of this analysis, I would like to wholeheartedly thank Vishal Bhardwaj.

I wish to thank every member of the Belle collaboration and the KEKB accelerator team for their hard work to provide the excellent smooth operation of the experiment - no analysis without data. Also, I am incredibly grateful to my Belle Note referees, Seema Bahinipati, Pavel Krokovny and Eiichi Nakano for their specific comments on a number of the more technical details and for monitoring my progress. For providing critical assessments and suggestions, I am particularly grateful to Karim Trabelsi, Yoshihide Sakai, Mikihiro Nakao, and all of the Belle physics analysis colleagues and the conveners of the Charm and New Physics Subgroup as well as BAM and BGM meetings.

I would like to thank my colleagues and friends, Jason Mansour, Philipp Hamer, Andrea Knue and Boris Lemmer, for proofreading and for their comments on early drafts of this work, a lot of encouragement and help with LaTeX and Root issues. I also have to say a big thank you to my long time friend Lisa Büschelberger for an outsider's view and valuable advice in all things linguistical (and probably another best-of list of particle physics lingo). A special thank you to Oliver Steffen, for proofreading in every stage of this thesis, useful comments, help with any technical questions and for general moral support at any hour. Thank you for being there for me when I really needed it.

For moral support and for reminding me to keep a healthy work-life balance I would like to say thank you to the "Bier & Schnitzel"-Crew and my lovely flatmates, Jason Mansour and Frauke Bergmann. I thank Lucie Hamdi for her patience with all the complicated paperwork for reimbursement for conferences and coming "home" to Göttingen.

Zuletzt möchte ich meinen lieben Eltern, Herbert und Trudelinde Panzenböck danken. Mein Leben lang haben sie mich bei all meinen Entscheidungen ermutigt, beim Überwinden der damit verbundenen Herausforderungen unterstützt und mich immer daran erinnert, mein Bestes zu geben. Ich bin sehr dankbar für all die aufmunternden Worte während der kurzen Telefonpausen, in den kleinen E-Mails zwischendurch und das Verständnis und die Geduld, mit denen sie meine Ausschweifungen über technische Analyse-Details ertragen haben. Ihr seid großartig!

Curriculum Vitæ

Personal Data:

Name: Elisabeth Patricia Panzenböck
Date of Birth: February 24, 1985
in Mainz, Germany
Nationality: German

Education:

Jan 2011 - Dec 2014 PhD student under Joint Doctoral Supervision
at Georg August University, Göttingen, Germany
and Nara Women's University, Nara, Japan
Doctoral Thesis: *Branching Fraction Measurement of $B^\pm \rightarrow \chi_{c1} \pi^+ \pi^- K^\pm$ and Search for a Narrow Resonance with the Belle Experiment*
under supervision of Prof. Dr. Ariane Frey (Göttingen)
and Assoc. Prof. Dr. Kenkichi Miyabayashi (Nara)

Apr 2012 - Mar 2014 Research period at Nara Women's University, Nara, Japan

Nov 2010 Graduation (Diplom): grade *very good*
Apr 2004 - Nov 2010 Study of Physics at Johannes Gutenberg University,
Mainz, Germany
Diploma Thesis: *Setup of a Test Station for the PANDA Luminosity Monitor System*
under supervision of Prof. Dr. Achim Denig

Mar 2004 Graduation (Abitur): grade *very good*

Scientific Schools:

- Sep 2014 46. Herbstschule für Hochenergiephysik
in Maria-Laach, Germany
- Oct 2012 First Asia-Europe-Pacific School of High-Energy Physics
in Fukuoka, Japan
- Sep 2011 Belle Analysis School
in Jeju, South Korea
- Aug 2011 School on Amplitude Analysis in Modern Physics
in Bad Honnef, Germany
- Aug 2010 Summer School on Hadron Physics
in Bad Honnef, Germany

Presentations:

- Feb 2014 *Study of $B^\pm \rightarrow \chi_{c1}\pi^+\pi^-K^\pm$*
Talk at Lake Louise Winter Institute, Lake Louise, Canada
- Nov 2013 *Study of $B^\pm \rightarrow \chi_{c1}\pi^+\pi^-K^\pm$*
Talk at XV International Conference on Hadron Spectroscopy,
Nara, Japan
- Mar 2013 *Study of $B^\pm \rightarrow \chi_{c1}\pi^+\pi^-K^\pm$*
Talk at 69th Annual Meeting of JPS, Hiroshima, Japan
- Mar 2013 *Study of $B^\pm \rightarrow \chi_{c1}\pi^+\pi^-K^\pm$*
Talk at DPG Spring Conference, Dresden, Germany
- Mar 2010 *A Luminosity Monitor for PANDA*
Poster presentation at DPG Spring Conference, Bonn, Ger-
many

Scholarships:

- Apr 2012 - Mar 2014 Japanese Government (MEXT) & DAAD Scholarship
as partial funding of PhD Thesis
- Apr - Sep 2010 Scholarship of Johannes Gutenberg University Mainz
as partial funding of Diploma Thesis